61. Top Quark

Revised September 2025 by F. Canelli (Zurich U.), A. Knue (TU Dortmund) and F. Maltoni (CP3 U. catholique de Louvain; Bologna U.).

61.1 Introduction and SM theory overview

In the Standard Model (SM), the left-handed top quark is the Q=2/3, $T_3=+1/2$ member of the weak-isospin doublet containing the bottom quark, while the right-handed top quark is an $SU(2)_L$ singlet. The phenomenology of the top quark is driven by its large mass, $m_t \simeq v/\sqrt{2}$, where v=246 GeV is the Higgs vacuum expectation value, implying a Yukawa coupling of order unity. Being heavier than the W boson, it is the only quark that can decay weakly into a real W boson and a b quark. Its lifetime is shorter than the timescale of non-perturbative strong interactions, which prevents hadronization and preserves properties such as its spin, allowing the top to behave almost as a free quark. Through loop effects, it gives important contributions to SM precision observables, and its unique role makes it central to many extensions of the SM, often linked to new particles or interactions. These features strongly motivate increasingly precise studies of top-quark physics, providing a unique laboratory for testing the SM at the electroweak symmetry-breaking scale (EWSB) and beyond. At the same time, the abundant production of top quarks at the LHC enables precision measurements of their mass, couplings, production cross sections, and decay branching ratios. This review summarizes the experimental and theoretical issues in determining these properties and reports on recent progress.

61.1.1 Mass

The top-quark mass largely determines its unique phenomenology. In the SM, quark masses are derived parameters that are determined by the Yukawa coupling and the vacuum expectation value. At the loop level, with the Higgs boson discovery and better than per mil measurement of its mass, the values of the W-boson and top-quark mass are correlated, so that their precise determinations provide a strong test of the SM (see Section 10 "Electroweak Model and constraints on new physics" of this Review). At present, there is some tension at the $1.7\,\sigma$ level, between the indirect top-quark (pole) mass determination from electroweak (EW) precision data of $175.2\pm1.8\,$ GeV (see Section 10 in this Review) and the combination of direct measurements at the LHC that yields $172.52\pm0.33\,$ GeV [1].

The top-quark mass value is also crucial in the issue of vacuum stability in the SM [2–4]. At high scales, the Higgs quartic coupling λ evolves to increasingly small values as m_t grows. Above $m_t = 171$ GeV, i.e., very close to the most precise measurements, λ becomes negative at the Planck scale, leading to a meta-stable EW vacuum, while for slightly larger values, $m_t > 176$ GeV, the EW vacuum would become unstable. Current top-quark measurements therefore point to a Higgs quartic coupling that is nearly vanishing at the Planck scale. While being quite suggestive, in the absence of a clear UV picture, this argument allows only to conclude that comparison between our best SM predictions and the data does not imply new physics below the Planck scale (see Section 11.2.3 of "Status of Higgs Boson Physics" in this Review).

Due to its fundamental importance, precisely determining the top-quark mass has been a central objective of precision measurement programs carried out by the ATLAS and CMS collaborations at the LHC, and previously by the CDF and DØ collaborations at the Tevatron. The basic methodology rests on the idea of fitting m_t -dependent kinematic distributions to fully-exclusive (Monte Carlo) predictions, via the full or partial reconstruction of the system of the t and \bar{t} decay products. These are called "direct measurements" and aim for a target accuracy in the per-mil range. With an absolute uncertainty of order or better than $\Lambda_{\rm QCD}$, however, a clear relation between the

extracted mass and a well-defined quantum field theory parameter of the underlying theory has become necessary.

Several mass parameter definitions exist with a precise field-theoretical meaning, which can be organized into two broad classes: the long-distance ones, such as the "pole mass", and short-distance masses, such as the $\overline{\rm MS}$ mass. An additional mass definition [5] interpolates between the two.

Direct determinations rely on mass-sensitive observables constructed from the kinematics of the top-quark decay products. Monte Carlo generators enforce the invariant mass of this system to follow, as closely as possible, the virtuality of the top quark, which is modeled by a Breit–Wigner distribution centered on the Monte Carlo mass parameter. In this framework, the latter acts as an effective proxy for the pole mass. At e^+e^- colliders, one can define a short-distance mass, e.g., the "potential mass" that can be determined by measurements at the $t\bar{t}$ threshold, and it does not suffer from non-perturbative ambiguities. At hadron colliders, all observables that can be connected to the top-quark mass involve a top-quark reconstruction from the final state, and at the end are connected to the pole mass.

A top-quark mass measurement cannot be defined solely in terms of the mass of the system of its decay products: the top quark is a colored object; therefore, it cannot be an asymptotic state of the theory, and no final-state hadronic system can be unambiguously associated with it. On the other hand, final state observables, such as those arising from its decay, can be related to the top-quark mass through computations that have both perturbative and non-perturbative components, as seen in Monte Carlo generators.

From a purely theoretical (calculational) point of view, the top-quark mass parameter is defined within a given renormalization scheme, since divergent perturbative corrections arise order by order in perturbation theory and need to be subtracted. The pole mass scheme prescribes to subtract the divergent mass corrections so that the pole in the quark propagator remains fixed order by order in perturbation theory. The $\overline{\rm MS}$ scheme prescribes to employ dimensional regularization and subtract the pure $1/\epsilon$ pole in the divergent mass correction. In doing so, the corresponding mass becomes scale-dependent. In this scheme, the pole in the top quark propagator receives corrections at all orders in perturbation theory. This scheme has the advantage of making the relation between the mass and the Yukawa coupling straightforward in the SM and independent of non-perturbative corrections.

The relation between the top quark pole mass m_t^{pole} and $m_t^{\overline{\text{MS}}}$ up to four loops reads [6]

$$m_t^{\text{pole}} = m_t^{\overline{\text{MS}}}(m_t)[1 + 0.4244 \,\alpha_s + 0.8345 \,\alpha_s^2 + 2.375 \,\alpha_s^3 + (8.49 \pm 0.25) \,\alpha_s^4],$$
 (61.1)

which for strong coupling constant $\alpha_s = \alpha_s^{(6)}(m_t) = 0.1088$ and $m_t^{\text{pole}} = 172.5$ GeV gives $m_t^{\overline{\text{MS}}}(m_t) = 162.69 \pm 0.006$ GeV. The two definitions lead to perturbatively equivalent theories: the perturbative expression of the pole mass in terms of the $\overline{\text{MS}}$ can be used to turn a result expressed in the pole mass scheme into the corresponding one in the $\overline{\text{MS}}$ scheme. However, the relation above has only a perturbative meaning, as the two masses differ by non-perturbative, long-distance effects. The difference between the top-quark pole mass and the mass extracted in direct measurements arises due to non-perturbative effects, which are currently modeled by shower Monte Carlo programs. It is expected to be of order $Q_0 \cdot \alpha_s(Q_0)$ with $Q_0 \sim 1$ GeV, i.e., of order 0.5 GeV. Recent efforts to precisely define and estimate the uncertainties of the top-quark mass can be found in Refs. [7,8].

61.1.2 Width

Like other unstable elementary particles in the SM, the top-quark lifetime, and thus its decay width, can be perturbatively calculated within the SM. With a mass exceeding the Wb production

threshold and given that $|V_{tb}| \gg |V_{td}|, |V_{ts}|$, the top-quark decay width is dominated by the twobody decay channel $t \to Wb$. At next-to-leading order (NLO) prediction for the width within the SM is given by [9]:

$$\Gamma_t = \frac{G_F m_t^3}{8\pi\sqrt{2}} \left(1 - \frac{M_W^2}{m_t^2} \right)^2 \left(1 + 2\frac{M_W^2}{m_t^2} \right) \left[1 - \frac{2\alpha_s}{3\pi} \left(\frac{2\pi^2}{3} - \frac{5}{2} \right) \right],$$
(61.2)

where m_t refers to the top-quark pole mass (to keep the formula simple, known m_b^2/m_t^2 , α_s^2 , and $(\alpha_s/\pi)(M_W^2/m_t^2)$ are not included). The known quantum chromodynamics (QCD) corrections of order α_s^2 to Γ_t , and the EW NLO corrections [10,11] improve the overall theoretical accuracy to better than 1%. As a result, between $m_t = 170$ GeV and 175 GeV, the width changes from 1.258 GeV to 1.394 GeV, with a linear dependence on m_t assuming $\alpha_s(M_Z) = 0.1179$ and $M_W = 80.377$ GeV. At the reference value of $m_t = 172.5$ GeV, one finds $\Gamma_t = 1.326$ GeV.

With its correspondingly short lifetime of about 0.5×10^{-24} s, the top quark is expected to decay before top-flavored hadrons or $t\bar{t}$ quarkonium-like bound states can form [12]. However, in the latter case, since the decay time is very close to the would-be-resonance binding time, a peak is predicted in e^+e^- scattering at the $t\bar{t}$ threshold [13] (whose position and width are linked to the "potential mass" of the top quark and its width, respectively), and it is also present in hadron collisions [14–16]. The short lifetime of the top quark also prevents strong interactions from efficiently scrambling its spin, as such processes would require a much longer timescale. Moreover, the purely left-handed structure of the weak interaction dictates that the top-quark decays predominantly via $t \to Wb$, followed by $W \to f\bar{f}'$, with the direction of the fermion f (the charged lepton or down-type quark component) being almost 100% correlated with the top-quark spin. Taken together, these features render the top quark unique among quarks, as they allow for direct experimental access to its spin properties through the angular distributions of its decay products.

Other decay modes of the top quark provide negligible contributions to the total width. For example, flavor-changing neutral current (FCNC) interactions, which are allowed starting at the one-loop level, give [17,18]:

$$\begin{split} & \text{Br}^{\text{SM}}(t \to gc) = 5 \cdot 10^{-12}, \ \text{Br}^{\text{SM}}(t \to gu) = 4 \cdot 10^{-14}, \\ & \text{Br}^{\text{SM}}(t \to \gamma c) = 5 \cdot 10^{-14}, \ \text{Br}^{\text{SM}}(t \to \gamma u) = 4 \cdot 10^{-16}, \\ & \text{Br}^{\text{SM}}(t \to Zc) = 1 \cdot 10^{-14}, \ \text{Br}^{\text{SM}}(t \to Zu) = 7 \cdot 10^{-17}, \\ & \text{Br}^{\text{SM}}(t \to Hc) = 3 \cdot 10^{-15}, \ \text{Br}^{\text{SM}}(t \to Hu) = 2 \cdot 10^{-17}. \end{split}$$

61.1.3 Couplings

The SM couplings involving top quarks are of two types: gauge couplings, which are universal, and Yukawa couplings, which instead depend on the generation. Following the notation of Sections 9 and 10 of this *Review*, after EWSB the top-quark interactions read

$$\mathcal{L}_{t}^{\text{SM}} = \bar{\psi}_{t} \left[i \partial \!\!\!/ - m_{t} \right] \psi_{t} - g_{s} \bar{\psi}_{t} \gamma^{\mu} t^{C} \psi_{t} \mathcal{A}_{\mu}^{C} - e Q_{t} \bar{\psi}_{t} \gamma^{\mu} \psi_{t} A_{\mu}
- \frac{g}{2\sqrt{2}} \bar{\Psi} \gamma^{\mu} (1 - \gamma^{5}) (T^{+} W_{\mu}^{+} + T^{-} W_{\mu}^{-}) \Psi - \frac{g}{2\cos\theta_{W}} \bar{\psi}_{t} \gamma^{\mu} \left(g_{V}^{t} - g_{A}^{t} \gamma^{5} \right) \psi_{t} Z_{\mu}
- \frac{m_{t}}{2} H \bar{\psi}_{t} \psi_{t} ,$$
(61.3)

where in the first line we include the kinetic term, the coupling to the SU(3) field \mathcal{A}_{μ}^{C} , to the EM field A_{μ} , to the weak bosons, W_{μ}^{\pm} , Z_{μ} and to the Higgs boson ($\Psi = (t, b')$ with $b' = V_{tb} b + V_{ts} s + V_{td} d$). As mentioned above, there are no neutral flavor-changing interactions in the SM at tree level.

In the absence of evidence for physics beyond the SM at the weak scale or below, the SM Effective Field Theory (SMEFT) [19–21] provides a simple and consistent framework to systematically

parameterize possible deviations from the SM predictions in the interactions among the known particles, using minimal theoretical assumptions. It amounts to extending the Lagrangian of the SM by all higher-dimensional operators that respect the gauge symmetry

$$\mathcal{L}^{\text{SMEFT}} = \mathcal{L}^{\text{SM}} + \sum_{D>4} \sum_{i}^{N_D} \frac{C_i^{(D)} O_i^{(D)}}{\Lambda^{D-4}},$$
 (61.4)

where D is the dimension of the operator $O_i^{(D)}$ and Λ provides an upper bound for the scale of new physics. An EFT model is generally characterized by power counting rules that identify a hierarchy among operators. In the case of the SMEFT, a minimal approach is considered, where the large-scale Λ provides a universal suppression factor for the higher-dimensional operators.

The currently adopted parametrization for SMEFT interpretations of top-quark measurements relies on the Warsaw basis of gauge-invariant dimension-six operators [21] and it is detailed in Ref. [22] (see [23,24] for early discussions of top-quark related operators). For convenience, often specific degrees of freedom are identified from combinations of Warsaw-basis operator coefficients aligned with the directions of the EFT parameter space, which appear in given processes, in interferences with SM amplitudes, and top-quark interactions with some of the gauge boson mass eigenstates. Model implementations are available for tree-level and even one-loop Monte Carlo simulations [25, 26].

The definitions of the SMEFT operators can be organized in four categories: Four-quark, two-quark-two-bosons, two-quark-two-lepton, and baryon-lepton-number-violating operators. The over-whelming number of four-fermion operators is tamed by adopting simplifying assumptions about beyond-the-standard-model flavor structures. A baseline flavor scenario in the quark sector and motivated by the minimal flavor violation ansatz [27–29] corresponds to imposing a $U(2)_q \times U(2)_u \times U(2)_d$ symmetry among the first two generations (q refers to the SU(2) left-handed doublet, while u,d are right-handed singlets). In this case, the following numbers of degrees of freedom are produced for the operators of each category of field content:

four heavy quarks 11 + 2 CPV two light and two heavy quarks 14 two heavy quarks and bosons 9 + 6 CPV two heavy quarks and two leptons (8 + 3 CPV) \times 3 lepton flavors

where we counted separately CP-conserving and CP-violating (CPV) parameters. These operators are collected in Tab. 61.1. Other less restricted scenarios, such as that obtained by imposing $U(2)_{q+u+d}$ symmetry featuring additional 10 + 10 CPV degrees of freedom, or more restricted ones, such as top-philic scenario where it is assumed that new physics couples dominantly to the left-handed doublet and right-handed up-type quark singlet of the third generation as well as to bosons, featuring only 19+6 (CPV) degrees of freedom, are often considered. It is also customary to analyze top-quark FCNCs separately, as at the tree level, they enter only quadratically.

61.1.4 Production

Top-quark production provides a powerful probe of QCD and the EW theory. Precise measurements of production rates and kinematic distributions constrain PDFs, α_s , and m_t . Since its discovery in 1995 at the Tevatron, direct measurements of top-quark production have been extensively performed. At the LHC, the broad range of center-of-mass energies, large production cross sections, and the ability to study forward production and heavy-ion collisions make top-quark measurements a uniquely sensitive tool for testing the SM and probing the partonic structure of matter.

Table 61.1: List of SMEFT operators at dimension six, assuming $U(2)_q \times U(2)_u \times U(2)_d$ flavor symmetry. For more details on notation and conventions, see the reference in the text.

Operator	Field content	Operator	Field content
Four-quark			wo-quark-two-lepton
$O_{qq}^{1(ijkl)}$	$(\bar{q}_i \gamma^\mu q_j)(\bar{q}_k \gamma_\mu q_l)$	$O_{lq}^{1(ijkl)}$	$(\bar{l}_i \gamma^\mu l_j)(\bar{q}_k \gamma^\mu q_l)$
$O_{qq}^{3(ijkl)}$	$\left (\bar{q}_i \gamma^\mu \tau^I q_j) (\bar{q}_k \gamma_\mu \tau^I q_l) \right $	$O_{lq}^{\overrightarrow{3}(ijkl)} \ O_{lu}^{(ijkl)} \ O_{lu}^{(ijkl)}$	$(\bar{l}_i \gamma^\mu \tau^I l_j)(\bar{q}_k \gamma^\mu \tau^I q_l)$
$O_{qu}^{1(ijkl)}$	$\left (\bar{q}_i \gamma^\mu q_j)(\bar{u}_k \gamma_\mu u_l) \right $	$O_{lu}^{(ijkl)}$	$(\bar{l}_i\gamma^\mu l_j)(\bar{u}_k\gamma^\mu u_l)$
$O_{qu}^{8(ijkl)}$	$\left (\bar{q}_i \gamma^\mu T^A q_j) (\bar{u}_k \gamma_\mu T^A u_l) \right $	O_{eq}	$(\bar{e}_i \gamma^\mu e_j)(\bar{q}_k \gamma^\mu q_l)$
$O_{qd}^{1(ijkl)}$	$(\bar{q}_i \gamma^{\mu} q_j)(\bar{d}_k \gamma_{\mu} d_l)$	$O_{eu}^{(ijkl)}$	$(\bar{e}_i \gamma^\mu e_j)(\bar{u}_k \gamma^\mu u_l)$
$O_{qd}^{\hat{8}(ijkl)}$	$(\bar{q}_i \gamma^{\mu} T^A q_j) (\bar{d}_k \gamma_{\mu} T^A d_l)$	$^{\ddagger}O_{lequ}^{1(ijkl)}$	$(\bar{l}_i e_j) \varepsilon (\bar{q}_k u_l)$
$O_{uu}^{(ijkl)}$	$\left((\bar{u}_i \gamma^\mu u_j)(\bar{u}_k \gamma_\mu u_l) \right)$	$^{\ddagger}O_{lequ}^{3(ijkl)}$	$(\bar{l}_i \sigma^{\mu\nu} e_j) \varepsilon (\bar{q}_k \sigma_{\mu\nu} u_l)$
$O_{ud}^{1(ijkl)}$	$\left (\bar{u}_i \gamma^\mu u_j)(\bar{d}_k \gamma_\mu d_l) \right $	$^{\ddagger}O_{ledq}^{(i\dot{j}kl)}$	$(ar{l}_i e_j)(ar{d}_k q_l)$
$O_{ud}^{8(ijkl)}$	$\left (\bar{u}_i \gamma^\mu T^A u_j) (\bar{d}_k \gamma_\mu T^A d_l) \right $		
$^{\ddagger}O_{quqd}^{1(ijkl)}$	$(\bar{q}_i u_j) \varepsilon (\bar{q}_k d_l)$		
$^{\ddagger}O_{quqd}^{8(ijkl)}$	$(\bar{q}_i T^A u_j) \varepsilon (\bar{q}_k T^A d_l)$		
Two	o-quark operators	Baryon- and lepton-number-violating	
$^{\ddagger}O_{u\varphi}^{(ij)}$	$\bar{q}_i u_{j,\tilde{\varphi}_i}(\varphi^\dagger \varphi)$	$^{\ddagger}O_{qqu}^{(ijkl)}$	$(\overline{q^c}_{i\alpha}\varepsilon q_{j\beta})(\overline{u^c}_{k\gamma}e_l)\;\epsilon^{\alpha\beta\gamma}$
$O_{\varphi q}^{1(ij)}$	$(\varphi^{\dagger} i \overrightarrow{D}_{\mu} \varphi) (\overline{q}_i \gamma^{\mu} q_j)$	$^{\ddagger}O_{qqq}^{1(ijkl)}$	$(\overline{q^c}_{i\alpha}\varepsilon q_{j\beta})(\overline{q^c}_{k\gamma}\varepsilon l_l) \ \epsilon^{\alpha\beta\gamma}$
$O_{\varphi q}^{3(ij)}$	$(\varphi^{\dagger} i \stackrel{\longrightarrow}{D}_{\mu}^{I} \varphi) (\bar{q}_i \gamma^{\mu} \tau^{I} q_j)$	$^{\ddagger}O_{qqq}^{3(ijkl)}$	$(\overline{q^c}_{i\alpha}\tau^I\varepsilon q_{j\beta})(\overline{q^c}_{k\gamma}\tau^I\varepsilon l_l)\;\epsilon^{\alpha\beta\gamma}$
$O_{\varphi u}^{(ij)}$	$\left(\varphi^{\dagger} i \overrightarrow{D}_{\mu} \varphi) (\bar{u}_i \gamma^{\mu} u_j)\right)$	$^{\ddagger}O_{duu}^{(ijkl)}$	$(\overline{d^c}_{i\alpha}u_{j\beta})(\overline{u^c}_{k\gamma}e_l)\;\epsilon^{\alpha\beta\gamma}$
$^{\ddagger}O_{arphi ud}^{(ij)}$	$\left (\tilde{\varphi}^{\dagger} i D_{\mu} \varphi) (\bar{u}_i \gamma^{\mu} d_j) \right $		
$^{\ddagger}O_{uW}^{(ij)}$	$(\bar{q}_i \sigma^{\mu\nu} \tau^I u_j) \tilde{\varphi} W^I_{\mu\nu}$		
$^{\ddagger}O_{dW}^{(ij)}$	$(\bar{q}_i \sigma^{\mu\nu} \tau^I d_j) \varphi W^I_{\mu\nu}$		
$^{\ddagger}O_{uB}^{(ij)}$	$\left(\bar{q}_i\sigma^{\mu\nu}u_j\right) \tilde{\varphi}B_{\mu\nu}$		
$^{\ddagger}O_{uG}^{\overline{(ij)}}$	$(\bar{q}_i \sigma^{\mu\nu} T^A u_j) \tilde{\varphi} G^A_{\mu\nu}$		

Top-quark production processes are classified according to the underlying interaction mechanism. The primary categories include: top-antitop quark pair production through QCD interactions $(t\bar{t})$, single top-quark production via EW interactions (t or $\bar{t})$, and associated production involving the creation of a single top quark or a top-quark pair alongside gauge bosons or other particles via EW or QCD interactions $(t\bar{t}+X,t/\bar{t}+X)$. Associated production also encompasses the rare scenarios where multiple top quarks are produced, specifically three-top $(tt\bar{t}/\bar{t}t\bar{t})$ and four-top $(t\bar{t}t\bar{t})$ production. Among these, pair production is the most abundant mode of top-quark production.

A key aspect of top-quark phenomenology is the study of its spin through the angular distributions of decay products, which directly reflect the production mechanism. In single-top-quark production via the weak interaction, the top quark is predicted to be fully polarized. In contrast, in $t\bar{t}$ production dominated by QCD interactions, individual top quarks are nearly unpolarized, but their spins exhibit nontrivial correlations. These spin effects are known up to NNLO in QCD and NLO in EW theory [30, 31]. In specific kinematic regimes, such as near threshold or at high transverse momentum (p_T) , the correlations are strong enough that the $t\bar{t}$ spin system becomes entangled [32]. Recent LHC measurements at threshold by ATLAS and CMS have provided experimental confirmation of this phenomenon [33–35], see Sec. 61.2.5.3. Fully exclusive predictions

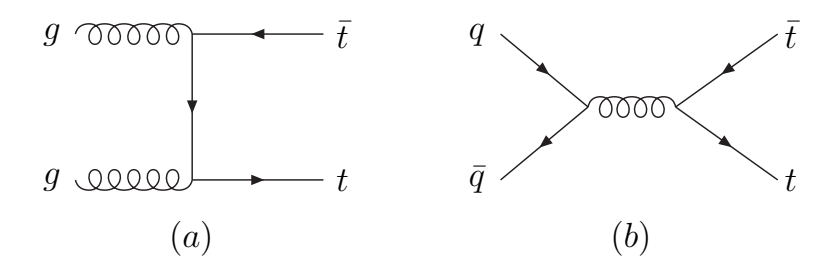


Figure 61.1: Representative Feynman diagrams for $t\bar{t}$ production (a) via gluon-gluon fusion and (b) via quark-antiquark annihilation.

via Monte Carlo generators for the $t\bar{t}$ and single top production processes at NLO accuracy in QCD are available, including top-quark decays and possibly off-shell effects [36–39] through the MC@NLO [40] and POWHEG [41] methods. The first Monte Carlo implementation of the NNLO QCD computation is also available [42, 43].

61.1.4.1 Pair production

The dominant production mode for top quarks in hadron collisions is top-antitop pair production via QCD interactions. Due to its significantly higher event rates compared to other production modes, this process is primarily used to extract top-quark properties. Additionally, it constitutes a significant background for many other collider physics measurements, making its thorough understanding and accurate modeling a key priority.

At leading order in QCD, the two principal partonic subprocesses that contribute to $t\bar{t}$ production are: gluon-gluon fusion $(gg \to t\bar{t})$ and quark-antiquark annihilation $(q\bar{q} \to t\bar{t})$, as shown in Fig. 61.1.

The relative contributions of these subprocesses depend on the collision energy and the PDFs of the incoming hadrons. At the Tevatron, where the initial state is proton-antiproton, and the energy is lower, the production of $t\bar{t}$ is dominated by quark-antiquark annihilation (approximately 85%), with gluon-gluon fusion contributing the remaining 15%. At the LHC, where protons collide at higher energies, the parton composition at low momentum fraction x is dominated by gluons, resulting in gluon-gluon fusion being the dominant production mechanism. At $\sqrt{s} = 13$ TeV, around 90% of $t\bar{t}$ pairs originate from gluon-gluon fusion, decreasing to approximately 80% at $\sqrt{s} = 7$ TeV.

Theoretical predictions for the inclusive $t\bar{t}$ production cross sections are available at NNLO in QCD, supplemented by next-to-next-to-leading logarithmic (NNLL) resummation of soft-gluon emissions [44,45]. A combination of NNLO in QCD and NLO EW corrections is also available [46].

Assuming a top-quark mass of 173.3 GeV, the NNLO+NNLL prediction for the $t\bar{t}$ cross section at the Tevatron at $\sqrt{s} = 1.96$ TeV is:

$$\sigma_{t\bar{t}} = 7.16^{+0.11}_{-0.20} \text{ (scale)}^{+0.17}_{-0.12} \text{ (PDF) pb},$$

where the first uncertainty reflects variations in the renormalization and factorization scales, and the second arises from PDF uncertainties [44].

The $t\bar{t}$ cross sections for pp collisions at various center-of-mass energies for a top quark mass of 172.5 GeV and $\alpha_s = 0.118$ are presented in Tab. 61.2. They are calculated with the ToP++2.0 program to NNLO in perturbative QCD (pQCD), including soft-gluon resummation to NNLL order (see [47] and references therein). The first uncertainty comes from the independent variation of the factorization and renormalization scales. In contrast, the second one is associated with variations

in the PDF and α_s , following the PDF4LHC prescription with the MSTW2008 68% C.L. NNLO, CT10 NNLO and NNPDF2.3 5f FFN PDF sets (see [48] and references therein, and [49–51]).

Table 61.2: Theoretical predictions for top quark pair production at LHC calculated at NNLO+NNLL in QCD. Results collected by the LHCTopWG, see https://twiki.cern.ch/twiki/bin/view/LHCPhysics/TtbarNNLO.

\sqrt{s} (TeV)	$\sigma_{t\bar{t}} \; (\mathrm{pb})$
5.02	$69.5^{+2.0}_{-2.3} (\text{scale})^{+2.9}_{-2.9} (\text{PDF})$
7	$179.6^{+4.8}_{-6.2} (\text{scale})^{+6.1}_{-6.1} (\text{PDF})$
8	$256.0_{-8.9}^{+6.7} (\text{scale})_{-8.0}^{+8.0} (\text{PDF})$
13	$833.9^{+20.5}_{-30.0} (\text{scale})^{+21.0}_{-21.0} (\text{PDF})$
13.6	$923.6^{+22.6}_{-33.4} \text{ (scale)}^{+22.8}_{-22.8} \text{(PDF)}$

The $t\bar{t}$ production is typically accompanied by additional QCD radiation, primarily driven by the initial states. Events with high jet multiplicities offer sensitivity to higher-order QCD radiation and to the accuracy of parton shower modeling. The exclusive $t\bar{t}+n$ —jet cross sections are known at NLO in QCD. Inclusive samples matched with parton shower (PS) can be obtained by merging samples that are accurate at NLO in QCD at fixed jet multiplicities [52,53].

Additional jets may originate from heavy quarks, such as b and c quarks. Predictions for these processes can be obtained in different flavor schemes. For example, in the 4-flavor (3-flavor) scheme, b (c) quarks are treated as massive and not included as initial-state partons [54], while in the 5-flavor (4-flavor) scheme they are treated as massless and included on the same footing as the light quarks [55]. Matching or merging with parton showers can also be applied [39]. Despite these advances, theoretical predictions still carry sizable uncertainties. In particular, measurements of $t\bar{t}$ +heavy-flavor production reveal moderate mismodeling, often requiring data-driven corrections in the background estimation for precise measurements.

61.1.4.2 Pair production in heavy-ion collisions

The top quark constitutes a novel and theoretically precise probe of the nuclear parton distribution functions (nuclear PDFs, or nPDFs), in the poorly explored region where partons have a significant fraction of the nucleon momentum, as well as of the properties of the produced quark-gluon plasma (QGP).

First, precise knowledge of nPDFs is a key prerequisite for extracting detailed information on QGP properties from experimental data. Second, on average, top quarks decay on a timescale similar to the formation of the QGP, offering a unique opportunity to study its time evolution [56].

For lead-lead (PbPb) collisions at center-of-mass energy of 5.02 TeV, the prediction for $t\bar{t}$ cross section is given by

$$\sigma_{\rm theory}^{t\bar{t}} = \sigma_{\rm PbPb \to t\bar{t} + X}^{\rm NNLO+NNLL} = 3.22^{+0.38}_{-0.35} \, (\rm nPDF4 \ PDF) \, ^{+0.09}_{-0.10} \, (\rm scale) \, \mu b,$$

calculated with the ToP++2.0 program at NNLO in QCD, including soft-gluon resummation at NNLL accuracy, with the nuclear EPPS16 and free-nucleon CT14 PDFs [47]. Results with a central value lower than about 7% are obtained from free-nucleon CT14 and NNPDF30 NNLO PDFs (scaled by the square of the number of nucleons in the Pb nucleus, $A^2 = 208^2$). A small difference between the cross sections obtained with nuclear and free-nucleon PDFs arises from the nPDF "antishadowing" effect, which is only mildly dependent on the center of mass energy.

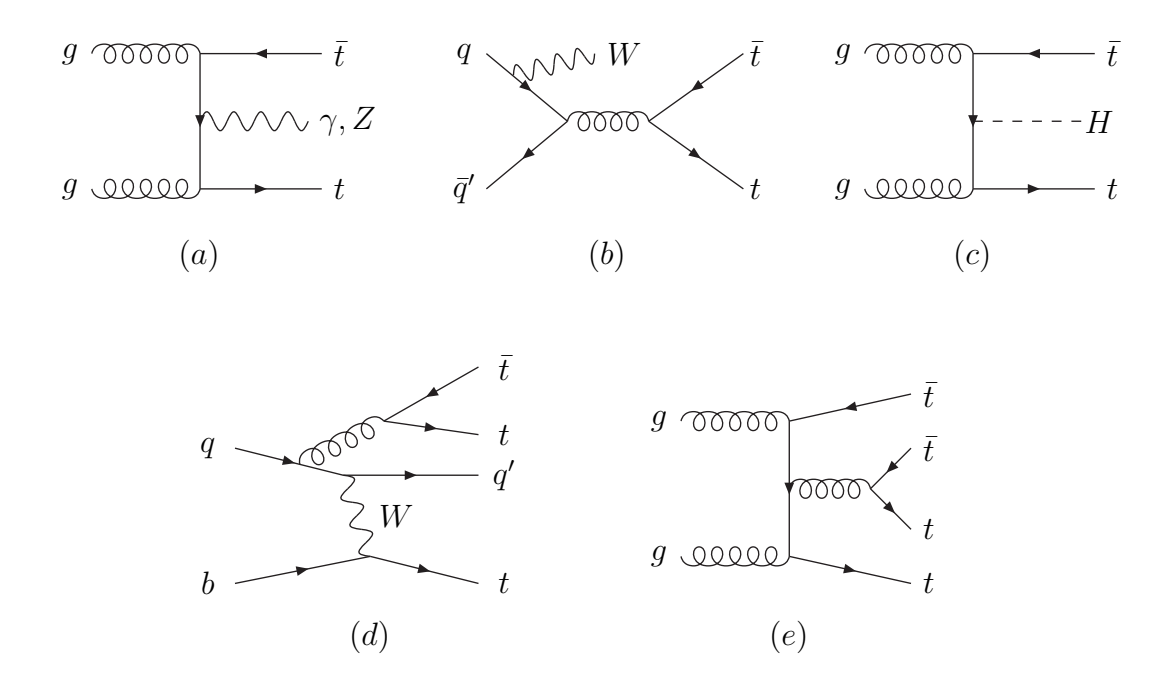


Figure 61.2: Representative Feynman diagrams for $t\bar{t}$ associated production with (a) γ, Z , (b) W, (c) Higgs, (d) a single-top, (e) an extra $t\bar{t}$ pair.

61.1.4.3 Associated pair production

The $t\bar{t}$ production in association with other particles has substantially smaller cross sections compared to standard top-quark production modes. Nevertheless, these associated production processes offer valuable possibilities for precise tests of the SM, specifically enabling detailed studies of the top-quark couplings and EW interactions. Representative diagrams for each production channel are given in Fig. 61.2.

 $t\bar{t}V$ ($V=W,Z,\gamma$): Associated $t\bar{t}$ production with vector bosons. Processes with γ and Z bosons in the final state test the neutral EW couplings of the top quark, see Fig. 61.2 (a). In $t\bar{t}W$, , on the other hand, the W-boson couples to the initial $q\bar{q}'$ state, see Fig. 61.2 (b). Predictions for $t\bar{t}W$ and $t\bar{t}Z$ are computed at complete NLO accuracy, including both QCD and EW effects, with resummation of soft emissions to NNLL accuracy in QCD [57]. Additionally, motivated by the large NLO QCD corrections, approximate NNLO QCD predictions have been obtained for $t\bar{t}W$ [58,59]. Approximate NNLO and N³LO predictions for $t\bar{t}Z$ production include, respectively, second- and third-order soft-gluon corrections added to the exact NLO QCD calculation, together with NLO EW contributions [60]. Predictions for $t\bar{t}\gamma$ are available at NLO in QCD [61].

 $t\bar{t}H$: This process directly explores the top-quark Yukawa coupling. Predictions have been computed similarly to the $t\bar{t}W$ and $t\bar{t}Z$ processes, incorporating NLO corrections with soft-gluon emission resummation [57]. Recently, approximate NNLO QCD predictions have also been derived for $t\bar{t}H$ production [62].

 $tt\bar{t}/\bar{t}t\bar{t}t$: EW production of single t or \bar{t} can be accompanied by the QCD emission of a $t\bar{t}$ pair. This leads to a final state with three top quarks. Depending on the EW single-top-quark production

channel, predictions can be calculated either at LO (for tW) or at NLO (for s- and t-channels) through automated codes. The LO expectation for the cross section at 14 TeV LHC is around 2 fb [63].

 $t\bar{t}t\bar{t}$: The production of four top quarks at hadron colliders probes very high scales and is sensitive to higher-order EW and QCD effects [64]. Predictions have been computed to next-to-leading log-arithmic (NLL') accuracy, matched to full NLO QCD and EW corrections. The NLL' corrections enhance the total production rate by approximately 26%, significantly reducing theoretical uncertainties from scale variations, which are now smaller than current experimental uncertainties [65].

Theoretical predictions for these processes are implemented in Monte Carlo event generators to at least NLO accuracy, and discussed in detail in the corresponding section in this *Review*. Many of these processes have already been observed at the LHC, and their computed cross sections are summarized in Tab. 61.3 at $\sqrt{s} = 13 \text{ TeV}$.

Table 61.3: Predictions for inclusive cross sections at LHC at $\sqrt{s} = 13 \,\text{TeV}$ for $t\bar{t}$ production in association with additional particles. The first uncertainty comes from scale variation, while the second (when present) comes from the PDF. The perturbative order refers to the highest order in QCD and EW available (aNNLO=approximated NNLO).

Process	Cross section [fb]	Perturbative order	Ref.
$t\bar{t}W$	745.3^{+37+14}_{-48-14}	aNNLO QCD +EW NLO	[59]
$t ar{t} Z$	811^{+89+19}_{-78-19}	NLO+NNLL QCD	[57]
$t\bar{t}\gamma$ (w/ cuts)	$1720^{+207+16}_{-208-16}$	NLO QCD + EW NLO	[66]
$t ar{t} H$	529_{-12}^{+8}	aNNLO+NNLL QCD +EW NLO	[67]
$t \overline{t} t \overline{t}$	$14.7_{-2.5}^{+\overline{1.2}}$	NLO+NLL'QCD + EWNLO	[65]

61.1.4.4 Single production

There are three main mechanisms to produce top quarks singly in pp and $p\bar{p}$ collisions, see Fig. 61.3: t-channel $(qb \to q't)$, mediated by a space-like (virtual) W boson [68], s-channel production $(q\bar{q}' \to t\bar{b})$ [69] mediated by a time-like W boson, and tW production $(bg \to tW^-)$ [70], where the W boson is on-shell. These processes have smaller cross sections than QCD-driven $t\bar{t}$ production but offer unique sensitivity to the EW sector and top-quark couplings. Separate measurements of the s- and t-channel processes provide sensitivity to physics beyond the SM [71]. Additionally, the production of single top-quarks associated with a Z or Higgs boson is classified as associated single top-quark production.

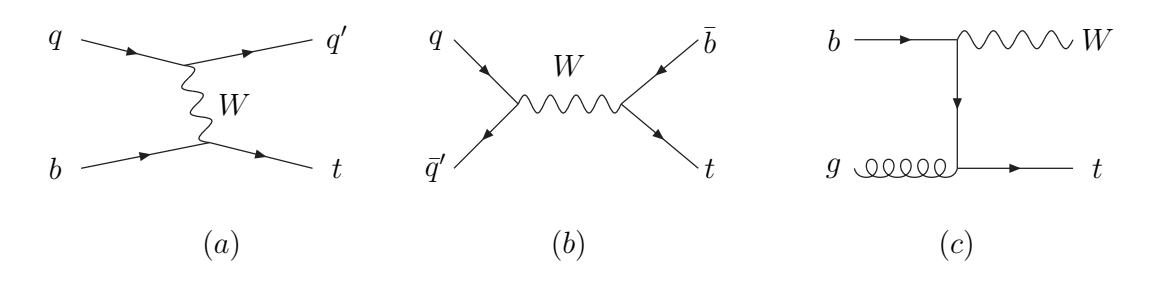


Figure 61.3: Representative Feynman diagrams for single top production (a) via t-channel, (b) via s-channel, and (c) via tW-channel.

Assuming $|V_{tb}| \gg |V_{td}|$, $|V_{ts}|$ (see the Section "The CKM Quark-Mixing Matrix" in this *Review*), the cross sections for single-top-quark production are proportional to $|V_{tb}|^2$. This brings the unique possibility that no additional assumptions about the number of quark families or CKM unitarity are required to extract $|V_{tb}|$.

While suppressed by the weak coupling relative to QCD $t\bar{t}$ production, t-channel single-topquark production is kinematically enhanced, leading to sizeable cross sections at both Tevatron and LHC energies. At the Tevatron, the s-channel production is symmetric, while t-channel exhibits a forward–backward asymmetry; at the LHC, the symmetric pp initial state yields different top and antitop production rates in the t-channel.

For $m_t = 173.2 \,\text{GeV}$, the NNLO prediction for t-channel single top $(t + \bar{t})$ in $p\bar{p}$ collisions at $\sqrt{s} = 1.96 \,\text{TeV}$ is [72]:

$$\sigma_{t\text{-ch}}^{t+\bar{t}} = 2.08^{+0.04}_{-0.03} \, (\text{scale})^{+0.08}_{-0.10} \, (\text{PDF}) \, \text{pb}.$$

Updated NNLO predictions for $m_t = 172.5$ GeV at the LHC are given in Tab. 61.4, where the first uncertainty reflects scale variation and the second PDF and α_s uncertainties [72–74].

Finite-order expansions of resummed cross sections, including soft and collinear gluon corrections, have been computed through NNLO for single-top-quark production in the s-channel. At the Tevatron, the results for single top and antitop quarks are identical. For $\sqrt{s} = 1.96$ TeV and $m_t = 173$ GeV, the NNLO prediction is [75]:

$$\sigma_{s\text{-ch}}^{t+\bar{t}} = 1.05^{+0.001}_{-0.005} \, (\text{scale})^{+0.030}_{-0.028} \, (\text{PDF}) \, \text{pb}.$$

At the LHC, the NNLO cross sections are summarized in Tab. 61.4, with uncertainties quoted from scale variation only.

Although negligible at Tevatron energies, tW production becomes sizeable at the LHC. Accurate predictions for this process are difficult to obtain as, starting at NLO in QCD, it interferes with $t\bar{t}$ production. Several schemes to proper account for this effect have been proposed [76] and implemented in MC generators [37,77]. Approximate NNLO predictions, obtained from NNLL-resummed calculations, are available for the combined $(t+\bar{t})$ production rates, which are expected to be equal for top and antitop quarks. These predictions, summarized in Tab. 61.4, include uncertainties from scale variation and PDFs [70]. The approximate NNLO corrections enhance the cross section by about 8% relative to the NLO result.

Table 61.4: Predictions for inclusive cross sections of single top-quark production at the LHC. The first uncertainty corresponds to renormalization and factorization scale dependence, while the second is due to $PDF+\alpha_s$ variations.

\sqrt{s} (TeV)	$\sigma_{t-ch}^{t+\bar{t}}$ (pb)	$\sigma_{s-ch}^{t+\bar{t}}$ (pb)	$\sigma^{t+\bar{t}}_{Wt-ch} ext{ (pb)}$
pp	(NNLO) [72–74]	(NNLO) [78]	(approx. NNLO) [70]
5.02	$30.3^{+0.4}_{-0.3}{}^{+0.6}_{-0.4}$	NA	$6.54^{+0.16}_{-0.14}{}^{+0.33}_{-0.33}$
7	$63.7^{+0.9}_{-0.5}{}^{+1.1}_{-0.7}$	$3.00^{+0.03}_{-0.03}$	$17.1^{+0.4}_{-0.3}{}^{+0.7}_{-0.7}$
8	$84.3^{+1.1}_{-0.7}^{+1.4}_{-0.9}$	$5.63^{+0.03}_{-0.03}$	$24.4^{+0.6}_{-0.5}^{+0.9}_{-0.9}$
13	$214.2^{+2.4}_{-1.7}^{+3.3}_{-2.0}$	$11.07_{-0.03}^{+0.06}$	$79.3^{+1.9}_{-1.8}{}^{+2.2}_{-2.2}$
13.6	$232.2^{+2.6}_{-1.7}{}^{+3.4}_{-2.2}$	$11.78_{-0.04}^{+0.06}$	$87.9^{+2.0}_{-1.9}{}^{+2.3}_{-2.4}$

61.1.4.5 Associated single production

These rare processes can probe the EW interactions of the top quark and are sensitive to potential contributions from new physics, such as anomalous couplings or effective operators. (Note

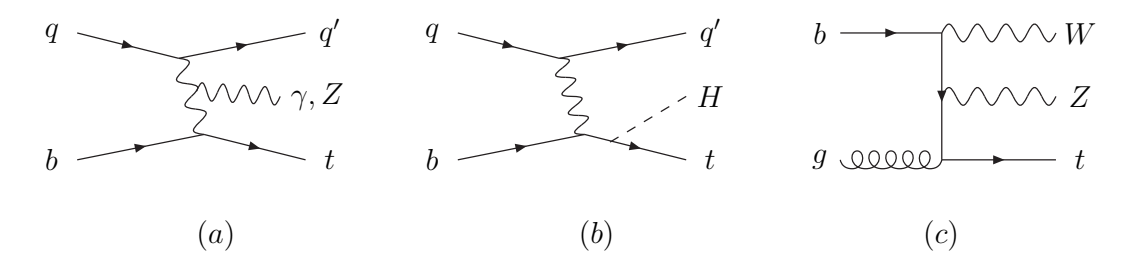


Figure 61.4: Representative Feynman diagrams for single top-quark associated production with (a) γ, Z (b) Higgs, and (c) WZ.

that in this section, with t we mean both top and antitop quarks). Representative diagrams for each production channel are given in Fig. 61.4.

tZ: In this process, a Z boson is radiated from the top quark, the initial-state quark, or an internal W-boson line, and it can occur in all three single-top-quark production channels, with the t-channel contribution dominating. It provides direct sensitivity to anomalous tqZ and FCNC couplings [79]. At the LHC, the cross section for t-channel+Z production at $\sqrt{s} = 13$ TeV has been computed at NLO in QCD and EW [80] and is listed in Tab. 61.5.

 $t\gamma$: Photon emission in association with single-top-quark production or decay gives rise to this process, which probes the electromagnetic structure of the top-quark coupling. It is sensitive to anomalous $tq\gamma$ and dipole interactions. At the LHC, the cross section for t-channel+ γ production at $\sqrt{s}=13$ TeV has been calculated at NLO in QCD and EW [66] (see Tab. 61.5), with predictions depending on photon identification ($p_{\rm T}>25$ GeV, $|\eta|<1.44$) and isolation requirements (see [66] for details).

tH: The associated production of a Higgs boson can occur through radiation from either the top quark or the intermediate W bosons. Non-trivial unitarity cancellations among diagrams make this final state highly sensitive to anomalous interactions [79], thereby playing a crucial role in global fits of top-quark EW couplings. At the LHC, the cross section for t-channel+H production at $\sqrt{s} = 13$ TeV has been calculated at NLO in QCD and EW [80] and is reported in Tab. 61.5.

tWZ: A rare mode, this process produces a single top quark together with a W and a Z boson, radiated from either initial-state quarks or intermediate propagators. The tWZ final state is sensitive to a broad range of anomalous interactions [81] and contributes to global analyses of top-quark EW couplings. At the LHC, the cross section for tWZ production at $\sqrt{s} = 13$ TeV has been computed at NLO in QCD [81] (see Tab. 61.5).

Table 61.5: Cross sections at $\sqrt{s} = 13 \text{ TeV}$ for $t(+\bar{t})$ in association with additional particles.

Process	Cross section [fb]	Perturbative order	Ref.
tZ (t-channel only)	$805^{+45}_{-89} (\text{scale})^{+3}_{-3} (\text{PDF})$	NLO QCD+EW	[80]
$t\gamma$ (t-channel only w/ cuts)	$806^{+57}_{-66} (\text{scale})^{+4}_{-4} (\text{PDF})$	NLO QCD+EW	[66]
tH (t-channel only)	$71.3^{+5.2}_{-7.7} \text{ (scale)} ^{+0.3}_{-0.3} \text{ (PDF)}$	NLO QCD+EW	[80]
tWZ	$106.8_{-6}^{+5.3}$ (scale)	NLO QCD	[81]

61.2 Top-quark and precision SM tests

The first direct observation of the top quark was made in 1995 at the Tevatron in $p\bar{p}$ collisions at $\sqrt{s} = 1.8$ TeV by the CDF and DØ experiments [82,83], followed by more precise measurements at $\sqrt{s} = 1.96$ TeV. Since 2010, the ATLAS and CMS experiments at the LHC have extended top-quark studies to higher energies, performing measurements in pp collisions at $\sqrt{s} = 5.02, 5.36, 7, 8, 13$, and 13.6 TeV. The LHCb experiment has further contributed by observing top-quark production in the forward region [84], a phase-space domain inaccessible to other detectors. Dedicated low-energy runs at $\sqrt{s} = 5.02$ TeV and $\sqrt{s} = 5.36$ TeV in PbPb collisions [85–87] and at $\sqrt{s} = 8.16$ TeV in proton–lead (pPb) collisions [88,89] have provided a novel and theoretically precise probe of nuclear parton distribution functions.

The experiments have collected approximately 10 fb⁻¹ of data at the Tevatron and substantial datasets at the LHC: 255 pb⁻¹ at 5 TeV, nearly 5 fb⁻¹ at 7 TeV, 20 fb⁻¹ at 8 TeV, 139 fb⁻¹ at 13 TeV, and about 250 fb⁻¹ at 13.6 TeV to date. These diverse datasets enable unprecedented precision in a wide range of top-quark measurements, including production mechanisms mediated by EW and QCD interactions, precise determinations of the top-quark mass, detailed studies of production dynamics such as $t\bar{t}$ spin correlations and charge asymmetries, extensive measurements of differential cross sections, investigations of the tWb vertex, and constraints on Wilson coefficients describing physics beyond the SM.

The top-quark mass has now been measured with a precision better than 0.2%, making it the most accurately determined quark mass to date [1]. Combined with precision measurements of the W-boson mass and Higgs-boson properties, these results provide stringent and comprehensive tests of the SM.

Significant progress has also been achieved in associated production processes involving the top quark, such as $t\bar{t}b\bar{b}$, $t\bar{t}t\bar{t}$, $t\bar{t}\gamma$, $t\bar{t}Z$, $t\bar{t}H$, tH, tZq, $t\gamma q$, and tWZ. Most of these processes have now been observed, including the recent observation of tWZ production, while tH associated production remains beyond current experimental reach. These channels probe novel aspects of top-quark physics, including its EW couplings to neutral gauge bosons and possible four-top production mediated by new contact interactions. The measurements of tH and $t\bar{t}H$ production are discussed in the Review "Status of Higgs Boson Physics" in Sec. 11.3.5.

Recent pioneering analyses have begun to explore quantum entanglement phenomena in topquark pair production, and an excess has been reported compatible with a pseudoscalar quasi-bound state [90,91], discussed further in chapters 61.2.5.3 and 61.2.5.5. In parallel, numerous searches for BSM physics exploit the top quark as a sensitive probe, either through its production dynamics or through decays involving hypothetical new particles.

The following sections review the current status of top-quark measurements and discuss their implications for our broader understanding of fundamental particle physics.

61.2.1 Cross-section measurements of pair production

Top quarks decay before they hadronize, and their presence is inferred from detecting their decay products. Each top quark decays almost exclusively to a W boson and a b quark. The $t\bar{t}$ final states are categorized based on the decays of the W bosons:

- All-hadronic (AH) channel (45.7%): $t\bar{t} \to W^+ b \, W^- \bar{b} \to q \bar{q}' b \, q'' \bar{q}''' \bar{b}$
- Lepton+jets (LJ) channel (43.8%): $t\bar{t} \to W^+ b \, W^- \bar{b} \to q \bar{q}' b \, \ell^- \bar{\nu}_\ell \, \bar{b}$ or $\ell^+ \nu_\ell b \, q \bar{q}' \bar{b}$
- Dilepton (DL) channel (10.5%): $t\bar{t} \to W^+ b W^- \bar{b} \to \ell^+ \nu_\ell b \, \ell'^- \bar{\nu}_{\ell'} \bar{b}$

The branching fractions in parentheses are computed assuming lepton universality for the decay of the W-boson. The symbol ℓ refers to any charged lepton $(e, \mu, \text{ or } \tau)$. However, most analyses focus on electrons and muons due to the challenges associated with reconstructing τ leptons. The

symbol q refers to any quark flavor other than a b quark. Final-state quarks hadronize into jets, whose reconstruction depends on the decay kinematics and the analysis algorithm. Neutrinos are not detected directly but are inferred as an imbalance in the event transverse momentum.

In general, the top-quark measurements extracted from $t\bar{t}$ are categorized depending on the number of leptons in the final state as dilepton (DL), lepton+jets (LJ), and all-hadronic (AH) decay channels. The DL channel offers the highest signal purity but is affected by larger statistical uncertainties due to its small branching ratio. The DL($e\mu$) channel specifically refers to events containing one electron and one muon in the final state. In contrast, the LJ channel benefits from a larger branching ratio and better statistical precision, although it is more susceptible to background contamination and larger systematic uncertainties. As data samples increased from the Tevatron to the LHC, the relative precision of these channels improved, with the DL channel often becoming the most precise. Measurements in the AH channel are less common due to the overwhelming QCD multijet background, which is challenging to model and suppress.

In some events, the top quarks are produced with high transverse momentum ($p_{\rm T} > 400-500$ GeV), resulting in a **boosted** topology where the decay products become collimated. In this case, traditional **resolved** analyses, which reconstruct separate jets, may not resolve individual decay products. Instead, jet substructure techniques are employed to identify large-radius jets consistent with hadronic top decays. Consequently, $t\bar{t}$ final states are further classified into resolved and boosted categories depending on the top-quark $p_{\rm T}$.

Experimentally, the measurement of the $t\bar{t}$ production cross section begins with the selection of collision events consistent with the expected $t\bar{t}$ signatures described above. After event selection, background contributions from processes that mimic the signal, such as W/Z+jets, single-top production, QCD multijet and nonprompt-lepton events, and diboson production, are carefully estimated. These estimates are typically obtained using data-driven techniques or Monte Carlo simulations, which are validated against control regions in the data.

To distinguish genuine $t\bar{t}$ events from background processes, analyses employ a variety of discriminating methods, ranging from simple event-counting or kinematic selections to advanced multivariate classifiers such as boosted decision trees, neural networks, or matrix-element techniques. Once suitable discriminants are defined, the signal yield and corresponding cross section are extracted using statistical inference methods, including template fits, profile likelihood fits, or simultaneous maximum-likelihood fits across analysis categories. These inference techniques optimize the use of information in the data and improve the overall precision of the measurement.

Subsequently, detector effects such as trigger efficiency, acceptance, and event-selection efficiency must be corrected to obtain the true $t\bar{t}$ production rate. In simple event-counting analyses, these corrections are typically applied multiplicatively to the observed signal yield, using factors derived from detailed detector simulations calibrated with data. In more sophisticated analyses, such effects are incorporated directly into the signal modeling used for the statistical inference, through templates or parameterized response functions, which allows the fit to constrain the corresponding uncertainties from data and improves the overall measurement precision.

Cross-section measurements rely on a specific Monte Carlo model of $t\bar{t}$ production and decay, which defines the kinematic properties, acceptance, and efficiency of the signal. These simulations assume a value for the top-quark mass, typically 172.5GeV, and a particular modeling of QCD radiation, hadronization, and parton showering. The assumed mass and modeling both affect the acceptance corrections and, in some cases, the shapes of key kinematic and topological distributions used in the analysis. The precision of the measurements, therefore, benefits greatly from Monte Carlo generators that accurately reproduce the observables studied in data.

Comprehensive evaluations of systematic uncertainties, including detector performance and object reconstruction, background and signal modeling uncertainties, and luminosity measurement

accuracy, are integral to ensuring the reliability and robustness of the measurement.

Systematic uncertainties related to object reconstruction include the jet energy scale (JES), b-tagging, and lepton identification. The JES uncertainty accounts for possible mismatches between the true jet energy and its reconstructed value in the detector, affecting all measurements that rely on jet kinematics. The b-tagging systematic reflects differences between data and simulation in the efficiency of correctly identifying b-jets or misidentifying other jet flavors. Since nearly all top-quark measurements rely on b-tagging, this uncertainty appears prominently in most analyses. The lepton identification uncertainty accounts for potential discrepancies between data and simulation in the efficiency of reconstructing and identifying electrons or muons, and tends to dominate in analyses with multiple leptons.

A dominant source of systematic uncertainty in these measurements is the integrated luminosity, which is typically quoted separately from other systematic uncertainties. To mitigate this, some analyses have measured the $t\bar{t}$ production cross section relative to the Z boson production cross section, thus reducing the dependence on the absolute luminosity estimate. This is typically done in the early stages of data-taking, when the luminosity uncertainty is still large.

Finally, the measured $t\bar{t}$ cross section is interpreted by comparing it with theoretical predictions. Agreement or deviation from these predictions provides essential tests of the SM and opens opportunities to explore potential new physics phenomena.

Figure 61.5 summarizes the measured $t\bar{t}$ production cross sections from Tevatron and LHC collisions at various center-of-mass energies, compared to theoretical predictions at NNLO+NNLL accuracy.

Studies of $t\bar{t}$ production in single-, double-, or, more recently, even triple-differential measurements are essential. Such measurements allow increasingly stringent tests of perturbative QCD as a description of the production mechanism and, in combination with other data, facilitate the extraction of PDFs. Measurements of the differential $t\bar{t}$ cross section also allow for the extraction of m_t , α_s , and the top Yukawa coupling to the Higgs boson. Moreover, such measurements enhance sensitivity to possible new physics contributions, particularly now that NNLO predictions for the main differential observables in $t\bar{t}$ production are available [92] and have been independently confirmed [45]. Finally, precise differential results also reduce uncertainties in modeling $t\bar{t}$ production as a background in other SM measurements and in searches for rare processes or physics beyond the SM.

Differential cross sections are typically determined by selecting candidate events, reconstructing their kinematics, and unfolding the measured event to the parton level, binned in kinematic variables to correct for detector resolution, acceptance, and migration effects. While bin-by-bin unfolding is used in some analyses, others apply more sophisticated approaches. The most commonly employed methods include iterative Bayesian unfolding (IBU) [93], often implemented through the RooUnfold package [94], and profile-likelihood unfolding [95,96]. Alternative techniques, such as singular value decomposition [97] and maximum likelihood fits [98], are also utilized. A general observation of $t\bar{t}$ differential measurements is that the measured top-quark $p_{\rm T}$ spectrum tends to be significantly softer than the corresponding NLO+PS theoretical predictions presented in the existing literature, while the agreement improves significantly when compared to NNLO+PS predictions [43].

At the Tevatron, both the CDF and DØ collaborations evolved from an initial search program aimed at discovering the top quark to performing precise measurements of the inclusive $t\bar{t}$ production cross section. Table 61.6 summarizes the earliest $t\bar{t}$ measurements, the most precise individual results, and the final combination.

The latest measurements of the $t\bar{t}$ production cross section from the DØ collaboration [101] and the CDF collaboration [102] assume a top-quark mass of 172.5 GeV, while earlier measurements assumed 175 GeV. Combining these measurements using the Best Linear Unbiased Es-

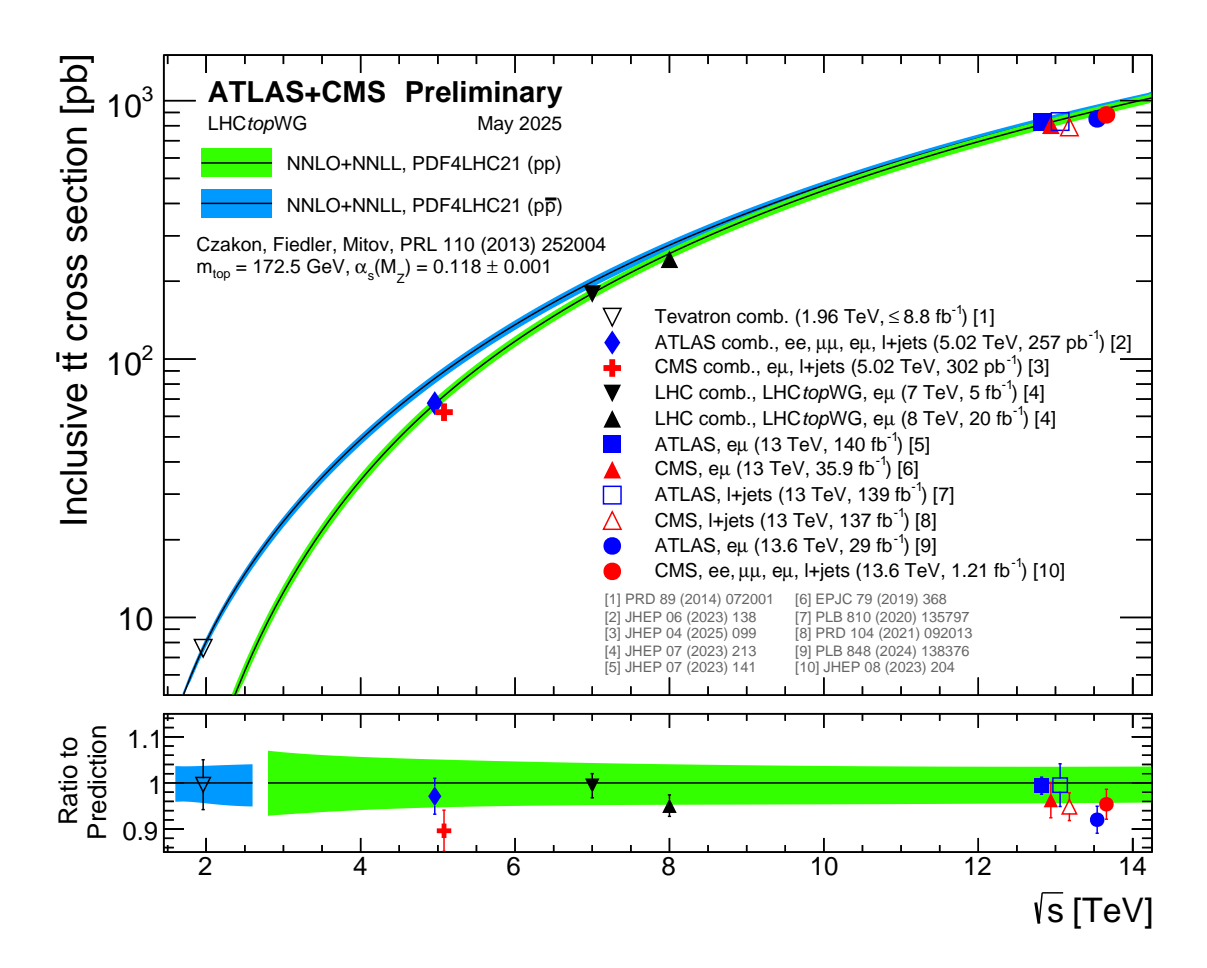


Figure 61.5: Measured and predicted $t\bar{t}$ production cross sections from Tevatron energies in $p\bar{p}$ collisions to LHC energies in pp collisions. The LHCtopWG working group kindly provides the plot, status as of May 2025, see https://twiki.cern.ch/twiki/bin/view/LHCPhysics/LHCTopWGSummaryPlots.

timator (BLUE) method, the Tevatron collaborations report a combined cross section: $\sigma_{t\bar{t}} = 7.60 \pm 0.20 \, (\mathrm{stat.}) \pm 0.29 \, (\mathrm{syst.}) \pm 0.21 \, (\mathrm{lumi.})$ pb, which is in agreement with the SM prediction calculated at the same top-quark mass [44]. The correlation coefficient between the measurements from the two experiments is determined to be 17%.

Additionally, CDF has measured the $t\bar{t}$ production cross section in the DL channel, including one hadronically decaying τ lepton, obtaining $\sigma_{t\bar{t}} = 8.1 \pm 2.1$ pb. By separately identifying the single- τ and di- τ leptons, CDF extracted the branching fraction of the top quark into a τ lepton, τ neutrino, and b-quark as $(9.6 \pm 2.8)\%$ [104]. CDF has also measured the $t\bar{t}$ production cross section normalized to the Z boson production cross section, thus reducing the impact of luminosity uncertainties [105].

The ATLAS and CMS experiments at the LHC employ similar techniques to measure the $t\bar{t}$ production cross section in pp collisions. The most precise determinations are typically obtained in the DL channel, particularly in the $e\mu$ final state, owing to the large statistical yield and high purity of this channel. Numerous measurements have been performed across a wide range of center-of-mass energies, including pPb and PbPb collisions, in different channels, and using a variety of techniques. The uncertainties are divided into statistical, systematic, luminosity, and beam components. In

Experiment [Ref.]	Lumi. (fb $^{-1}$)	\sqrt{s} (TeV)	Topology	Measurement (pb)
CDF (first observation) [82]	0.0067	1.8	LJ	$6.8^{+3.6}_{-2.4}$
DØ (first observation) [83]	0.0050	1.8	LJ	5.9 ± 1.7
CDF [99]	0.00109	1.8	DL+LJ	$6.5^{+1.7}_{-1.4}$
DØ [100]	0.00125	1.8	DL+LJ	5.9 ± 1.4
DØ [101]	9.7	1.96	DL+LJ	$7.26^{+0.58}_{-0.51}$
CDF [102]	8.8	1.96	DL	7.09 ± 0.84
CDF [103]	4.3-8.8	1.96	DL+LJ+AH	7.63 ± 0.50
DØ [103]	5.3-9.7	1.96	DL+LJ+AH	7.56 ± 0.59
Tevatron [103]	4.3-9.7	1.96	DL+LJ+AH	7.60 ± 0.41

Table 61.6: Summary of $t\bar{t}$ cross-section measurements at the Tevatron.

CMS measurements, the uncertainty associated with the beam energy is typically included within the quoted systematic uncertainty. As the beam energy determination improved, this convention was also adopted in later ATLAS measurements. The systematic uncertainties strongly depend on the final state and include experimental contributions, related to the identification of objects and background estimates, as well as theoretical contributions that rely on the modeling assumptions used to extract the measurement.

Most results are summarized in Tab. 61.7 and found to be consistent with theoretical predictions. A description of the measurements at different collision energies follows.

61.2.1.1 Measurements at $\sqrt{s} = 5.02$ TeV

In a dedicated LHC run at this energy, both ATLAS and CMS measured the $t\bar{t}$ production cross section in the DL and LJ channels. Each experiment subsequently combined the results from its individual channels. The ATLAS combination yields $\sigma_{t\bar{t}} = 67.5 \pm 0.9 \text{ (stat.)} \pm 2.3 \text{ (syst.)} \pm 1.1 \text{ (lumi.)} \pm 0.2 \text{ (beam)}$ pb, with the dominant uncertainty arising from background modeling [106]. The corresponding CMS combination gives $\sigma_{t\bar{t}} = 62.3 \pm 1.5 \text{ (stat.)} \pm 2.4 \text{ (syst.)} \pm 1.2 \text{ (lumi.)}$ pb, where the main contributions to the uncertainty come from the integrated luminosity and from the b-tagging scale factors for b-jets [107]. The two measurements are consistent with each other and with the SM prediction within two standard deviations. These measurements provide important constraints on the proton PDFs at large Bjorken-x.

61.2.1.2 Measurements at $\sqrt{s} = 7$ TeV

At this energy, a wide variety of final states and methods were explored. The ATLAS measurement in the $DL(e\mu)$ channel yields $\sigma_{t\bar{t}}=182.9\pm3.1(\mathrm{stat.})\pm4.2(\mathrm{syst.})\pm3.6(\mathrm{lumi.})\pm3.3(\mathrm{beam})$ pb [108], with the dominant uncertainty arising from the modeling of $t\bar{t}$ production, evaluated by comparing different Monte Carlo generators and hadronization models. CMS obtained its most precise measurement also in the $DL(e\mu)$ final state, using a binned likelihood fit to multi-dimensional distributions related to b-quark jets and other jets identified in the event. The measured cross-section is $\sigma_{t\bar{t}}=173.6\pm2.1(\mathrm{stat.})^{+4.5}_{-4.0}(\mathrm{syst.})\pm3.8(\mathrm{lumi.})$ pb [109].

In the LJ channel, ATLAS utilized a three-class, multidimensional event classifier based on

support vector machines to distinguish $t\bar{t}$ from W/Z + bb and other background processes, obtaining $\sigma_{t\bar{t}} = 168.5 \pm 0.7 (\text{stat.})^{+6.2}_{-5.9} (\text{syst.})^{+3.4}_{-3.2} (\text{lumi.})$ pb [110].

Additional measurements using partial datasets by ATLAS and CMS played a crucial role in refining techniques and enhancing data understanding. These studies were carried out in several channels, including e/μ +jets [111], DL [112] [113], AH [114], lepton+ τ [115], hadronic τ +lepton [116], and τ +jets [117] [118]. These results are consistent with theoretical predictions, although they are characterized by larger uncertainties due to limited data statistics and systematic effects.

Furthermore, both collaborations have jointly published a combined "legacy" cross-section measurement at $\sqrt{s} = 7$ TeV, which is also included in Tab. 61.7.

The first observation of $t\bar{t}$ production in the forward region of pp collisions was performed by LHCb using the e+jets and μ +jets channels. The inclusive $t\bar{t}$ production cross section measured in the fiducial region is $\sigma_{t\bar{t}} = 239 \pm 53 ({\rm stat.}) \pm 33 ({\rm syst.}) \pm 24 ({\rm theo.})$ fb [84]. This result is in agreement with the SM predictions of 180^{+51}_{-41} fb at 7 TeV obtained at NLO using MCFM program [119].

ATLAS and CMS measured single-differential $t\bar{t}$ cross sections for the jet multiplicity, the topquark $p_{\rm T}$, and m_t , and the rapidity of the top quark as well as of the $t\bar{t}$ system or kinematic properties of the final-state charged leptons and jets associated with b-quarks. While CMS finds in general good agreement with the pQCD calculations [120–122], ATLAS finds the data to be softer, in particular in the $t\bar{t}$ mass and the top-quark $p_{\rm T}$ than the ALPGEN+HERWIG generator. Also, some disagreement in the rapidity spectrum is observed, indicating a preference for the HERAPDF1.5 PDF set over CT10 [123–125].

61.2.1.3 Measurements at $\sqrt{s} = 8$ TeV

The DIL $(e\mu)$ channel provided the most precise measurements of the $t\bar{t}$ production cross section at this energy, which is included in Tab. 61.7. ATLAS determined $\sigma_{t\bar{t}}=242.9\pm1.7({\rm stat.})\pm5.5({\rm syst.})\pm5.1({\rm lumi.})\pm4.2({\rm beam})$ pb through a simultaneous extraction of the b-tagging efficiency [126]. CMS conducted a measurement by fitting multidimensional final-state distributions involving identified b-quark jets and other jets, obtaining $\sigma_{t\bar{t}}=244.9\pm1.4({\rm stat.})^{+6.3}_{-5.5}({\rm syst.})\pm6.4({\rm lumi.})$ pb [109, 127]. This measurement was also used to determine the $m_t^{\rm pole}$ and set constraints on potential new physics models.

In the LJ channel, ATLAS modeled the W+jets background using Z+jets data and employed neural networks to classify events across three regions defined by jet and b-jet multiplicities. This analysis resulted in $\sigma_{t\bar{t}} = 248.3 \pm 0.7 (\mathrm{stat.}) \pm 13.4 (\mathrm{syst.}) \pm 4.7 (\mathrm{lumi.})$ pb [128]. CMS performed a template fit to the invariant mass distribution M_{lb} , extracting from it $\sigma_{t\bar{t}} = 228.5 \pm 3.8 (\mathrm{stat.}) \pm 13.7 (\mathrm{syst.}) \pm 6.0 (\mathrm{lumi.})$ pb [129].

Additionally, both ATLAS and CMS measured the cross section in the hadronic τ +jets channel, producing consistent but less precise results [130, 131]. CMS also obtained a measurement in the AH final state [132].

ATLAS and CMS combined their $\mathrm{DL}(e\mu)$ channel results [133], performing cross-section ratio studies to verify the internal consistency of the measurements and to reduce sensitivity to specific systematic uncertainties. Ratios of measurements taken at $\sqrt{s}=7$ TeV and 8 TeV provided precise tests of perturbative QCD and constraints on PDFs. Additionally, ratios between $t\bar{t}$ and Z-boson production cross sections were analyzed to minimize luminosity uncertainties while maintaining sensitivity to the gluon-to-quark PDF ratio. These combined analyses also enabled the extraction of m_t^{pole} and the determination of α_s .

LHCb measured $t\bar{t}$ production in the forward region of pp collisions at 8 TeV in the e+jets and $\mu+$ jets channels. The measured cross section is $\sigma_{t\bar{t}}=289\pm43({\rm stat.})\pm40({\rm syst.})\pm29({\rm theo.})$ fb [84], which agrees with the NLO SM prediction of 312^{+83}_{-68} fb calculated using MCFM. Additionally, the measured differential yield distributions and charge asymmetry are consistent with SM predictions.

ATLAS measured single-differential cross sections in the DL and LJ channels, analyzing observables such as m_t , top-quark $p_{\rm T}$., rapidity of the $t\bar{t}$ system, and other event-level kinematic variables [134,135]. These measurements demonstrate good or fair agreement with theoretical predictions across a wide kinematic range, with predictions beyond NLO accuracy notably improving the consistency at high $p_{\rm T}$.

CMS performed extensive measurements of normalized differential cross sections for $t\bar{t}$ production in the LJ channel, examining kinematic variables such as missing transverse energy, scalar sums of jet $p_{\rm T}$, scalar sums of the $p_{\rm T}$ of all event objects, and the $p_{\rm T}$ of the leptonically decaying W bosons originating from top-quark decays [121]. Furthermore, CMS has measured differential cross sections in both the LJ and DL decay channels, focusing on kinematic properties of charged leptons, jets associated with b quarks, top quarks, and the entire $t\bar{t}$ system, comparing the results to predictions at approximate NNLO precision [136]. Notably, in the DL($e\mu$) channel, CMS's normalized double-differential cross-section measurements as a function of paired kinematic observables significantly impacted the determination of gluon distributions in PDF fits [137].

Additionally, ATLAS and CMS carried out targeted differential $t\bar{t}$ measurements in the boosted topology using the LJ channel. In these analyses, the hadronically decaying top quark was reconstructed as a single large-radius jet and identified as a top candidate through jet substructure techniques. ATLAS focused on events with hadronic top quarks of $p_T > 300$ GeV [138], while CMS used a threshold of $p_T > 400$ GeV [139]. Predictions from NLO and LO matrix-element calculations interfaced with parton-shower Monte Carlo generators generally overestimate the measured cross sections. This can be explained by the softer p_T spectra in the data compared to the simulation.

61.2.1.4 Measurements at $\sqrt{s} = 13$ TeV

The most precise measurement of the $t\bar{t}$ cross section is obtained in the DL($e\mu$) final state with b-tagged jets by ATLAS, yielding $\sigma_{t\bar{t}} = 829 \pm 1 ({\rm stat.}) \pm 13 ({\rm syst.}) \pm 8 ({\rm lumi.}) \pm 2 ({\rm beam})$ pb [140]. This analysis includes differential and double-differential measurements of kinematic variables of leptons from top-quark decays, comparing results against predictions from several Monte Carlo generators. Although no single prediction matches all distributions, reweighting the simulated $t\bar{t}$ events to align with the top-quark $p_{\rm T}$ distribution calculated at NNLO significantly improves agreement, especially for lepton $p_{\rm T}$ distributions.

CMS measured the $t\bar{t}$ cross section in the DL channel using a likelihood fit, reporting $\sigma_{t\bar{t}} = 803 \pm 2 ({\rm stat.}) \pm 25 ({\rm syst.}) \pm 20 ({\rm lumi.})$ pb [141]. This result facilitated the extraction of the $m_t^{\rm pole}$ and $\overline{\rm MS}$ schemes at NNLO and allowed the determination of α_s .

In the LJ channel, ATLAS measured the inclusive $t\bar{t}$ cross section using a profile-likelihood fit, obtaining $\sigma_{t\bar{t}} = 830 \pm 0.4 ({\rm stat.}) \pm 36 ({\rm syst.}) \pm 14 ({\rm lumi.})$ pb [142]. CMS measured this channel, dividing events into regions based on top-quark $p_{\rm T}$ and b-tag scores, and employed a combined χ^2 fit with migration matrices, measuring $\sigma_{t\bar{t}} = 791 \pm 1 ({\rm stat.}) \pm 21 ({\rm syst.}) \pm 14 ({\rm lumi.})$ pb, noting generally good agreement with SM predictions except for certain double-differential distributions [143].

ATLAS utilized partial datasets in the DL $e\mu$ channel with one or two b-tags to determine the $m_t^{\rm pole}$, compute ratios and double ratios of $t\bar{t}$ to Z cross sections across different energies, and measure absolute and normalized differential cross sections as functions of LJ and DL kinematic variables [144]. A pioneering measurement of inclusive and normalized differential cross sections in the LJ channel was also conducted by CMS [145]. Other significant results using partial datasets include CMS measurements in the DL channel featuring a hadronically decaying τ [146].

CMS-TOTEM performed the first search for the central exclusive production of $t\bar{t}$ pairs using proton-tagged events with an integrated luminosity of 29.4 fb⁻¹. The top-quark pair decay products were reconstructed by the central CMS detector, while forward protons were measured using the TOTEM precision proton spectrometer. An observed (expected) upper limit on the production

cross section of 0.59 (1.14) pb was established at a 95% C.L. for proton collisions with fractional momentum losses ranging from 2% to 20% [147].

LHCb measured the forward production of $t\bar{t}$ in the μeb final state, consisting of a muon, an electron, and a b-jet. The cross section is measured in a fiducial region defined by both leptons $p_{\rm T}$ and pseudorapidities as well as their angular separation, the b-jet $p_{\rm T}$ and its angular separation from the leptons, yielding $\sigma_{t\bar{t}} = 126 \pm 19 ({\rm stat.}) \pm 16 ({\rm syst.}) \pm 5 ({\rm lumi.})$ fb [148].

Single- and double-differential cross-section measurements for $t\bar{t}$ production have been extensively performed in various channels. Both ATLAS and CMS have performed high-precision measurements of these cross sections in the DL and LJ channels, probing the kinematic properties of leptons, b-quark jets, top quarks, top-quark pairs, and jet multiplicities [149–153]. All results are compared with SM predictions from Monte Carlo simulations with NLO accuracy in QCD at matrix-element level interfaced to parton-shower simulations. While these measurements generally agree well with theoretical predictions, notable discrepancies have been observed in specific DL analyses. CMS has used these results to constrain the top-quark chromomagnetic dipole moment [154] within an EFT framework at NLO QCD, and to extract $t\bar{t}$ and leptonic charge asymmetries [155].

CMS performed the first triple-differential measurement of the $t\bar{t}$ production cross section in the dilepton (DL) channel, as a function of the invariant mass and rapidity of the $t\bar{t}$ system and the multiplicity of additional jets, using a partial Run 2 dataset. From this measurement, α_s , $m_t^{\rm pole}$, and PDFs were extracted [156]. With the full Run 2 dataset, CMS measured differential $t\bar{t}$ and $t\bar{t}$ +jets cross sections as functions of up to three kinematic variables, unfolded to both parton and particle levels. Comparisons with QCD predictions show that theoretical calculations do not consistently reproduce the data, with the most considerable deviations appearing in multi-differential observables. Predictions beyond NLO provide similar or improved agreement for top-quark and $t\bar{t}$ observables, while improvements for lepton and b-jet variables remain limited. The observed dependence on PDF choice indicates that these measurements can provide valuable input to future global PDF fits [157].

ATLAS measured absolute and normalized differential cross sections for the $t\bar{t}$ process in the $e\mu$ DL channel as functions of different observables. Also, it provided complementary measurements of $e\mu b\bar{b}$ production, treating both $t\bar{t}$ and Wt as signal. Comparisons with event generator predictions show that state-of-the-art generators such as Powheg MiNNLO or Powheg bb4l better model the lepton kinematics than the Powheg hvq process traditionally used for LHC physics analyses. These precise measurements provide input that can be used to further refine the modeling of the top quark production at hadron colliders [158].

ATLAS has performed measurements in the AH channel, examining the resolved regime with individually reconstructed jets [159], and measuring differential cross sections as a function of various kinematic properties of the top quarks and the overall $t\bar{t}$ system, both at the stable-particle level within a fiducial phase space and at the parton level in the full phase space.

In boosted topologies, CMS and ATLAS have performed dedicated analyses of $t\bar{t}$ cross sections as a function of top-quark and $t\bar{t}$ system kinematics. CMS measured these cross sections in the AH and LJ channels using large-radius jets with b-tags, finding absolute cross sections notably lower than theoretical predictions [160]. ATLAS carried out similar measurements in these channels, focusing on high- $p_{\rm T}$ hadronic decays, characterizing additional radiation, and setting limits on Wilson coefficients describing potential physics beyond the SM [161]. Mild discrepancies with the data were observed in the modeling of additional radiation. ATLAS has also measured differential $t\bar{t}$ cross sections in AH events in boosted topologies [162]. CMS has further performed single- and double-differential measurements in the LJ channel, categorized by top-quark $p_{\rm T}$, boosted versus resolved topologies, and b-tagging scores, extending momentum measurements well into the TeV range [143].

Several differential $t\bar{t}$ cross-section measurements have been performed to aid in the tuning of Monte Carlo generators. ATLAS measured one- and two-dimensional differential cross sections for eight jet substructure variables, defined using charged jet components and corrected for detector effects [140, 163]. QCD predictions agree well with measured energy-flow variables, whereas discrepancies arise for variables sensitive to the three-body structure of top-quark jets. Additionally, observables sensitive to color reconnection effects in top-quark pair-production events, such as charged-particle multiplicity and scalar sums of charged-particle $p_{\rm T}$, were measured and unfolded to the stable-particle level. These data disfavor certain color reconnection models, informing future Monte Carlo parameter optimizations [164].

Furthermore, ATLAS measured observables related to b-quark fragmentation into b-hadrons. Observables characterizing longitudinal and transverse momentum distributions of b-hadrons within jets were corrected for detector effects. The unfolded results were compared to various Monte Carlo generators, showing varying levels of agreement. These measurements complement similar results from e^+e^- collider experiments, where b-quarks originate from color-singlet Z/γ^* states [165].

61.2.1.5 Measurements at $\sqrt{s} = 13.6$ TeV

The LHC began colliding protons at $\sqrt{s} = 13.6$ TeV in 2022 and is expected to continue until mid-2026. ATLAS and CMS have already performed inclusive $t\bar{t}$ cross-section measurements using partial Run 3 datasets at this energy.

The first result was reported by the CMS collaboration using 1.21 fb⁻¹ of data in events in the LJ channel [166]. Events were categorized according to lepton flavor and multiplicity, the number of jets, and the number of b-tagged jets, and the cross section was extracted from a profile-likelihood fit. CMS measured $\sigma_{t\bar{t}} = 881 \pm 23 \text{ (stat+syst)} \pm 20 \text{ (lumi)} \text{ pb.}$

ATLAS performed a complementary measurement in the DIL($e\mu$) final state with b-tagged jets using 29 fb⁻¹ of data [167]. The result, $\sigma_{t\bar{t}} = 850 \pm 3 \text{ (stat.)} \pm 18 \text{ (syst.)} \pm 20 \text{ (lumi.)}$ pb, corresponds to a relative uncertainty of 3.2%, dominated by the luminosity calibration. To reduce its impact, ATLAS also extracted the ratio of $t\bar{t}$ to Z+jets production, obtaining $R_{t\bar{t}/Z} = 1.145 \pm 0.003 \text{ (stat.)} \pm 0.021 \text{ (syst.)} \pm 0.002 \text{ (lumi.)}$ with a relative uncertainty of 1.9%, benefitting from cancellations of common systematic effects.

Both ATLAS and CMS results are consistent with SM expectations and the NNLO+NNLL prediction, and already achieve percent-level precision despite being based on early Run 3 datasets.

61.2.2 Cross-section measurements of associated pair production

The associated production of a $t\bar{t}$ pair with an additional particle (ttX, with $X = \gamma$, W, Z, H, top quarks or jets) provides direct probes of the top-quark couplings. The $t\bar{t}H$ process offers the most direct access to the top-Higgs Yukawa coupling, while $t\bar{t}Z$ and $t\bar{t}W$ test the EW couplings of the top quark and are sensitive to anomalous interactions in the EFT framework.

Measurements typically require the reconstruction of a $t\bar{t}$ final state in the DL or LJ channels, together with the specific signature of the associated particle (isolated photon, additional leptons, $b\bar{b}$ pair from $H\to b\bar{b}$, or extra jets), and employ multivariate techniques to separate signal from background. CDF reported the first measurement of the associated $t\bar{t}\gamma$ production, while studies of $t\bar{t}W$, $t\bar{t}Z$, $t\bar{t}H$, and $t\bar{t}t\bar{t}$ processes were initiated at the LHC. Evidence and subsequent observations of several of these processes began to emerge during Run 1.

This has become a very active area of research, with many new associated production processes observed in recent years. As larger datasets are collected, these measurements are becoming increasingly precise, and analyses are moving toward differential cross sections, which provide enhanced sensitivity to EFT coefficients.

The next section is organized by associated production processes, beginning with the most common production channel and progressing to increasingly rare ones.

Experiment [Ref.]	Lumi. (fb $^{-1}$)	\sqrt{s} (TeV)	Topology	Measurement (pb)
ATLAS [106]	0.257	5.02	DL+LJ	67.5 ± 2.7
CMS [168], [169]	0.302, 0.0274	5.02	$DL(e\mu)+LJ$	63.0 ± 5.1
ATLAS [108]	4.6	7	$DL(e\mu)$	182.9 ± 7.1
ATLAS [110]	4.6	7	LJ	$168.5^{+7.1}_{-6.7}$
CMS [109]	5	7	$DL(e\mu)$	$173.6^{+6.3}_{-5.9}$
ATLAS+CMS [133]	5	7	DL,LJ	178.5 ± 4.7
LHCb [84]	1	7	LJ (fwd)	0.239 ± 0.067
ATLAS [126]	20.3	8	$DL(e\mu)$	242.9 ± 8.8
ATLAS [128]	20.2	8	LJ	248.3 ± 14.2
CMS [109]	19.7	8	$DL(e\mu)$	$244.9^{+9.1}_{-8.6}$
CMS [129]	19.6	8	LJ	228.5 ± 15.4
ATLAS+CMS [133]	20	8	DL	$243.3^{+6.0}_{-5.9}$
LHCb [84]	2	8	LJ (fwd)	0.289 ± 0.065
ATLAS [126]	140	13	$\mathrm{DL}(e\mu)$	829 ± 15.4
ATLAS [142]	139	13	LJ	830 ± 38.6
CMS [141]	35.9	13	DL	803 ± 32.1
CMS [143]	137	13	LJ	791 ± 25.3
LHCb [148]	1.93	13	$DL(e\mu)$ (fwd)	126 ± 25.3
AFRI A C. [1.67]	20	10.0	DI	

Table 61.7: Summary of $t\bar{t}$ cross-section measurements at LHC.

61.2.2.1 Associated pair production with jets

29

1.21

ATLAS [167]

CMS [166]

The production of $t\bar{t}$ in association with jets, denoted as $t\bar{t}$ +jets, where the additional jets originate from the fragmentation of quarks of any flavor or gluons, offers a valuable probe of QCD radiation in a multi-scale environment. Within this context, the subset of events involving additional b-quarks, $t\bar{t}+b$ -jets, is of particular interest due to the added complexity introduced by heavy-flavor production. Although NLO QCD calculations are available for both $t\bar{t}$ +jets and $t\bar{t}+b\bar{b}$ final states [170], these predictions are subject to sizable theoretical uncertainties. A major source of uncertainty lies in the choice of factorization and renormalization scales, which is complicated by the presence of at least two relevant physical scales: the m_t and the p_T of the additional jets. The measurements of $t\bar{t}$ +jets offer useful constraints for tuning theoretical models of QCD radiation in $t\bar{t}$ events.

13.6

13.6

DL

DL+LJ

 850 ± 27

 881 ± 30

Measurements are usually performed in fiducial regions and unfolded to the particle level to enable direct comparisons with NLO calculations and Monte Carlo simulations.

At $\sqrt{s} = 7$ TeV, ATLAS performed a study of $t\bar{t}$ production with a veto on central jet activity,

measuring the fraction of events that pass the jet veto as a function of the $p_{\rm T}$ threshold across multiple rapidity intervals [171]. Following, ATLAS measured the fiducial $t\bar{t}$ production cross section as a function of jet multiplicity, including up to eight jets, in both the LJ and DL decay channels [172]. The precision of these measurements ranged from approximately 10% to 30%, with the dominant uncertainties arising from background modeling at low jet multiplicities and uncertainties in the jet energy scale at higher multiplicities.

CMS conducted similar measurements of normalized differential $t\bar{t}$ cross sections as a function of jet multiplicity in the LJ and DL channels [122]. In the LJ channel, the cross section was studied as a function of the number of additional jets, while in the DL channel, the fraction of events with no additional jets above a specified threshold was measured. Comparisons with perturbative QCD predictions revealed no significant deviations.

At $\sqrt{s}=8$ TeV, CMS extended these studies with measurements of absolute and normalized differential $t\bar{t}$ +jets cross sections in the DL channel, exploring various jet $p_{\rm T}$ thresholds and the kinematics of the leading additional jets [173]. The fraction of events without additional jets was also determined as a function of the $p_{\rm T}$ of the leading additional jet and the scalar sum of the transverse momenta of all additional jets. These results were compared with predictions from a range of perturbative QCD event generators and NLO calculations, and were found to agree within uncertainties.

ATLAS performed studies in the $DL(e\mu)$ channel with two identified b-jets and measured the multiplicity and kinematic properties of additional jets for several p_T thresholds [174]. Normalized differential cross sections were reported for the five highest- p_T additional jets, as well as gap fraction observables, defined as the fraction of events lacking additional jets in a central rapidity region, as functions of jet p_T thresholds or the scalar p_T sum. These observables were also explored in different regions of the $e\mu b\bar{b}$ system invariant mass. After correcting for detector effects, the results were found to be largely consistent with LO and NLO event generator predictions, provided suitable parameter settings were used.

At $\sqrt{s} = 13$ TeV, both ATLAS and CMS significantly extended the study of $t\bar{t}$ +jets, offering more precise tests of QCD radiation patterns and generator modeling. These analyses focused on inclusive and differential cross sections in both the LJ and DL decay channels, probing jet multiplicities and detailed jet kinematics.

ATLAS measured normalized differential $t\bar{t}$ +jets cross sections in the LJ channel as functions of jet multiplicity and the properties of the leading additional jets [175]. These measurements, unfolded to particle level, were compared to predictions from several Monte Carlo event generators. While the Monte Carlo simulations described the general features of the data, notable discrepancies appeared in high jet multiplicity regions and in specific jet kinematic distributions.

In the DL channel, ATLAS performed a complementary study of $t\bar{t}$ +jets production [176], which included differential measurements of jet multiplicities, transverse momenta, and gap fractions, defined as the fraction of events without additional jet activity above a given threshold. The results provided sensitivity to soft and collinear QCD radiation and were used to test both leading-order and NLO predictions matched to parton showers. Although broad agreement was observed, no single generator configuration consistently described all observables.

CMS measured differential and double-differential $t\bar{t}$ +jets cross sections in the DL channel across a wide range of observables, including additional-jet momenta, angular separations, and global event variables [177]. This extended set of observables provides tighter constraints on parton-shower modeling and on the treatment of initial- and final-state radiation. Normalized $t\bar{t}$ +jets cross sections were also measured as a function of jet multiplicity and the kinematics of additional jets in both the DL and LJ channels [178]. The measurements are performed in a fiducial phase space and extrapolated to the full phase space. The values of $\sigma_{t\bar{t}b\bar{b}}$ are extracted from the product of $\sigma_{t\bar{t}ij}$ and

the measured cross-section ratio. Results unfolded to the particle level are broadly consistent with NLO+PS predictions, although some tension is observed in observables sensitive to hard radiation and color-reconnection effects.

Together, the ATLAS and CMS results at 13 TeV form a comprehensive dataset for validating QCD predictions in top-quark production with jets. They highlight the strengths and limitations of current theoretical tools and serve as benchmarks for improving Monte Carlo simulations used throughout top-quark physics and beyond.

61.2.2.2 Associated pair production with b-jets

The production of $t\bar{t}$ in association with additional b-jets arising from gluon radiation provides a stringent test of perturbative QCD. This process is particularly challenging to predict due to the interplay of multiple mass scales: the large mass of the top quark, the smaller but non-negligible b-quark mass, and the energy scale associated with gluon splitting into $b\bar{b}$ pairs. The hierarchy among these scales introduces significant theoretical uncertainties, especially in modeling the emission of heavy-flavor jets in the presence of top quarks.

Beyond its theoretical significance, $t\bar{t}$ production with additional b-jets is also an important background in several key analyses, such as those targeting $t\bar{t}H$ and $t\bar{t}t\bar{t}$ production, where its modeling uncertainty can significantly impact the overall sensitivity. The most precise theoretical predictions for these final states rely on fixed-order calculations at NLO accuracy in pQCD, typically matched to parton showers. These calculations are still limited by significant uncertainties from missing higher-order corrections, making direct experimental measurements of these processes especially valuable for improving the theoretical modeling.

To reduce the model dependence, experimental measurements are often performed in fiducial phase-space regions that are closely aligned with the detector acceptance. This strategy enables a more robust comparison with theoretical predictions, which are evaluated within the same fiducial region, thereby minimizing extrapolation uncertainties into unmeasured regions.

The first measurements of $t\bar{t}$ production with b-jets were performed by ATLAS at $\sqrt{s}=7$ TeV [179]. Events with at least three b-tagged jets were selected, where two b-jets are attributed to top-quark decays and the third to additional heavy-flavor jets, defined to include both b- and c-jets. The result was expressed as the ratio of events with heavy-flavor jets to the total number of $t\bar{t}$ events with additional jets.

At $\sqrt{s} = 8$ TeV, CMS measured fiducial cross sections in the DL channel, requiring at least four jets, of which two were identified as *b*-jets [180]. ATLAS performed similar measurements in both the LJ and DL channels, targeting $t\bar{t}$ production in association with one or two additional *b*-jets [181].

CMS extended these studies with the first differential measurements of $t\bar{t}$ cross sections as functions of the jet multiplicity, exploring various jet transverse momentum thresholds and the kinematics of the leading additional jets. Furthermore, it provided differential cross-section measurements for $t\bar{t} + b$ and $t\bar{t} + b\bar{b}$ final states as a function of the kinematic properties of the leading additional b-jets [173].

At $\sqrt{s}=13$ TeV, ATLAS measured inclusive and differential cross sections for $t\bar{t}+b\bar{b}$ production in both DL and LJ channels using a partial dataset [182]. The measured inclusive fiducial cross sections were generally found to exceed theoretical predictions from various NLO matrix element generators matched to parton showers.

CMS has performed complementary measurements of $t\bar{t} + b\bar{b}$ production across diverse event topologies: first in the DL channel [183], later in both the DL and LJ channels [184], and in the AH channel [185] using partial datasets. In the AH final state, events with at least eight jets, including at least two b-jets, were analyzed. A combination of multivariate techniques was used

to suppress the substantial multijet background and to discriminate jets from top-quark decays from those originating from additional radiation. A two-dimensional likelihood fit yielded a $\sim 25\%$ precision on the $t\bar{t}+b\bar{b}$ cross section in this channel.

CMS reported comprehensive measurements of inclusive and normalized differential $t\bar{t}+bb$ cross sections using the full dataset in the LJ channel [186], providing results in four distinct fiducial phase-space regions optimized to probe different aspects of the process. Distributions were unfolded to the particle level using maximum likelihood fits, enabling direct comparisons with theoretical predictions from a range of event generators. The measured inclusive cross sections tend to exceed the predictions obtained with the default settings of these generators. At the differential level, the data exhibit varying degrees of agreement, with discrepancies observed particularly in regions sensitive to additional b-jet radiation.

ATLAS performed differential measurements in the DL final state, analyzing events with exactly one electron and one muon and requiring at least three or four identified b-jets [187]. Results were unfolded to the particle level and reported for both inclusive and normalized differential cross sections. The differential measurements encompass global event properties, individual jet kinematics, and observables sensitive to correlations among b-jets, including those stemming from top-quark decays as well as those originating from additional heavy-flavor radiation. After correcting for detector effects, the measured integrated fiducial cross sections are generally consistent with predictions from various NLO matrix-element calculations matched to parton showers, within the quoted theoretical and experimental uncertainties.

In both ATLAS and CMS results, the unfolded differential measurements are compared with state-of-the-art theoretical predictions. While some event generators describe certain kinematic distributions well, none achieves a fully consistent agreement across all observables. The differences among the various theoretical predictions are generally smaller than the experimental uncertainties for most measured quantities, underscoring the need for further theoretical improvements and more precise data to better discriminate between modeling approaches.

61.2.2.3 Associated pair production with c-jets

Predicting and detecting production of $t\bar{t}$ in association with additional c-jets arising from gluon radiation is even more challenging than with additional b-jets. Both ATLAS and CMS have published such measurements using the 13 TeV dataset. The first measurement was performed by the CMS collaboration using a partial 13 TeV dataset [188]. The measurement is based on events with dileptonic $t\bar{t}$ final states and differentiates the three processes $t\bar{t}$ +light, $t\bar{t}+b\bar{b}$ and $t\bar{t}+c\bar{c}$. The events are categorised using a neural-network approach that utilises charm-jet tagging information. The output probabilities of the different classes are then used to construct a two-dimensional discriminator that is used in a binned profile-likelihood fit to extract the cross-sections for the three processes. The measurement is performed in a fiducial and in the inclusive phase space. Also the ratios of cross-sections are extracted, which benefit from the cancellation of several uncertainties. The measured cross-sections agree with the MC generator predictions within the uncertainties. The cross-section of the $t\bar{t}+c\bar{c}$ process has an uncertainty of 18%, which is dominated by statistical uncertainties as well as uncertainties in the c-tagging calibration and the ME-PS matching uncertainties.

The ATLAS measurement based on the full 13 TeV datasets uses top-quark pairs with either one or two charged leptons in the final state [189]. The cross-sections are extracted for two $t\bar{t}$ +charm categories, namely $t\bar{t}+\geq 2c$ and $t\bar{t}+1c$. A new flavour-tagging algorithm is employed that allows to tag b and c jets simultaneously. The discriminating variables in this approach are either the invariant masses of the two closest c-jets or b-jets, or the number of events in the specific region. Seven signal-enriched regions are included in the fit alongside 12 control regions. The cross-sections

of the two signal processes as well as for the $t\bar{t}$ and $t\bar{t}+b$ processes are extracted simultaneously, both for the fiducial and the inclusive cross-sections. Also ratios of cross-sections are measured. The signal cross-sections have uncertainties of 20% and 14% for $\sigma(t\bar{t}+\geq 2c)$ and $\sigma(t\bar{t}+1c)$, respectively. They are consistent with the predictions within the uncertainties, but are all slightly below the predictions. The precision is limited by data statistics as well as the tagger calibration and the modelling of the signal process.

61.2.2.4 Associated pair production with massive vector bosons

The associated production of $t\bar{t}$ with a vector boson V (V=W,Z) is a rare but powerful probe of the SM, accessible only at high energies and luminosities. These heavy final states allow precision studies of EW couplings in the top sector and offer unique sensitivity to new physics. In particular, $t\bar{t}W$ production features complex QCD and EW corrections, charge asymmetry from the initial state, and same-sign dilepton signatures, key ingredients in many beyond-the-SM searches. It also forms a major background in rare processes such as $t\bar{t}H$ and $t\bar{t}t\bar{t}$ production. Meanwhile, $t\bar{t}Z$ production provides the most direct probe of the t-Z coupling. In the SM, the W boson is expected to arise primarily from initial-state radiation. In contrast, the Z boson can also be emitted from a final-state top quark, offering direct sensitivity to the top-quark neutral-current interactions and, in particular, to the third component of its weak isospin, a property not yet directly measured. Together, $t\bar{t}V$ processes are central to both precision tests of the SM and the ongoing search for new phenomena at the LHC.

Experimental measurements of $t\bar{t}Z$ and $t\bar{t}W$ typically rely on leptonic decays of the Z and W bosons to suppress the large backgrounds from $t\bar{t}$ +jets and $t\bar{t}$ +b-jets. The most sensitive channels are final states with three or more charged leptons and events with two same-sign leptons (electrons or muons), which provide substantial background reduction. These analyses require lepton identification with high efficiency and purity to maximize the signal and minimize systematic uncertainties from misidentified leptons.

A summary of the LHC measurements of the inclusive $t\bar{t}V$ cross sections is given in Tab. 61.8. The first measurement of $t\bar{t}V$ in pp collisions was performed by CMS at $\sqrt{s}=7$ TeV using two independent analysis channels: a trilepton analysis targeting $t\bar{t}Z$ events and a same-sign dilepton analysis sensitive to $t\bar{t}V$ production. The trilepton channel enabled a direct measurement of the $t\bar{t}Z$ production rate, observed with a significance of 3.3 standard deviations above the background-only hypothesis. The same-sign dilepton analysis yielded evidence for $t\bar{t}V$ production with a significance of 3.0 standard deviations. In both cases, the measured rates were found to be consistent with NLO SM predictions within uncertainties [190].

At $\sqrt{s}=8$ TeV, both ATLAS and CMS observed the production of $t\bar{t}$ with a W or Z boson. Both collaborations made simultaneous measurements of the $t\bar{t}W$ and $t\bar{t}Z$ cross sections using final states with two same-sign leptons, three leptons, and four leptons. ATLAS obtained significances of 5.0 and 4.2 standard deviations above the background-only hypothesis for $t\bar{t}W$ and $t\bar{t}Z$, respectively [191]. CMS also reported significances of 4.8 standard deviations for $t\bar{t}W$ and 6.4 for $t\bar{t}Z$ [192]. All results were found to be consistent with NLO SM predictions. In addition, the CMS analysis was used to set constraints on five dimension-six operators in the framework of EFT that could modify the $t\bar{t}W$ and $t\bar{t}Z$ production rates.

At $\sqrt{s} = 13$ TeV, the SM cross sections for $t\bar{t}Z$ and $t\bar{t}W$ production increase by factors of approximately 3.5 and 2.4, respectively, compared to 8 TeV. As Tab. 61.3 shows, these cross sections, calculated at different orders in EW and QCD, carry an uncertainty of about 10%, primarily from renormalization and factorization scale variations. At this center-of-mass energy, ATLAS and CMS performed various measurements in final states with two same-sign leptons or three and four leptons. Using partial datasets, ATLAS simultaneously measured the $t\bar{t}Z$ and $t\bar{t}W$ cross sections via a

combined fit across multiple analysis regions [193]. The results are consistent with SM predictions and were used to set constraints on dimension-six SMEFT operators involving the top quark and the Z boson. CMS also reported measurements of the $t\bar{t}V$ cross section using similar final states. For $t\bar{t}W$ production in the same-sign dilepton channel, the observed (expected) significance reached 5.3 (4.5) standard deviations. In the three- and four-lepton channels targeting $t\bar{t}Z$, both observed and expected significances exceeded 5 standard deviations. These results agree with SM predictions and were further used to constrain Wilson coefficients of eight dimension-six EFT operators that would modify $t\bar{t}W$ and $t\bar{t}Z$ production [194].

The first differential $t\bar{t}Z$ measurement by CMS used events with three or four leptons, with the Z boson reconstructed from an oppositely charged lepton pair [195]. Results were presented as functions of the Z $p_{\rm T}$ and the angular distribution of the negatively charged decay lepton, providing a detailed characterization of the process and enabling stringent limits on anomalous tZ couplings.

ATLAS measured inclusive and differential $t\bar{t}Z$ cross sections [196] also using events with three or four isolated leptons. Differential results were unfolded at both the particle and parton levels in specific fiducial regions and are reported as absolute and normalized cross sections. A range of kinematic observables was studied to probe the dynamics of the $t\bar{t}Z$ system. The measurements were compared with predictions from several fixed-order calculations and Monte Carlo generators, showing good overall agreement.

An updated and extended $t\bar{t}Z$ measurement by ATLAS was later performed using the same dataset [197]. This analysis introduced an additional final state targeting the AH decay of the $t\bar{t}$, alongside the multilepton channels. The measurement benefits from improved calibrations, better background modeling, and reduced experimental and theoretical uncertainties. The inclusive and differential cross sections were extracted using a simultaneous profile-likelihood fit across all analysis regions. Unfolding was performed at both particle and parton levels using a consistent fiducial volume, yielding robust and precise results. These measurements were further interpreted in the EFT framework to constrain dimension-six operators relevant to the tZ interaction. Additionally, the spin density matrix coefficients of the $t\bar{t}Z$ system were extracted for the first time, offering a new perspective on the polarization structure of this process.

CMS measured inclusive and differential cross sections of $t\bar{t}Z$ simultaneously with tWZ and tZq in events with three or more leptons. A multiclass deep neural network was employed to separate $t\bar{t}Z+tWZ$, tZq, and background processes. The inclusive cross sections for $70 < m_{\ell\ell} < 110$ GeV are measured to be 1.14 ± 0.07 pb for $t\bar{t}Z+tWZ$ and 0.81 ± 0.10 pb for tZq, both consistent with SM predictions [198].

A pioneering study of $t\bar{t}Z$ and $t\bar{t}H$ production in the LJ final state has been performed by CMS to probe potential effects of BSM in top-quark interactions with the Z and Higgs bosons [199]. The analysis selected events with a single charged lepton, multiple jets, two of which are b-tagged, and an additional large-radius jet with high $p_{\rm T}$, identified as a boosted Z or Higgs boson decaying into a $b\bar{b}$ pair. Signal strengths for boosted $t\bar{t}Z$ and $t\bar{t}H$ production were measured, and upper limits are set on their differential cross sections as functions of the boson $p_{\rm T}$. These results are translated into constraints on eight dimension-six EFT operators. Limits are also placed on eight leading-order EFT parameters that significantly impact boosted $t\bar{t}Z$ and $t\bar{t}H$ production.

Using the full Run 2 datasets, both ATLAS and CMS have measured the $t\bar{t}W$ production cross section. CMS determined the inclusive cross section and the separate contributions from $t\bar{t}W^+$ and $t\bar{t}W^-$ production [200], obtaining values slightly higher than but consistent with SM predictions within two standard deviations. It also measured differential cross sections in final states with two same-sign or three leptons, using multivariate and selection-based methods. The normalized results agree with SM expectations, while the absolute cross sections are somewhat higher, in line with previous measurements [201].

CMS [192]

CMS [192]

ATLAS [193]

ATLAS [193]

ATLAS [196]

ATLAS [197]

CMS [199]

CMS [200]

ATLAS [202]

CMS [195]

8

8

13

13

13

13

13

13

13

13

ATLAS performed both inclusive and differential measurements of $t\bar{t}W$ production [202]. The inclusive result lies slightly above the NNLO QCD prediction. At the same time, the unfolded differential cross sections show good overall agreement with various theoretical models and provide detailed insight into the $t\bar{t}W$ process. In addition, ATLAS reported separate measurements of the $t\bar{t}W^+$ and $t\bar{t}W^-$ cross sections.

Experiment [Ref.]	\sqrt{s} (TeV)	Measurement	Comment
CMS [190]	7	$\sigma_{t\bar{t}Z} = 280^{+152.3}_{-114.0} \text{ fb}$	3.3σ
CMS [190]	7	$\sigma_{t\bar{t}V} = 430^{+192.4}_{-165.5} \text{ fb}$	3.0σ
ATLAS [191]	8	$\sigma_{t\bar{t}W} = 369^{+100}_{-91} \text{ fb}$	$5.0\sigma \ (3.2\sigma \ \text{expected})$
ATLAS [191]	8	$\sigma_{t\bar{t}Z} = 176^{+58}_{52} \text{ fb}$	4.2σ (4.5 σ expected)

 $\sigma_{t\bar{t}W} = 382^{+117}_{-102} \text{ fb}$

 $\sigma_{t\bar{t}Z} = 242^{+65}_{-55} \text{ fb}$

 $\sigma_{t\bar{t}W} = 870 \pm 191 \text{ fb}$

 $\sigma_{t\bar{t}Z} = 950 \pm 128 \text{ fb}$

 $\sigma_{t\bar{t}Z} = 950 \pm 78 \text{ fb}$

 $\sigma_{t\bar{t}Z} = 990 \pm 94 \text{ fb}$

 $\sigma_{t\bar{t}Z} = 860 \pm 57 \text{ fb}$

 $\mu(t\bar{t}Z) = 0.65^{+1.04}_{-0.98}$ $\mu(t\bar{t}H) = 0.27^{+0.86}_{-0.83}$

 $\sigma_{t\bar{t}W} = 868 \pm 65;$

 $R_{t\bar{t}W^+/t\bar{t}W^-} = 1.61^{+0.17}_{-0.16}$

 $R_{t\bar{t}W^+/t\bar{t}W^-} = 1.96 \pm 0.22$

 $\sigma_{t\bar{t}W} = 880 \pm 80 \text{ fb};$

Table 61.8: Summary of $t\bar{t}V$ cross-section measurements from LHC.

 4.8σ (3.5 σ expected)

 6.4σ (5.7 σ expected)

 4.3σ (3.4 σ expected)

first differential, EFT limits

updated result, EFT limits

 $>5\sigma$

EFT limits

first differential

61.2.2.5 Associated pair production with one or two photons

The $t\bar{t}\gamma$ production provides a direct probe of the top-quark EM interactions. In particular, deviations in the p_T spectrum of the photon from the SM prediction could point to new physics through anomalous dipole moments of the top quark or the production of excited top quarks decaying radiatively via $t^* \to t\gamma$ [203–206].

The EM coupling of the top quark can be accessed experimentally by studying final states where a photon is radiated in $t\bar{t}$ events via measurements of the absolute cross sections, cross section ratios (e.g. $\sigma_{t\bar{t}\gamma}/\sigma_{t\bar{t}}$), or through fits within the framework of EFT using differential distributions.

In $t\bar{t}\gamma$ measurements, the cross section must be defined within a well-specified fiducial phase space because the photon can originate from different parts of the event, such as top-quark decay products or initial-state radiation. A clear fiducial selection area is required to unambiguously define which phase-space region and photon kinematics are included in the measurement.

A summary of the Tevatron and LHC measurements of the inclusive $t\bar{t}\gamma$ cross sections is given

in Tab. 61.9.

The first evidence for $t\bar{t}\gamma$ production was reported by the CDF collaboration [207]. The analysis targeted events with a lepton, a photon, significant missing transverse momentum, at least one b-tagged jet, three or more additional jets, and large total transverse energy. The first observation of the $t\bar{t}\gamma$ process was reported by ATLAS in pp collisions at $\sqrt{s}=7$ TeV, using events with an electron or muon and a high- p_T photon, with results consistent with LO theoretical predictions [208]. At $\sqrt{s}=8$ TeV, ATLAS measured the $t\bar{t}\gamma$ cross section for photons with $p_T>15$ GeV and $|\eta|<2.37$, selecting events with an isolated high- p_T lepton, large missing transverse momentum, and at least four jets, including at least one b-tagged jet [209]. The results are in good agreement with the NLO prediction [210]. CMS performed a similar measurement in the LJ channel, requiring photons with $p_T>25$ GeV and $|\eta|<1.44$ [211]. When the measured cross-section is extrapolated to the cross-section times branching fraction by dividing by the kinematic acceptance, it is also consistent with theoretical predictions.

At $\sqrt{s}=13$ TeV, ATLAS measured the fiducial and differential cross sections for $t\bar{t}\gamma$ production in LJ and DL final states containing exactly one isolated photon [212]. Differential cross sections were extracted as functions of the photon $p_{\rm T}$, $|\eta|$, and the angular distance between the photon and the nearest lepton $(\Delta R(\gamma,\ell))$ in both channels. In the DL channel, additional observables include the azimuthal opening angle and the absolute pseudorapidity difference between the two leptons. All results are found to be consistent with theoretical predictions.

ATLAS measured the inclusive and differential cross-sections of combined $t\bar{t}\gamma$ and $tW\gamma$ in $e\mu+\gamma$ events with at least two jets, including at least one b-tagged jet [213]. Differential cross sections were measured as functions of the photon $p_{\rm T}$, $|\eta|$, and angular correlations between the photon and leptons, as well as between the two leptons. The results are in good agreement with NLO predictions and state-of-the-art Monte Carlo simulations.

A subsequent ATLAS analysis measured inclusive and differential $t\bar{t}\gamma$ cross sections in both the LJ and DL channels [214], focusing on events where the photon was radiated in the production stage. The combined measurement achieves a relative uncertainty of 5.2%. Differential distributions were further used to set limits on EFT parameters related to the EW dipole moments of the top quark, with a significant improvement obtained when combining $t\bar{t}\gamma$ and $t\bar{t}Z$ differential measurements in a joint interpretation.

CMS measured $t\bar{t}\gamma$ production in the LJ channel in a fiducial phase space defined at particle level [215], requiring an isolated high- $p_{\rm T}$ lepton, at least three jets (including one or more b-tagged jets), and a single isolated photon. For photons with $p_{\rm T}^{\gamma} > 20$ GeV and $|\eta^{\gamma}| < 1.4442$, the inclusive fiducial cross section agrees with NLO QCD predictions. Differential cross sections were measured as functions of the photon $p_{\rm T}$ and η , and the angular separation between the photon and the lepton, and were interpreted in the EFT framework to constrain the Wilson coefficients c_{tZ} and c_{tZ}^I .

CMS also measured the inclusive $t\bar{t}\gamma$ cross section in the DL channel [216], selecting events with exactly one isolated photon with $p_{\rm T}^{\gamma} > 20$ GeV and at least one b-tagged jet. Differential cross sections were extracted as functions of observables related to the photon, leptons, and jets, and combined with the LJ results in a joint EFT interpretation, further improving the constraints on c_{tZ} and c_{tZ}^{I} . In addition, CMS measured in the DL channel the ratios of the inclusive and differential $t\bar{t}\gamma$ to $t\bar{t}$ cross sections, performed differential studies including the kinematics of the top quarks, and extracted the top-quark charge asymmetry, A_C , in $t\bar{t}\gamma$ events [217].

The production of a $t\bar{t}$ pair in association with two photons has been observed by ATLAS [218]. This process constitutes an important background to $t\bar{t}H(\gamma\gamma)$ and provides sensitivity to the top-quark chromomagnetic and electric dipole moments [154], the latter also probed through the ratio of $t\bar{t}$ events with one or two photons. The measurement includes both the fiducial cross-section and the cross-section ratio, extracted using a boosted decision tree as the final discriminant in a

profile-likelihood fit. In the fiducial phase space at stable-particle level, events with at least one high- $p_{\rm T}$ electron or muon are selected, requiring two photons with $p_{\rm T}^{\gamma} > 20$ GeV. ATLAS measured a fiducial cross section of $\sigma_{t\bar{t}\gamma\gamma} = 2.42^{+0.46}_{-0.38} \, ({\rm stat})^{+0.35}_{-0.38} \, ({\rm syst})$ fb, with an observed significance of $5.2 \, \sigma$.

61.2.2.6 Four top quarks

BSM effects that modify top-quark couplings are particularly relevant in rare processes with small SM cross sections, such as $t\bar{t}t\bar{t}$ production, where they can notably enhance the rate or distort kinematic distributions. Because of its tiny SM cross section, this process is highly sensitive to such effects and is widely used in EFT fits to constrain four-fermion operators, especially the four-top-quark operator. While $t\bar{t}t\bar{t}$ production offers the cleanest and most sensitive probe due to its low SM background, other processes—such as high-energy tails of $t\bar{t}$ production and other rare top-quark final states—also exhibit sensitivity to the same operators. Owing to this, the study of $t\bar{t}t\bar{t}$ production has attracted substantial theoretical and experimental interest in recent years.

Given its heavy final state and extremely low production rate, the first searches for $t\bar{t}t\bar{t}$ production were conducted at a center-of-mass energy of 13 TeV. Similar to $t\bar{t}V$ analyses, these studies target multilepton channels to improve signal purity and rely extensively on multivariate techniques to separate signal from background. The large number of b-jets in the final state makes efficient and well-calibrated b-tagging crucial, together with high reconstruction efficiency and small systematic uncertainties for all final-state objects.

Table 61.10 summarizes recent measurements. Throughout this review, quoted signal significances are taken directly from the corresponding publications; however, it should be noted that these are sometimes evaluated relative to different theoretical hypotheses. While this caveat applies broadly, it is particularly relevant for $t\bar{t}t\bar{t}$ production, where variations in the assumed signal theoretical cross section can lead to notably different significance estimates.

CMS initiated the effort with a search in the one-lepton and two-lepton opposite-sign channels [219]. This was followed by the first measurement using events with two same-sign leptons or at least three leptons, which benefit from relatively low backgrounds but cover only a small fraction of the total branching ratio [220], achieving an observed (expected) significance of 2.6σ (2.7 σ), approaching the threshold for evidence.

ATLAS measured $t\bar{t}t\bar{t}$ production in the same-sign dilepton and trilepton channels [221]. The analysis was extended to include the one-lepton and opposite-sign dilepton channels, which are dominated by $t\bar{t}$ + heavy-flavor backgrounds [222]. The combination of these channels yielded an observed (expected) significance of 4.7 σ (2.6 σ), providing the first evidence for the $t\bar{t}t\bar{t}$ production.

CMS later reported evidence for $t\bar{t}t\bar{t}$ production using a complementary approach targeting the traditional $t\bar{t}$ channels: DL, LJ, and AH final states [223]. Combining this result with the previous multilepton measurements further increased the overall significance to 4.0σ (expected 3.2σ).

The first observations of $t\bar{t}t\bar{t}$ production were made following improvements in object reconstruction and analysis techniques. ATLAS reported the observation in events with two same-sign leptons or at least three leptons [224]. A graph neural network was employed to enhance signal-to-background discrimination, and dedicated control regions were used to constrain dominant backgrounds. The observed (expected) significance reached 6.1σ (4.3 σ). In addition, the measurement was interpreted to constrain the top-Higgs Yukawa coupling and EFT operator coefficients.

CMS reported the observation of the $t\bar{t}t\bar{t}$ production process using events with two same-sign, three, or four charged leptons and multiple jets [225]. The analysis featured improved lepton and b-jet identification, as well as a multivariate classification based on a multi-class boosted decision tree, and achieved an observed (expected) significance of 5.6σ (4.9σ) .

The cross-sections measured by ATLAS and CMS are almost twice the SM prediction and

Table 61.9: Summary of $t\bar{t}\gamma$ cross-section measurements from Tevatron and LHC (see text for photon selection criteria).

Experiment [Ref.]	\sqrt{s} (TeV)	Measurement
CDF [207]	$1.96~(p\bar{p})$	Evidence for $t\bar{t}\gamma$ production
		$\sigma_{t \bar{t} \gamma} = 0.18 \pm 0.08 \text{ pb}$
		$\sigma_{t\bar{t}\gamma}/\sigma_{t\bar{t}}=0.024\pm0.009$
ATLAS [208]	7	Observation of $t\bar{t}\gamma$ production with 5.3 σ significance
		$\sigma^{\rm fid.}(t\bar{t}\gamma)\times BR=63^{+19}_{-15}~{\rm pb}$ per lepton flavor
ATLAS [209]	8	Fiducial cross section: $\sigma_{t\bar{t}\gamma} = 139 \pm 18 \text{ fb}$
CMS [211]	8	Normalized cross sections:
		$\mathcal{R}_{e+\text{jets}} = (5.7 \pm 1.8) \times 10^{-4}$
		$\mathcal{R}_{\mu + \text{jets}} = (4.7 \pm 1.3) \times 10^{-4}$
		Fiducial cross section: $\sigma_{t\bar{t}\gamma} = 244.9^{+9.1}_{-8.6} \text{ pb}$
ATLAS [212]	13	Fiducial cross section:
		$\sigma_{t\bar{t}\gamma} = 521 \pm 42 \text{ fb LJ channel}$
		$\sigma_{t\bar{t}\gamma}=69\pm5~{ m fb}~{ m DL}$ channel
ATLAS [213]	13	Fiducial cross section:
		$\sigma_{t\bar{t}\gamma}=39.6^{+2.7}_{-2.3}~{ m fb}~{ m DL}~e\mu+\gamma~{ m channel}$
ATLAS [214]	13	Fiducial cross section (LJ+DL):
		$\sigma_{t\bar{t}\gamma} = 319^{+16}_{-15} \; \text{fb} - \gamma \; \text{only radiated in production}$
		$\sigma_{t\bar{t}\gamma} = 788^{+38}_{-37} \text{ fb}$
		c_{tZ}, c_{tB} and $c_{t\gamma}$ limits
CMS [215]	13	Fiducial cross section:
		$\sigma_{t\bar{t}\gamma}=798\pm49$ fb LJ channel
		c_{tZ} and c_{tZ}^{I} limits
CMS [216]	13	Fiducial cross section:
		$\sigma_{t\bar{t}\gamma}=174.4\pm6.6~{ m fb}~{ m DL}~{ m channel}$
		c_{tZ} and c_{tZ}^{I} limits
CMS [217]	13	Fiducial cross section:
		$\sigma_{t \bar{t} \gamma} = 54 \pm 5 \text{ fb DL channel}$
		$R(t\bar{t}\gamma/t\bar{t}) = 0.0125 \pm 0.0005$
		$A_C = (-0.012 \pm 0.042)\%$

compatible with it within 2 standard deviations.

Table 61.10: Chronological summary of $t\bar{t}t\bar{t}$ production measurements at LHC at $\sqrt{s} = 13$ TeV.				
Table 01.10. Chronological summary of titt production measurements at Line at $\sqrt{s} = 15$ feV.	Table 61.10: Chronological	I summary of tttt production	measurements at LHC at	$\sqrt{s} = 13 \text{ TeV}.$

Experiment [Ref.]	$\begin{array}{c} \textbf{Lumi.} \\ (\mathbf{fb}^{-1}) \end{array}$	Topology	Measurement (fb)	Significance (obs/exp)
CMS [219]	35.8	LJ, DL	Search only	_
CMS [220]	137	Same-sign DL, ≥ 3 leptons	$\sigma = 12.6^{+5.8}_{-5.2}$	2.6σ / 2.7σ
ATLAS [221]	139	Same-sign DL, ≥ 3 leptons	$\sigma = 24^{+7}_{-6}$	4.3σ / 2.4σ
ATLAS [222]	139	LJ, DL	$\sigma = 26^{+17}_{-15}$	$1.9\sigma / 1.0\sigma$
ATLAS [222]	139	Combined channels	$\sigma = 24^{+7}_{-6}$	4.7σ / 2.6σ
CMS [223]	137	LJ, DL, AH	$\sigma = 36^{+12}_{-11}$	$3.9\sigma / 1.5\sigma$
CMS [223]	137	Combined channels	$\sigma = 17 \pm 5$	$4.0\sigma / 3.2\sigma$
ATLAS [224]	140	Same-sign DL, ≥ 3 leptons	$\sigma = 22.5^{+6.6}_{-5.5}$	$6.1\sigma / 4.3\sigma$
CMS [225]	137	Same-sign DL, 3 and 4 leptons	$\sigma = 17.7^{+4.4}_{-4.0}$	5.6σ / 4.9σ

61.2.3 Cross-section measurements of single production

The traditionally considered mechanisms for single-top-quark production are the t-channel exchange of a virtual W boson $(qb \to q't)$ and the s-channel process $(q\bar{q}' \to t\bar{b})$. Additionally, the associated production with a W boson tW-channel $(b\bar{q} \to tW)$ is also regarded as a main production mode. The primary motivation for precise measurements of single-top production is that they enable a direct determination of the CKM matrix element V_{tb} , without relying on assumptions about the number of quark generations or the unitarity of the CKM matrix.

At the Tevatron, the t-channel dominates, with a cross section approximately twice that of the s-channel. At the LHC, the t-channel is further enhanced by the large gluon and light-quark parton fluxes, while the s-channel rate is more than a factor of three smaller. Associated production of a single top quark with a vector boson (W, Z, γ) is negligible at the Tevatron but becomes non-negligible at the LHC.

In t-channel production, the final state contains a single top quark and a light spectator quark. A characteristic signature is a forward, high- $|\eta|$ spectator jet, typically well separated in rapidity from the b-jet originating from the top-quark decay. Events generally have little additional jet activity, and the absence of a second central b-jet provides further discrimination from $t\bar{t}$ production.

In s-channel production, the final state consists of a single top quark produced together with a second b-quark from the hard interaction. This process is of particular interest because deviations from the SM cross section could signal physics beyond the SM, as predicted in scenarios involving non-SM mediators such as a W' boson or a charged Higgs boson.

In tW channel, the signal is difficult to isolate because of its close resemblance to the $t\bar{t}$ signature. Its definition is also non-trivial, as at NLO a subset of diagrams leads to the same final state as $t\bar{t}$ production, resulting in interference between the two processes [77]. The tW channel is particularly interesting since it probes the Wtb vertex in a kinematic regime different from that of the s- and t-channels, and because of its similarity to the associated production of a charged Higgs boson with a top quark.

The top-quark decays almost exclusively via $t \to Wb$, producing a high- p_T central b-jet accom-

panied by an isolated lepton and missing transverse momentum in leptonic W decays, or by two additional jets in hadronic decays. Because the t-, s-, and tW-channel final states are relatively simple and contain only a few reconstructed objects, they are easily mimicked by background processes. Consequently, measurements of the t- and s-channels primarily use the single-lepton plus jets (LJ) final state, where the lepton is an electron or muon, which provides a favorable signal-to-background ratio. In contrast, the presence of two W bosons in the tW final state makes dileptonic topologies (DL), characterized by two leptons, missing transverse energy, and jets, the most sensitive channel for this mode.

61.2.3.1 Measurements at the Tevatron

The single-top production process was first observed in 2009 by the DØ collaboration [226–228] and by CDF [229–231] at the Tevatron. Although the single-top production cross section at the Tevatron is about half that of $t\bar{t}$ production, its final states are more difficult to isolate due to large backgrounds from W+jets and other processes. Comprehensive reviews of these early measurements and the analysis strategies employed to extract the signal from background-dominated datasets are provided in [232, 233].

At the Tevatron, searches targeted single-top production in both the t-channel and s-channel modes. These processes can in principle be separated kinematically, which is of particular interest since various new-physics scenarios—such as a fourth-generation quark, heavy W'/Z' bosons, flavor-changing neutral currents [71], or a charged Higgs boson—affect the two channels differently. In practice, however, this separation proved challenging, and the initial Tevatron results focused on the combined s and t contributions.

Due to the diverse backgrounds, the experiments developed multiple parallel analyses to optimize signal discrimination, employing advanced multivariate techniques, including likelihood fits, artificial neural networks, matrix-element methods, and BDTs. Each approach provided an independent cross-section measurement and statistical assessment of the excess over background expectations. To maximize sensitivity, the analyses were combined using a higher-level discriminant that took as input the outputs of the individual analysis discriminants for each event [231].

The CDF and DØ collaborations later combined their results, first for the s+t channel using partial datasets [234], and subsequently with the full Run 2 dataset to measure the t-channel cross section [235]. In the latter publication, simultaneous extractions of the s-, t-, and combined s+t cross sections were reported. The measurements were consistent with theoretical predictions at $\sqrt{s} = 1.96$ TeV and $m_t = 172.5$ GeV, yielding for both t and \bar{t} production $\sigma_{s+t} = 2.08 \pm 0.13$ pb [75, 236].

These results were also used to extract the CKM matrix element $|V_{tb}|$, again in agreement with theoretical expectations. It is worth noting that theoretical cross sections are typically quoted separately for top and antitop quarks, whereas the Tevatron results refer to their sum. Since the two contributions are equal in $p\bar{p}$ collisions, the quoted theory predictions include a factor of two.

Finally, CDF and DØ combined their data to achieve the first observation of single-top production in the s-channel, with an observed significance of 6.3 standard deviations [237].

A summary of Tevatron single-top measurements is provided in Tab. 61.11.

61.2.3.2 Measurements at the LHC

At the LHC, single-top-quark production is enhanced by the higher energy and gluon-rich initial state with respect to the Tevatron. The t channel dominates, exceeding the combined rates of the s channel and tW production by a factor of more than three. While the t and tW channels have been observed, the s-channel process still has significance below 4σ .

Figure 61.6 summarizes the measured single-top-quark production cross sections in the t-channel, s-channel, and tW-channel from LHC collisions at various center-of-mass energies, com-

Experiment [Ref.]	Luminosity (fb ⁻¹)	Measurement	Note
DØ [226]	2.3	$\sigma_{s+t} = 3.94 \pm 0.88 \text{ pb}$	Observation single top
CDF [229, 231]	up to 3.2	$\sigma_{s+t} = 2.3^{+0.6}_{-0.5} \text{ pb}$ $\sigma_{s} = 1.8^{+0.7}_{-0.5} \text{ pb}$ $\sigma_{t} = 0.8^{+0.4}_{-0.4} \text{ pb}$	Observation single top
Tevatron [235]	up to 9.7	$\sigma_t = 2.25^{+0.29}_{-0.31} \text{ pb}$ $\sigma_{s+t} = 3.30^{+0.52}_{-0.40} \text{ pb}$ $ V_{tb} = 1.02^{+0.06}_{-0.05}$ $ V_{tb} > 0.92 \text{ at } 95\% \text{ C.L}$	t -channel only without assuming the SM ratio of σ_s/σ_t
Tevatron [237]	up to 9.7	$\sigma_s = 1.29^{+0.26}_{-0.24} \text{ pb}$	Observation s-channel

Table 61.11: Single-top-quark production measurements from the Tevatron at $\sqrt{s} = 1.96$ TeV.

pared to theoretical predictions at NNLO+NNLL accuracy. The following sections provide a detailed description of these measurements.

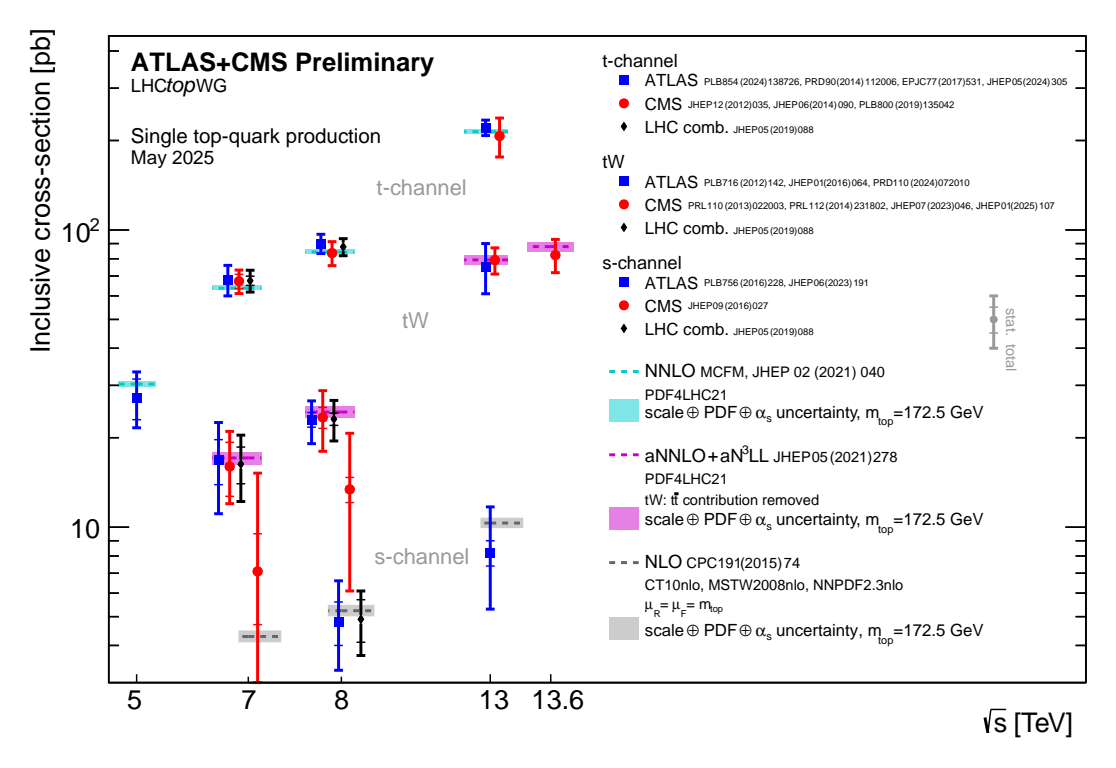


Figure 61.6: The LHC measured and predicted single-top-quark production cross sections as a function of the center-of-mass energy. The measurements are compared to theoretical calculations based on: NLO QCD, aNNLO QCD complemented with aN³LL resummation and NNLO QCD. The LHCtopWG working group kindly provides the plot, status as of May 2025, see https://twiki.cern.ch/twiki/bin/view/LHCPhysics/LHCTopWGSummaryPlots.

t-channel at the LHC

Studies of the t-channel process focus on precise measurements of the single top-quark (σ_t) and top-antiquark $(\sigma_{\bar{t}})$ production cross sections, which differ at the LHC, as well as their ratio (R_t)

and the inclusive cross section $(\sigma_{t+\bar{t}})$. Comparing these measured cross sections with theoretical predictions allows the extraction of $|V_{tb}|^2$. The measurements are performed separately for each production mode and center-of-mass energy.

Measurements of t-channel single-top-quark production have been performed at several LHC energies and are summarized in Tab. 61.12. Figure 61.7 summarizes the ATLAS and CMS measurements of R_t compared to NLO QCD calculations using the PDF4LHC21 and CT18 PDF sets.

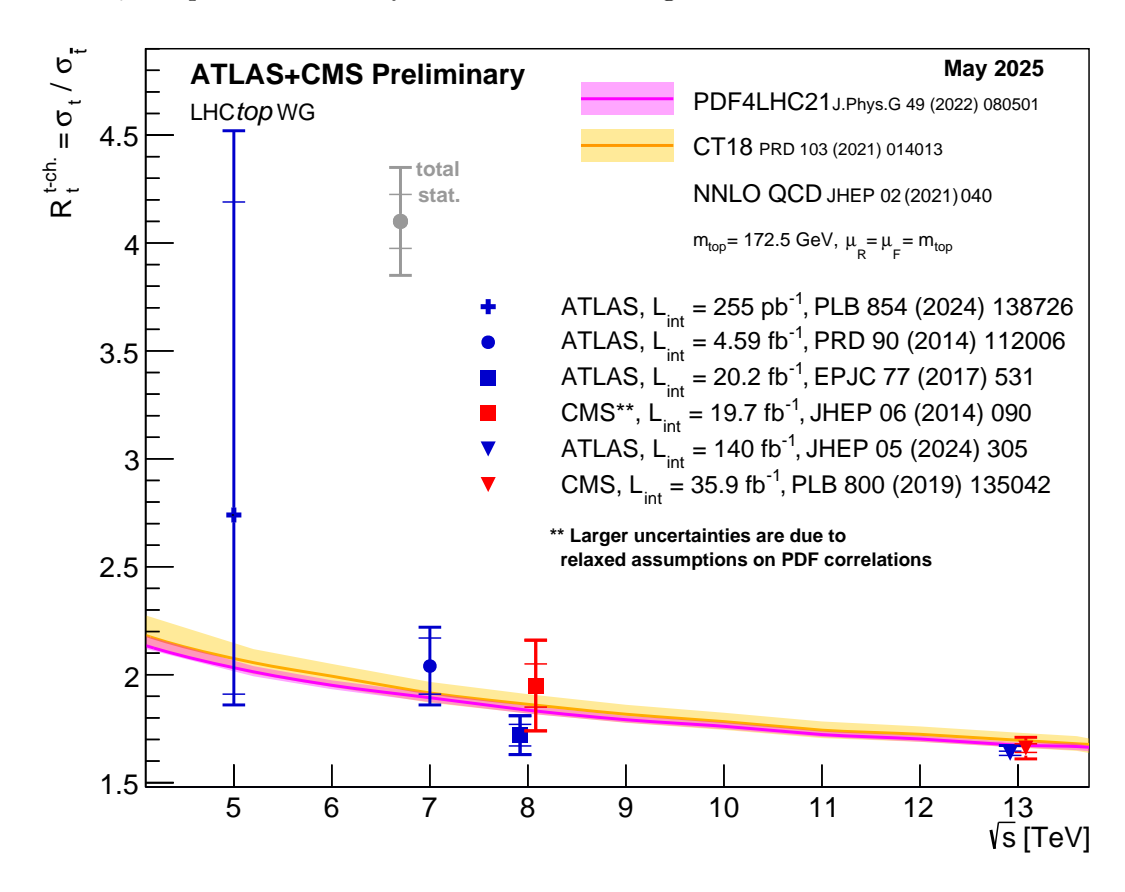


Figure 61.7: Summary of the ATLAS and CMS measurements of R_t , the ratio of the t-channel top-quark production cross section to the t-channel top-antiquark production cross section. The data measurements are compared to NLO QCD calculations using the PDF4LHC21 and CT18 PDF sets. The colored bands represent the uncertainties on the theoretical predictions (scale and PDF uncertainties). The plot is kindly provided by the LHCtopWG working group, status as of May 2025, see https://twiki.cern.ch/twiki/bin/view/LHCPhysics/LHCTopWGSummaryPlots

At $\sqrt{s} = 5.02$ TeV, ATLAS and CMS reported the observation of single-top production in the t-channel [238, 239]. Separate measurements of top and antitop quark production allowed the determination of their production ratio and an extraction of $|V_{tb}|$. This lower-energy result provides an independent test of the SM, with backgrounds and systematic uncertainties distinct from those at higher LHC energies.

At $\sqrt{s}=7$ TeV, ATLAS measured the t-channel cross section in the LJ channel with one b-tagged jet, relying on a neural-network discriminant [240, 241]. Differential cross sections for top-and antitop-quark production were reported as functions of $p_{\rm T}$ and |y|. CMS carried out analogous measurements in the same channel [242]. One approach used the η distribution of the recoil jet

and the reconstructed m_t with background estimates from data control samples, while another employed multivariate techniques. A combined ATLAS+CMS result at this energy shows good agreement with SM predictions [243].

At $\sqrt{s}=8$ TeV, both experiments extended and refined their studies. ATLAS measured total, fiducial, and differential cross sections for top- and antitop-quark production evaluated at both the parton and particle levels, extracting $|V_{tb}|$ [244], and probed the structure of the Wtb vertex using polarization observables, with asymmetries in angular distributions consistent with the SM [245]. CMS performed measurements in the LJ channel, extracting the signal yield through maximum-likelihood fits to the $|\eta_j|$ distribution of the recoil jet [246], and reported separate fits for top and antitop quark cross sections. Combined ATLAS+CMS results again confirmed SM expectations [243]. CMS measured the top-quark spin asymmetry to be $A_{\mu}=0.26\pm0.03$ (stat.) ±0.10 (syst.), derived from the angular distribution of the charged lepton relative to the top-quark spin axis, defined by the spectator quark direction in t-channel production [247]. The measurement assumes the SM spin-analyzing power of 100% for the charged lepton and corresponds to a p-value of 4.6% (a 2.0σ deviation from the SM prediction, corresponding to $A_{\mu}^{\rm TH}=0.44$ with very small uncertainty). The asymmetry probes the correlation between the lepton direction and the top-quark spin, providing sensitivity to the polarization and chiral structure of the top-quark interaction.

At $\sqrt{s} = 13$ TeV, the first analyses were performed with partial datasets. ATLAS extracted cross sections and their ratio using a binned maximum-likelihood fit to the output of a neural-network discriminant [248], while CMS employed simultaneous fits to the transverse W-mass and the output of a neural network to measure the cross section and determine $|V_{th}|$ [249]. CMS later refined the measurement with a larger dataset, categorizing events by jet and b-jet multiplicity and applying multivariate discriminators [250]. From these data, cross sections and their ratio were measured, differential distributions obtained [251], and constraints placed on $|V_{tb}|$ and other CKM elements in a model-independent framework [252]. The spin asymmetry was measured as 0.440 ± 0.070 , consistent with the SM but in tension with the 8 TeV result. Using the full dataset, ATLAS measured top and antitop quark cross sections with precisions of 6% and 8%, respectively [253], in agreement with NNLO QCD predictions. These results are also sensitive to PDFs, interpreted in terms of EFT operators, and used to measure $|V_{tb}|$ and set 95% C.L. limits on $|V_{td}|$ and $|V_{ts}|$. ATLAS further determined the three components of the polarization vectors for top and antitop quarks in t-channel events [254], reporting values consistent with SM expectations, and presented normalized differential cross sections as functions of charged-lepton angles, used to bound the complex Wilson coefficient of the dimension-six O_{tW} operator.

s-channel at the LHC

The growth of the s-channel cross section from $\sqrt{s}=8$ to 13 TeV is slightly larger than that of W-boson production, the second most important background, but smaller than that of $t\bar{t}$ production, which remains dominant. Theory predicts that the ratio of the s-channel single-top cross section to the W-boson cross section is 1.4×10^{-4} (1.7×10^{-4}) at $\sqrt{s}=8$ (13) TeV, and its ratio to the $t\bar{t}$ cross section is 2.1×10^{-2} (1.2×10^{-2}). Consequently, the analysis of this process becomes increasingly challenging as the center-of-mass energy rises.

A summary of results at different center-of-mass energies is given in Tab. 61.13.

At $\sqrt{s} = 7$ TeV, CMS analyzed events in the LJ channel using a maximum-likelihood fit to a BDT discriminant, presenting results that were later combined with those at 8 TeV [255].

At $\sqrt{s}=8$ TeV, ATLAS reported the first evidence for s-channel single-top-quark production at the LHC [256], employing a discriminant based on the Matrix Element Method optimized against the dominant $t\bar{t}$ and W+jets backgrounds. CMS measured the s-channel cross section using a maximum-likelihood fit to a BDT discriminant [255] and combined the result with the 7 TeV measurement, obtaining a best-fit value of 2.0 ± 0.9 for the ratio of the measured to the expected

Table 61.12: Single top-quark t-channel production measurements from the LHC.

Experiment [Ref.]	\sqrt{s} (TeV)	Measurement
ATLAS [238]	5.02	$\sigma_{t+\bar{t}} = 27.1^{+6.2}_{-5.5} \text{pb}$ $R_t = 2.73^{+1.75}_{-0.87}$ $f_{LV} \cdot V_{tb} = 0.94^{+0.11}_{-0.10}$
CMS [239]	5.02	$\sigma_{t+\bar{t}} = 30.2^{+5.8}_{-5.6} \text{pb}$ $R_t = 2.6^{+1.3}_{-0.7}$
ATLAS [240]	7	$\sigma_t = 46 \pm 6 \text{pb}; \ \sigma_{\bar{t}} = 23 \pm 4 \text{pb}$ $R_t = 2.04 \pm 0.18$ $\sigma_{t+\bar{t}} = 68 \pm 8 \text{pb}$
CMS [242]	7	$\sigma_{t+\bar{t}} = 67.2 \pm 6.1 \text{pb}$ $ V_{tb} = 1.020 \pm 0.049$
LHC [243]	7	$\sigma_{t+\bar{t}} = 67.5 \pm 5.7 \mathrm{pb}$
ATLAS [244]	8	$\sigma_t = 56.7^{+4.3}_{-3.8} \text{pb}; \ \sigma_{\bar{t}} = 32.9^{+3.0}_{-2.7} \text{pb}$ $R_t = 1.72 \pm 0.09$ $f_{LV} \cdot V_{tb} = 1.029 \pm 0.048$ $ V_{tb} > 0.92 \text{ at } 95\% \text{ C.L.}$
CMS [246]	8	$\sigma_t = 53.8 \pm 4.6 \text{pb}; \ \sigma_{\bar{t}} = 27.6 \pm 3.9 \text{pb}$ $R_t = 1.95 \pm 0.21$ $\sigma_{t+\bar{t}} = 83.6 \pm 7.7 \text{pb}$ $ V_{tb} = 0.998 \pm 0.041$
LHC [243]	8	$\sigma_{t+\bar{t}} = 87.7 \pm 5.8 \mathrm{pb}$
CMS [250] [252]	13	$\sigma_t = 130 \pm 19 \text{ pb}; \ \sigma_{\bar{t}} = 77 \pm 12 \text{ pb}$ $R_t = 1.68 \pm 0.054$ $ V_{tb} > 0.970$ $ V_{tb} = 0.988 \pm 0.024$ $ V_{td} ^2 + V_{ts} ^2 = 0.06 \pm 0.06$
ATLAS [253]	13	$\sigma_{t} = 137^{+8}_{-8} \text{pb}; \ \sigma \bar{t} = 84^{+6}_{-5} \text{pb}$ $R_{t} = 1.636^{+0.036}_{-0.034}$ $\sigma_{t+\bar{t}} = 221 \pm 13 \text{pb}$ $f_{LV} \cdot V_{tb} = 1.015 \pm 0.031$ $f_{LV} \cdot V_{td} < 0.13$ $f_{LV} \cdot V_{ts} < 0.31$ EFT coefficients constraints

cross section. A joint ATLAS+CMS combination confirmed consistency with the SM [243], but did not allow for observing the process.

At $\sqrt{s}=13$ TeV, ATLAS studied the s-channel cross section using the full Run 2 dataset in events with an electron or muon, missing transverse momentum, and exactly two b-tagged jets. A discriminant based on Matrix-Element Method calculations was used to separate the s-channel signal from $t\bar{t}$ and W+jets backgrounds. The result was found to be consistent with the SM

prediction [257], but the significance of the result is still below 4σ .

Table 61.13: Single top-quark s-channel production measurements from the LHC.

Experiment [Ref.]	\sqrt{s} (TeV)	Measurement
ATLAS [258]	7	$\sigma_s < 26.5 \; (20.5) \; \mathrm{pb}$
CMS [255]	7	$\sigma_s = 7.1 \pm 8.1 \text{ pb}$
ATLAS [256]	8	$\sigma_s = 4.8^{+1.8}_{-1.5} \text{ pb}$ 3.2 σ obs. (3.9 σ exp.)
CMS [255]	8	$\sigma_s = 13.4 \pm 7.3 \text{ pb}$ $R_s = 2.0 \pm 0.9 \text{ combining 7 and 8 TeV}$ $2.5\sigma \text{ obs. } (1.1\sigma \text{ exp.})$
LHC [243]	8	$\sigma_s = 4.9 \pm 1.4 \text{ pb}$
ATLAS [257]	13	$\sigma_s = 8.2^{+3.5}_{-2.9} \text{ pb}$ 3.3 σ obs. (3.9 σ exp.)

61.2.3.3 tW-channel at LHC

The tW signal is difficult to isolate because of its similarity to the $t\bar{t}$ final state. Its definition is further complicated at NLO, where part of the contributing diagrams lead to identical final states as $t\bar{t}$ production, giving rise to interference between the two processes [77]. The standard approach is to define the signal using the diagram-removal technique [76], in which the interfering diagrams are removed at the amplitude level. An alternative method, diagram subtraction, removes these contributions at the cross-section level, leading to similar results [76]. Both techniques are valid provided that the event selection cuts are chosen to keep interference effects small, which is typically the case.

Experimentally, the presence of two W bosons in the final state makes dileptonic topologies the most sensitive, requiring two leptons, missing transverse energy, and jets. A summary of results is given in Tab. 61.14.

At $\sqrt{s} = 7$ TeV, both ATLAS and CMS reported evidence for this process [259,260]. ATLAS employed template fits to BDT classifiers, while CMS used a multivariate analysis. Both of them used events in the DL channel with exactly one *b*-tagged jet. The combination of ATLAS and CMS results is consistent with SM predictions [243].

At $\sqrt{s}=8$ TeV, the two experiments strengthened their measurements. ATLAS observed tW production with a significance of 7.7 σ using a BDT discriminant and extracted the cross section with a profile-likelihood fit; a fiducial cross section was also reported [261]. In a separate analysis, ATLAS studied the LJ channel with at least three jets, training a neural network to discriminate signal from $t\bar{t}$ and extracting the cross section with a two-dimensional fit involving the neural network output and the invariant mass of the hadronic W boson [262]. CMS analyzed the DL channel with a b-tagged jet, employing a multivariate discriminant to suppress the $t\bar{t}$ background and observing the signal with a significance of 6.1σ [263]. ATLAS and CMS combined their results to determine σ_{tW} and extract $|V_{tb}|f_{LV}$, where f_{LV} is a real form factor parameterizing potential anomalous left-handed vector couplings. The extraction is based on the ratio of the measured to the predicted cross section, under the assumption that $|V_{td}|, |V_{ts}| \ll |V_{tb}|$. The combined result shows good agreement with the NLO+NNLL SM prediction [243].

At $\sqrt{s}=13$ TeV, analyses progressed with increasingly larger datasets. ATLAS first studied the DL channel, defining signal and control regions by jet and b-tag multiplicities and employing BDTs to separate the tW signal from backgrounds, measuring a cross section consistent with the SM [264]. Differential cross sections were also obtained as functions of the b-jet energy, the energy of the $\ell\ell b$ system, and various invariant and transverse masses involving the leptons, b-jet, and neutrinos [265].

A subsequent ATLAS analysis using the full Run 2 dataset improved precision by employing a BDT discriminant in three jet and b-tag-defined signal regions, with the cross section extracted from a profile-likelihood fit [266]. The measurement is dominated by systematic uncertainties, and a value of V_{tb} was also extracted.

CMS performed measurements in the DL channel with a partial dataset, selecting events with one tight and one loose lepton and at least one b-tagged jet. A BDT was used to separate signal from background, and the cross section was extracted with a likelihood fit [267]. The same dataset enabled a preliminary differential measurement in a fiducial region requiring exactly one b-tagged jet [268]. CMS also analyzed the LJ channel, where a BDT was employed to discriminate tW from $t\bar{t}$, with other backgrounds constrained using data-driven methods. This led to the first observation of tW production in the LJ final state, with a significance exceeding 5σ [269].

Finally, using the full Run 2 dataset, CMS measured inclusive and normalized differential cross sections in $e\mu$ events [270]. A multivariate discriminant was used to isolate the signal for the inclusive measurement, yielding a cross section consistent with the SM. The differential distributions were unfolded to the particle level in a fiducial region requiring exactly one b jet and were found to agree with NLO QCD predictions.

At $\sqrt{s} = 13.6$ TeV, CMS measured tW production using a partial dataset of 34.7 fb⁻¹ [271]. The analysis includes both inclusive and differential cross sections in the DL($e\mu$) channel. For the differential measurements at the stable-particle level in a fiducial phase space, good agreement was observed with the predictions. The inclusive cross section is consistent with the NNLO QCD prediction, with the overall precision limited by systematic uncertainties.

61.2.4 Cross-section measurements of associated single production

Beyond the primary single-top-quark production channels, rarer processes occur in association with EW bosons, such as tZ, $t\gamma$, tH, and tWZ. Although their cross sections are much smaller, these modes provide unique sensitivity to the couplings of the top quark to the Z boson, photon, and Higgs boson. They thus serve as precision tests of the SM and impose powerful constraints on anomalous couplings and possible effects of new physics [272, 273]. The Tevatron lacked the sensitivity to observe these processes, and only with the increased energy and luminosity of the 13 TeV LHC dataset has evidence for them been obtained. The following sections summarize these measurements in order of decreasing production rate, and Fig. 61.8 presents an overview of the ATLAS and CMS results for associated single-top-quark production at 13 TeV.

61.2.4.1 Associated single production with a photon

As in the case of $t\bar{t} + \gamma$, the measurement of single-top+ γ production requires a well-defined fiducial phase-space definition that specifies the photon kinematic and isolation criteria, as well as its separation from other objects, to ensure that the measured cross section corresponds to a clearly defined and reproducible region of phase space.

The first evidence for the associated production of a single top quark with a photon was reported by CMS at $\sqrt{s} = 13$ TeV using a partial dataset [274]. A multivariate discriminant was applied to events containing a muon, a photon, and jets. For isolated photons with $p_T > 25$ GeV in the central detector region ($|\eta_{\gamma}| < 1.44$), the measured cross section times branching fraction was found to be consistent with the SM expectation. At the same center-of-mass energy, ATLAS achieved the first

Table 61.14: Single top-quark tW-channel measurements from the LHC. Unless indicated, measurements are extracted in the DL channel.

Experiment [Ref.]	\sqrt{s} (TeV)	Measurement
ATLAS [259]	7	$\sigma_{tW} = 16.8 \pm 5.7 \text{ pb}$ $ V_{tb} = 1.03^{+0.16}_{-0.19}$ $3.3\sigma \text{ obs. } (3.4\sigma \text{ exp.})$
CMS [260]	7	$\sigma_{tW} = 16^{+5}_{-4} \text{ pb}$ $4.0\sigma \text{ obs. } (3.6\sigma \text{ exp.})$
LHC [243]	7	$\sigma_{tW} = 16.3 \pm 4.1 \text{ pb}$
ATLAS [261]	8	$\sigma_{tW} = 23.0^{+3.6}_{-3.9} \text{ pb}$ $ V_{tb} = 1.01 \pm 0.10 \text{ at } 95\% \text{ C.L.}$
ATLAS [262]	8	$\sigma_{tW} = 26 \pm 7 \text{ pb (LJ channel)}$
CMS [263]	8	$\sigma_{tW} = 23.4 \pm 5.4 \text{ pb}$ $ V_{tb} = 1.03 \pm 0.13$
LHC [243]	8	$\sigma_{tW} = 23.1 \pm 3.6 \text{ pb}$ $ V_{tb} = 1.02 \pm 0.045 > 0.79$, with 7 and 8 TeV
ATLAS [264]	13	$\sigma_{tW} = 94^{+30}_{-24} \text{ pb}$
ATLAS [266]	13	$\sigma_{tW} = 75^{+15}_{-14} \text{ pb}$ $ V_{tb} = 0.97 \pm 0.10$
CMS [267]	13	$\sigma_{tW} = 63.1 \pm 7.0 \text{ pb}$
CMS [269]	13	$\sigma_{tW} = 89 \pm 13 \text{ pb (LJ channel)}$
CMS [270]	13	$\sigma_{tW} = 79.2^{+7.8}_{-8.1} \text{ pb}$
CMS [271]	13.6	$\sigma_{tW} = 82.3^{+10.6}_{-10.5} \text{ pb}$

observation of this process [275], exploiting the presence of a forward jet and using neural networks for signal discrimination. Requiring a photon with $p_{\rm T}>20$ GeV within the detector acceptance ($|\eta_{\gamma}|<2.37$), ATLAS measured a fiducial cross section consistent with the NLO QCD prediction of 515^{+36}_{-42} fb, with $t\bar{t}\gamma$ modeling among the leading sources of uncertainty. The results are summarized in Table 61.15.

Table 61.15: Associated single top-quark production with a photon measurements from the LHC.

Experiment [Ref.]	\sqrt{s} (TeV)	Measurement
CMS [274]	13	$\sigma_{t\gamma} = 115 \pm 34 \text{fb } (p_{\text{T}}^{\gamma} > 25 \text{ GeV}; \eta_{\gamma} < 1.44)$ 4.4 σ obs. (3.0 σ exp.)
ATLAS [275]	13	$\sigma_{t\gamma} = 688^{+78}_{-75} \text{fb } (p_{\mathrm{T}}^{\gamma} > 20 \text{ GeV}; \eta_{\gamma} < 2.37)$ 9.3 σ obs. (6.8 σ exp.)

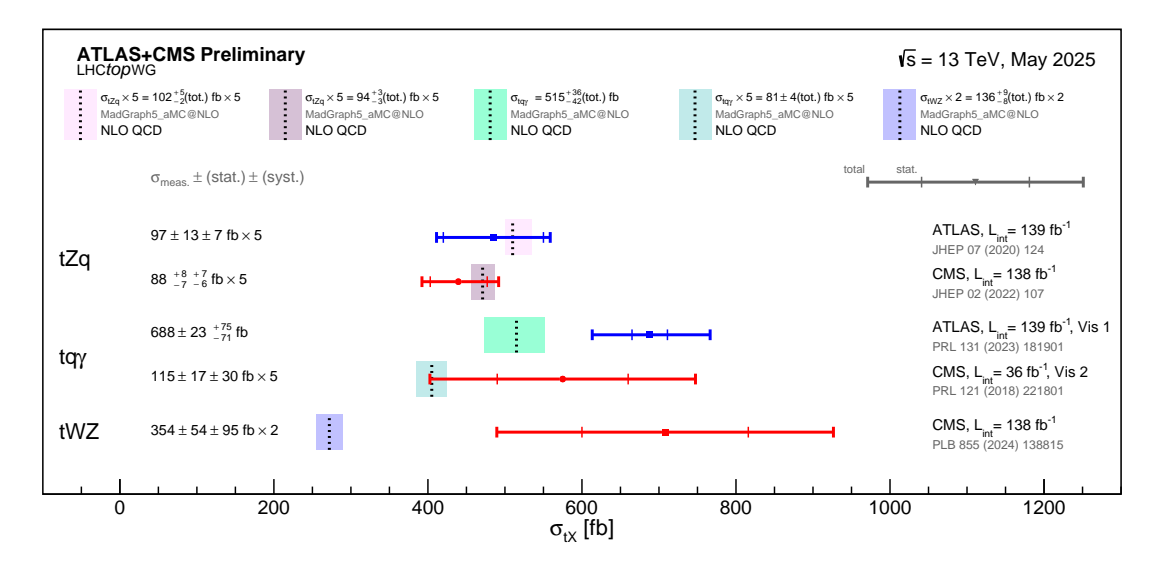


Figure 61.8: Summary of ATLAS and CMS measurements of t+WZ, t+Z and $t+\gamma$ cross sections at 13 TeV. The cross-section measurements are compared to the NLO QCD theoretical calculation. "Vis 1" and "Vis 2" highlight that the relevant phase space used for the ATLAS and CMS $t\gamma$ measurements is different. The theory prediction and experimental results of tZ, and those of the CMS $t\gamma$ measurement, are multiplied by a factor of 5 to allow for easy visualization on the same scale; those of the CMS tWZ measurement are multiplied by a factor of 2. The theory bands represent uncertainties due to renormalization and factorization scales and parton density functions. The LHCtopWG working group kindly provides the plot, status as of May 2025, see https://twiki.cern.ch/twiki/bin/view/LHCPhysics/LHCTopWGSummaryPlots.

61.2.4.2 Associated single production with a Z boson

The tZq process probes both the WWZ coupling, when the Z boson is emitted from the t-channel W in single-top production, and the tZ coupling, when the Z is radiated from the top quark.

At $\sqrt{s} = 8$ TeV, CMS searched for tZq production in trilepton events and reported a hint of signal with a significance of 2.4σ relative to the background-only hypothesis [276].

At $\sqrt{s} = 13$ TeV, both CMS and ATLAS measured tZq production in events with three leptons from $Z \to \ell^+\ell^-$ and top quark decay. CMS reported evidence using a partial dataset [274], followed by an observation with the full dataset [277], and later a comprehensive analysis of inclusive and differential cross sections [278]. The latter included the ratio of cross sections for top-and antitop-associated production, as well as the first differential measurements at both parton and particle levels. The spin asymmetry, sensitive to top-quark polarization, was also determined from the parton-level distribution of the polarization angle. All results were consistent with NLO SM predictions. ATLAS employed a simultaneous binned maximum-likelihood fit with neural-network discriminants to improve background rejection, extracting a signal also consistent with the SM expectation [279].

These results are summarized in Tab. 61.16.

61.2.4.3 Associated single production with a W and Z boson

At $\sqrt{s} = 13$ TeV, CMS reported the first evidence for single-top-quark production in association with a W and a Z boson in multilepton final states [280], with the Z reconstructed from e^+e^- or $\mu^+\mu^-$ pairs. The analysis made extensive use of multivariate techniques applied across multiple

Experiment [Ref.]	\sqrt{s} (TeV)	Measurement
CMS [278]	13	$\sigma_{tZq} = 87.9^{+10.5}_{-9.5}$ fb for $m(\ell\ell) > 30$ GeV $R_t = 2.37^{+0.62}_{-0.44}$ $A_l = 0.58^{+0.16}_{-0.17}$
ATLAS [279]	13	$\sigma_{tZq} = 97 \pm 15 \text{ fb for } m(\ell\ell) > 30 \text{ GeV}$

Table 61.16: Associated single top-quark production with a Z boson measurements from the LHC.

regions and event categories to suppress backgrounds and extract the signal. A key challenge was separating the tWZ signal from the dominant $t\bar{t}Z$ background, which was addressed using improved tWZ modeling.

This result was recently updated using both 13 and 13.6 TeV datasets, corresponding to an integrated luminosity of about 200 fb⁻¹ [281]. Events with three or four leptons were divided into distinct signal regions based on the output of a machine-learning classifier with multiple output nodes, and the distributions in these categories were used in a profile-likelihood fit. For the 13 TeV dataset alone, the expected significance increased from 1.4σ in the first analysis to approximately 3σ . Combining the 13 and 13.6 TeV results, summarized in Tab. 61.17, led to the first observation of the tWZ process.

Table 61.17: Associated single top-quark production with a W and Z bosons measurements from the LHC.

Experiment [Ref.]	\sqrt{s} (TeV)	Measurement
CMS [280]	13	$\sigma_{tWZ} = 354 \pm 109 \text{ fb}$ 3.5 σ obs. (1.4 σ exp.)
CMS [281]	13 13.6	$\sigma_{tWZ} = 248 \pm 52 \text{ fb}$ $\sigma_{tWZ} = 244 \pm 74 \text{ fb}$
		5.8σ obs. $(3.5\sigma$ exp.) in combination

61.2.5 Properties

The following sections provide an overview of experimental results on **top-quark properties**, that is, the intrinsic or fundamental characteristics of the particle itself, rather than how it is produced or which process it participates in. In this context, "top-quark properties" serves as an umbrella term for all observables that characterize the nature of the top quark itself, independent of the particular process used to measure them. Measurements of these properties provide stringent tests of the SM and sensitivity to new physics.

Intrinsic properties are quantities that define the top quark as a fundamental particle in the SM, including its mass (m_t) , electric charge (+2/3 e), spin (1/2), and lifetime or decay width (Γ_t) . Interaction properties describe how the top quark couples to other SM particles, its couplings to the W, Z, and Higgs bosons, as well as to gluons and photons. These reflect the particle's gauge and Yukawa interactions, which are part of its defining characteristics within the SM. Derived properties, such as polarization, spin correlations, and charge asymmetries, characterize the behavior of the top quark in production and decay and reveal how its intrinsic features manifest dynamically.

This section begins with measurements of m_t and Γ_t , followed by studies of its decay and spin structure, including polarization, spin correlations in $t\bar{t}$ pairs, and the observation of quantum entanglement in $t\bar{t}$ events. In this context, results on the production of a pseudo-bound state at the $t\bar{t}$ threshold are also reviewed. The V-A structure of the Wtb vertex is examined through measurements in both single-top-quark and $t\bar{t}$ events. Finally, results on asymmetries in $t\bar{t}$ and $t\bar{t}+X$ production are summarized and compared with theoretical expectations.

Most results are obtained from $t\bar{t}$ events, with analyses categorized according to the final state: lepton+jets (LJ), dilepton (DL), and all-hadronic (AH), as described in Sect. 61.2.1.

61.2.5.1 Mass

In the early 1990s, indirect constraints from precision measurements at CERN's LEP collider suggested that m_t lay between about 150 and 200 GeV, based on radiative corrections to EW observables involving the Z boson. In 1995, the top quark was directly discovered by the CDF and D0 collaborations at the Tevatron $p\bar{p}$ collider at Fermilab, with an initial mass estimate in the range of 151–197 GeV. Subsequent measurements at the Tevatron rapidly improved the precision, establishing the top-quark mass near 175 GeV. With the start of the LHC program, measurements by ATLAS and CMS further reduced the uncertainty to below 1 GeV, making m_t one of the most precisely determined parameters of the SM.

Final state topologies The top-quark mass has been determined in both top-quark pair and single-top-quark production, exploiting a variety of decay channels, each with distinct sensitivities to systematic uncertainties. This diversity enables internal consistency checks and improved precision when results are combined. The "standard" analyses use inclusive $t\bar{t}$ final states, classified into the DL, LJ, and AH channels, and further distinguished as **resolved**, when all decay products can be individually reconstructed, or **boosted**, when the large $p_{\rm T}$ of the top quarks causes two or more decay products to merge into a single reconstructed object in the detector, as described in Sec. 61.2.1. Since final states with many jets lead to larger overall systematic uncertainties, alternative channels have also been explored for measuring the m_t . Examples include events in which the b hadron decays semileptonically and produces a low- $p_{\rm T}$ ("soft") lepton, which can be combined with other objects to form an observable sensitive to m_t , or decays containing a J/ψ meson. These approaches benefit from a reduced impact of jet-related uncertainties but suffer from the low branching ratios of the relevant b-hadron decays, resulting in larger statistical uncertainties.

Reconstruction of observables

The first step in a top-quark mass measurement is to identify an observable sensitive to m_t and reconstruct it from the event. The calculation of such observables requires assigning the parton-level objects to the reconstructed objects in the detector. An assignment is considered correct ("matched") if ΔR (parton, detector object) < 0.3 or 0.4. Three categories are defined: correctly matched events, incorrectly matched events, and unmatched events, the latter occurring when at least one parton cannot be matched to a reconstructed object, for example, because it fails the selection criteria or lies outside the detector acceptance. While leptons are matched with very high efficiency, the matching efficiency for jets is significantly lower.

Several methods exist for jet-parton assignment. Kinematic fits are widely used, as they both improve the resolution of reconstructed observables and provide a goodness-of-fit estimator, which helps identify correctly matched events [282]. Matching can be further enhanced using machine-learning techniques, such as deep neural networks trained with correct assignments as signal and incorrect assignments as background. Since combinatorial mismatches worsen mass resolution and increase overall uncertainty, removing unmatched or incorrectly matched events is crucial. One

common strategy is to reject events in the tails of reconstructed mass distributions, which are rarely populated by correctly matched events. The goodness-of-fit from kinematic fits also enables event selection with high probability of correct assignment [283–286]. In another approach, a BDT was trained to distinguish correctly from incorrectly or unmatched events, and events were selected by applying a cut on the classifier output [282].

In the LJ and AH final states, the invariant mass of the objects assigned to their parton-level particles, $m_t^{\rm reco}$, is often used for the measurement. In the DL channel, a full reconstruction of the events is more challenging due to the presence of two neutrinos in the final state. To address this, several methods have been developed, such as full kinematic reconstruction [287,288]. At the Tevatron, the neutrino-weighting and matrix-element-weighting techniques were introduced [289–291].

In the neutrino-weighting method, for each assumed value of m_t , energy and momentum conservation is applied to the decay, yielding up to four possible solutions for the neutrino and antineutrino momenta. The missing transverse energy calculated from these solutions is then compared with the observed missing E_T to assign a weight. In the matrix-element weighting method, the neutrino momenta are likewise solved up to a fourfold ambiguity, but each solution is assigned a weight proportional to the likelihood of the kinematics arising from $t\bar{t}$ production and decay at that mass hypothesis. By scanning over m_t values (typically in the range 80–280 GeV), one obtains a weight distribution that reflects the production kinematics, decay distributions, and available phase space, which is then used to extract m_t .

Alternatively, without requiring full event reconstruction, several observables directly sensitive to the top-quark mass can be used, albeit with larger systematic uncertainties. One example is the invariant mass of the b-jet-lepton pair, $m_{\ell b}^{\rm reco}$ [292], or event variables such as the scalar sum of jet transverse energies and the missing transverse energy [293], both of which reduce the dependence on jet-related uncertainties. In final states with additional leptons from b-hadron decays, the invariant mass of all leptons can be used [294–296]. Another approach exploits the invariant mass of a charged lepton from the W decay and the tracks forming a secondary vertex from the b hadron [297].

In addition to observables directly sensitive to the top-quark mass, auxiliary observables are often employed to reduce specific groups of uncertainties. The invariant mass of the hadronically decaying W boson, $m_W^{\rm reco}$, is widely used to constrain the jet-energy scale (JES). This can be achieved either by extracting a dedicated jet-energy scale factor (JSF) simultaneously with m_t [298, 299], or by using the ratio of the jet energies assigned to the top quark and to the W boson [300,301].

When the uncertainty in the b-JES is also relevant, an additional observable can be introduced to determine the b-to-light jet scale factor (bJSF) [282]. To ensure sensitivity primarily to the bJSF rather than the overall JSF, the ratio of jet momenta assigned to the W boson and to the b jets is used, denoted $R_{bg}^{\rm reco}$ in the following.

$Measurement\ techniques$

A wide range of techniques has been developed to extract m_t , many of which have subsequently found applications in other areas of particle physics. The most precise determinations proceed by reconstructing an observable in data and comparing it to the same observable obtained from Monte Carlo simulations generated with different input values of m_t . This so-called template method has been the most widely used approach, see for example Refs. [283, 284, 302, 303]. The template method has been used to extract m_t since the first direct measurement at the Tevatron. It remains in use today, now often fitting multiple observables simultaneously to constrain the main systematic uncertainties.

Owing to its good signal-to-background ratio and the ability to use the hadronic W decay to constrain the dominant JES uncertainty, the LJ channel is considered the golden channel for

top-quark mass measurements.

At the Tevatron, considerable effort was devoted to improving the statistical precision of m_t measurements, leading to the development of new techniques. In the DL channel, methods were introduced that fit the dynamics of the decay products and evaluate per-event weights (matrix-element weighting) as mentioned above. In the LJ channel, the so-called matrix-element method was pioneered [304]. In this approach, a probability density is calculated for each event as a function of m_t , using a leading-order matrix element for $t\bar{t}$ production and decay. The probability densities are calculated using the four-momenta of the reconstructed objects, taking into account all possible jet-parton assignments. An in situ calibration of dijet pairs to the $W \to jj$ hypothesis is simultaneously performed to constrain the JES uncertainty [299]. The top-quark mass is then extracted from a likelihood fit to the ensemble of events, with each event contributing its own likelihood distribution, in contrast to the template method, where each event contributes a single number.

In the template method, templates are constructed from simulated samples generated with different input values of m_t for the observables used in the measurement. Typically, only one jet–parton permutation is considered per event. The top-quark mass is then extracted from a binned or unbinned maximum-likelihood fit. In the LJ channel, simultaneous fits of m_t together with the JSF and bJSF parameters have also been performed [282, 298].

The *ideogram* m_t method [305] is an unbinned likelihood fit that incorporates up to four jet–parton permutations, weighted to reduce the impact of incorrect assignments. The weights are derived from the goodness-of-fit probabilities obtained from the kinematic reconstruction. CMS employed this method to measure m_t simultaneously with an overall JSF, where the JSF was constrained by a Gaussian prior whose width was set to the total uncertainty of the JES corrections [306].

As the available statistics increased, methods aimed at reducing systematic uncertainties became more widely developed. In recent years, the use of profile-likelihood fits has grown. These are maximum-likelihood fits in which systematic uncertainties are incorporated as nuisance parameters. The nuisance parameters can be constrained in the fit, resulting in a reduction in overall uncertainty compared to traditional methods. However, greater care is required for uncertainties derived from comparisons of different Monte Carlo setups, which combine the effects of multiple variations. A notable example is the modeling uncertainty associated with hadronization, which is often evaluated by comparing simulations based on string and cluster models.

Results from the Tevatron

Both the DØ and CDF experiments performed numerous top-quark mass measurements, exploring various strategies to reduce the overall uncertainty in different final states. These included the use of matrix-element and template techniques, as well as alternative approaches such as exploiting soft-muon decays [294], the transverse momentum of the lepton [307], and global event variables like the scalar sum of jet transverse energies and the missing transverse energy [293].

The most precise results from both experiments are summarized in Tab. 61.18, which also shows their combination. This average incorporates published Run 1 (1992–1996) results together with the most precise published and preliminary Run 2 (2001–2011) measurements, based on up to 9.7 fb⁻¹ of Tevatron data. Accounting for correlations among uncertainties, and combining statistical and systematic contributions in quadrature, the Tevatron average yields $m_t = 174.30 \pm 0.65$ GeV, corresponding to a relative precision of 0.37% [308].

Results from the LHC

In the following, the precision of top-quark mass measurements at the LHC is examined across

Experiment [Ref.]	Lumi. (fb $^{-1}$)	Topology	m_t (GeV)
CDF (Run 1) [283]	0.1	LJ	$176.1 \pm 5.1 \text{ (stat)} \pm 5.3 \text{ (syst)}$
CDF (Run 1) [291]	0.1	DL	$167.4 \pm 10.3 \text{ (stat)} \pm 4.9 \text{ (syst)}$
CDF (Run 1) [309]	0.1	AH	$186.0 \pm 10.0 \text{ (stat)} \pm 5.7 \text{ (syst)}$
DØ(Run 1) [304]	0.1	LJ	$180.1 \pm 3.6 \text{ (stat)} \pm 3.9 \text{ (syst)}$
DØ(Run 1) [290]	0.1	DL	$168.4 \pm 12.3 \text{ (stat)} \pm 3.9 \text{ (syst)}$
CDF (Run 2) [310]	8.7	LJ	$172.9 \pm 0.5 \text{ (stat)} \pm 1.0 \text{ (syst)}$
CDF (Run 2) [311]	1.9	L_{XY}	$166.9 \pm 9.0 \text{ (stat)} \pm 2.8 \text{ (syst)}$
CDF (Run 2) [312]	8.7	E_T	$173.9 \pm 1.3 \text{ (stat)} \pm 1.4 \text{ (syst)}$
CDF (Run 2) [313]	9.1	DL	$171.5 \pm 1.3 \text{ (stat)} \pm 2.5 \text{ (syst)}$
CDF (Run 2) [314]	9.3	AH	$175.1 \pm 1.2 \text{ (stat)} \pm 1.6 \text{ (syst)}$
DØ(Run 2) [315]	9.7	LJ	$175.0 \pm 0.4 \text{ (stat)} \pm 0.6 \text{ (syst)}$
DØ(Run 2) [316]	9.7	DL	$173.5 \pm 1.3 \text{ (stat)} \pm 0.8 \text{ (syst)}$
CDF+DØ [308]	0.1-9.7	all	$174.30 \pm 0.35 \text{ (stat)} \pm 0.54 \text{ (syst)}$

Table 61.18: Summary of Tevatron top-quark mass measurements.

different decay topologies and analysis methods. Due to the large number of measurements that were carried out at the LHC, the focus will be on the most precise ones. Further measurements and more detailed discussions can be found in the reviews of the ATLAS and CMS experiments, published in Refs. [288, 317].

For the direct measurements, the most precise individual result is presented in Tab. 61.19 for each topology. Except for the measurement using J/ψ mesons in b-hadron decays, performed with the 8 TeV dataset, all results are based on 13 TeV data. Owing to the very large $t\bar{t}$ dataset available at the LHC (the 13 TeV sample alone contains more than 115 million events per experiment), statistical uncertainties are negligible for most analyses and become relevant only in rare topologies that exploit additional leptons from b-hadron decays.

The use of auxiliary observables in combination with profile-likelihood fits has substantially reduced the overall uncertainty in the LJ channel. In the resolved analysis [286], several auxiliary variables are included, such as $m_W^{\rm reco}$ and $R_{bq}^{\rm reco}$. The former helps constrain uncertainties from JES corrections and final-state radiation (FSR). These sources, however, still dominate the overall uncertainty, with jet-flavor-dependent jet-energy corrections being the largest component.

In the boosted analysis [318], the observable sensitive to m_t is the average mass of the large-R jets, \bar{m}_J . As in the resolved analysis, $m_W^{\rm reco}$ is used to reduce sensitivity to jet-related uncertainties. A significant uncertainty in this channel arises from modeling the recoil scheme in PYTHIA for secondary and subsequent gluon emissions. This effect is mitigated by introducing a third observable, m_{tj} , defined as the invariant mass of the leptonically decaying top quark and the nearest additional jet. After these improvements, the dominant remaining uncertainties stem from the JES and $t\bar{t}$ modeling, particularly FSR and color-reconnection effects.

The systematic models used by ATLAS and CMS are not identical, leading to different dominant uncertainties in the measurements discussed here.

Table 61.19: Comparison of the most precise individual measurements of m_t per decay topology. The uncertainties displayed are the statistical and systematic uncertainties. In the soft-muon-tag and the boosted topology, an additional uncertainty related to recoil effects in the simulation is also considered. The * indicates that the measurement was performed using 8 TeV data, while all others use 13 TeV datasets. The last row shows the LHC combination of 7 and 8 TeV results.

Exp. [Ref.]	m_t (GeV)	Topology	Method	Dominant uncert.
CMS [286]	$171.77 \pm 0.04 \pm 0.37$	Resolved (LJ)	profile LH (5D)	JES, FSR
CMS [141]	$172.33 \pm 0.14 ^{+0.66}_{-0.72}$	Resolved (DL)	profile LH	JES, MC statistics
CMS [285]	$172.34 \pm 0.20 \pm 0.70$	Resolved (AH)	ideogram	JES, color reconnection
ATLAS [318]	$172.95 \pm 0.27 \pm 0.46$	Boosted (LJ)	profile LH (3D)	JES, $t\bar{t}$ modelling
CMS [296]	$173.5 \pm 3.0 \pm 0.9$	J/Ψ (LJ)*	template	data statistics
ATLAS [295]	$174.41 \pm 0.39 \pm 0.66 \pm 0.25$	Soft muon tag (LJ)	profile LH	b fragmentation/decay, data statistics
CMS [267]	$172.13 \pm 0.32 ^{~+0.69}_{~-0.71}$	Single top	particle-level profiled	JES
LHC [1]	$172.52 \pm 0.14 \pm 0.30$	7 and 8 TeV results	BLUE	b-JES

Each experiment has produced a combined measurement of the top-quark mass using its individual results. The CMS combination gives $m_t = 172.44 \pm 0.13$ (stat.) ± 0.47 (syst.) GeV [319], while the ATLAS combination yields $m_t = 172.69 \pm 0.25$ (stat.) ± 0.41 (syst.) GeV [282].

Global combinations from the Tevatron and the LHC account for correlations both within individual experiments and between different experiments. A Tevatron–LHC combination released in 2014 reported $m_t = 173.34 \pm 0.76$ GeV (0.44%) [320], but this result, based only on the 7 TeV LHC data, has since been superseded by the most recent LHC combination [1]. In this latest combination, ATLAS and CMS included fifteen individual measurements in leptonic and hadronic top-quark decays, as well as a measurement in events enriched with single-top production via the EW t-channel. The datasets correspond to the full 7 and 8 TeV samples. The combination was performed using the BLUE method [321], incorporating estimator correlations both within and across experiments. The impact of correlation choices on the final result was investigated and found to be small. The combined result is $m_t = 172.52 \pm 0.33$ GeV, corresponding to a relative precision of 0.2%, and is limited primarily by the b-jet energy scale (b-JES) uncertainty.

The direct measurements of the top-quark mass correspond to the parameter used in Monte Carlo generators, which is closely related to the pole mass [8]. The relation between the pole mass and short-distance mass definitions, such as $\overline{\rm MS}$, is affected by non-perturbative effects. Recent calculations estimate the renormalon ambiguity to be below 250 MeV, which remains smaller than the current measurement uncertainty [322, 323]. Other ambiguities, for example, the one related to the parton-shower cut-off value, can be of the order of 500 MeV [8, 324]. A calibration of the

top-quark mass parameter in Powheg+Pythia 8 with respect to the MSR mass scheme [325] was performed by ATLAS. Using simulated $t\bar{t}$ events in the LJ channel and the mass distribution of large-radius jets containing the three quarks from the hadronic top decay, a difference between the Monte Carlo mass and the MSR mass of about 80 MeV was obtained, with large associated uncertainties [326].

As a result of renormalization at higher orders in perturbation theory, m_t depends on the scale at which it is defined. The first measurement of the running of the top-quark mass in the $\overline{\rm MS}$ scheme was reported by CMS [327]. The running mass was extracted from the differential cross section as a function of the $t\bar{t}$ invariant mass, unfolded to parton level in ${\rm DL}(e\mu)$ final states. The result shows a variation of about 15% between $M_{t\bar{t}}=400~{\rm GeV}$ and $M_{t\bar{t}}\approx 1~{\rm TeV}$, in good agreement with the one-loop renormalization-group prediction. Relative to the hypothesis of no running, the significance of the observed effect is 2.6σ , although the interpretation is subject to large theoretical uncertainties [328].

Measurements of $m_{\rm t}$ based on inclusive and differential cross sections of $t\bar{t}$ and $t\bar{t}$ +jet final states are summarized in Fig. 61.9. These have been performed at center-of-mass energies between 7 and 13 TeV using observables related to the production cross section. The most recent result, not yet included in this comparison, obtained by ATLAS at 13 TeV in the DL channel with $t\bar{t}$ +jet final states, yields $m_{\rm t} = 170.9 \pm 1.5$ GeV [329].

Vacuum stability

With the discovery of a Higgs boson at the LHC with a mass of about 125 GeV [330, 331], the precise determination of the top-quark mass has taken a central role in assessing the stability of the EW vacuum. Radiative corrections from the top quark tend to drive the Higgs quartic coupling λ negative, potentially leading to vacuum instability. An NNLO calculation [2] indicates vacuum stability for a Higgs mass satisfying $M_H \geq 129.4 \pm 5.6$ GeV [332]. Within this uncertainty, a Higgs boson mass of 125 GeV is compatible with stability, although the central values of the Higgs boson and top-quark masses still allow for a metastable scenario.

In the context of the European Strategy for Particle Physics 2025 update, ATLAS and CMS prepared projections of future Higgs boson and m_t determinations [333], shown in Fig. 61.10. These projections are based on two m_t measurements at 8 and 13 TeV, obtained from differential cross-section measurements in $t\bar{t}$ +jets final states. For the projections, different scenarios for reducing systematic uncertainties and employing alternative analysis methods are explored. Further projections can be found in the same document.

CPT test based on m_t measurements

The CPT theorem requires that particles and their antiparticles have identical masses, lifetimes, and absolute charges. A test of this symmetry has been performed by measuring the mass difference between the top and antitop quarks, $\Delta m_t = m_t - m_{\bar{t}}$, which is expected to vanish if CPT is conserved. The top and antitop quarks are distinguished through the charge of the decay lepton, and such measurements have been performed at both the Tevatron and the LHC. The results, summarized in Tab. 61.20, are consistent with the SM expectation of no mass difference, with a current sensitivity at the level of a few hundred MeV.

61.2.5.2 Width

The top-quark width, inversely proportional to its lifetime, is expected to be of order 1 GeV (Eq. 1). Early measurements made at CDF [340] and CMS [341] established confidence-level intervals for the width but lacked the sensitivity to make a direct measurement.

The total width of the top quark can be inferred from the partial decay width $\Gamma(t \to Wb)$ and

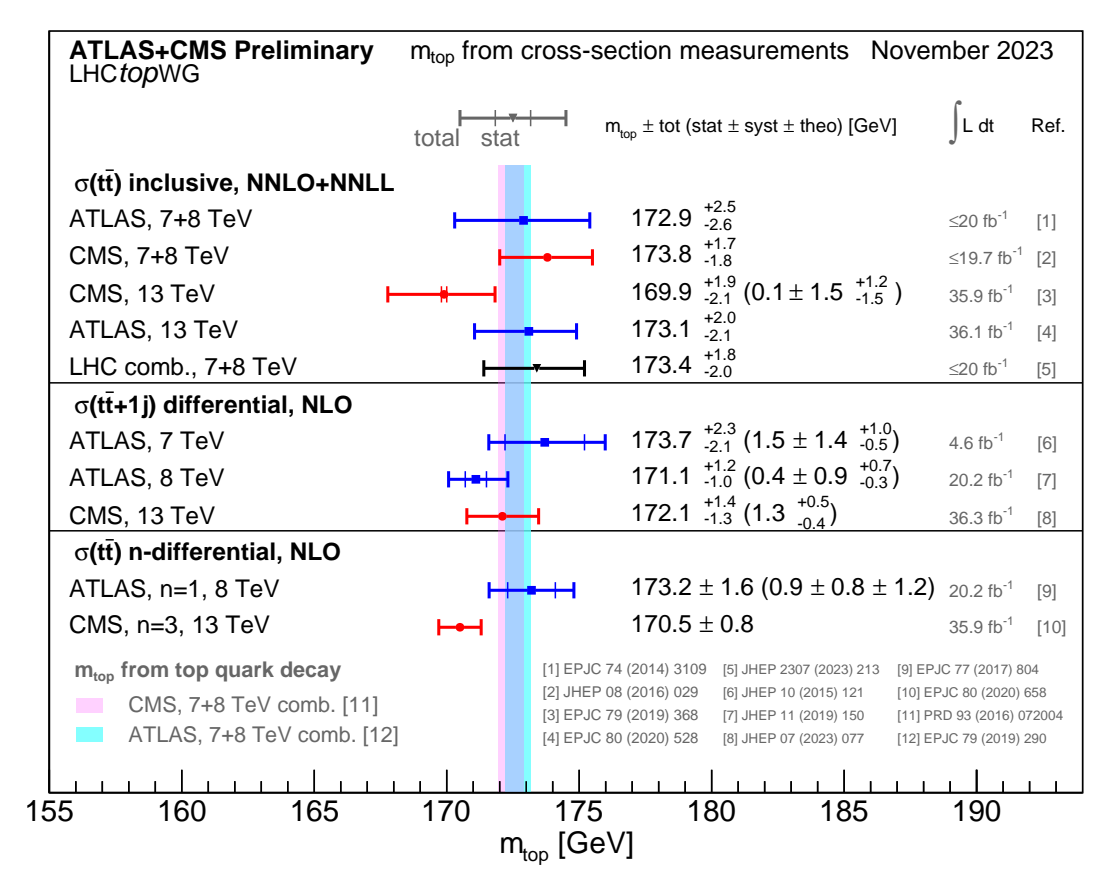


Figure 61.9: Comparison of ATLAS and CMS measurements of the top-quark mass using observables related to $t\bar{t}$ and $t\bar{t}$ +jet production. The LHCtopWG working group kindly provides the plot, status as of November 2023, see https://twiki.cern.ch/twiki/bin/view/LHCPhysics/LHCTopWGSummaryPlots.

Table 61.20: Comparison of the measurements of $\Delta m_t = m_t - m_{\bar{t}}$ in $t\bar{t}$ and single-top events.

Exp. [Ref]	\sqrt{s} (TeV)	$\Delta m_t \; [{ m GeV}]$	Topology
CDF [334]	1.96	$-1.95 \pm 1.11(stat.) \pm 0.59(syst.)$	$t \bar{t} \; \mathrm{LJ}$
$D\emptyset$ [335]	1.96	$0.84 \pm 1.81(stat.) \pm 0.48(syst.)$	t ar t LJ
ATLAS [336]	7	$0.67 \pm 0.61(stat.) \pm 0.41(syst.)$	$tar{t}~{ m LJ}$
CMS [337]	7	$-0.44 \pm 0.46(stat.) \pm 0.27(syst.)$	$tar{t}~{ m LJ}$
CMS [338]	8	$-0.15 \pm 0.19(stat.) \pm 0.09(syst.)$	$tar{t}~{ m LJ}$
CMS [339]	13	$0.83^{+1.79}_{-1.35}(stat. + syst.)$	single-top LJ

the branching fraction $B(t \to Wb)$. DØ extracted $\Gamma(t \to Wb)$ from the measured t-channel single-top-quark production cross section, and $B(t \to Wb)$ from the ratio $R = B(t \to Wb)/B(t \to Wq)$ in $t\bar{t}$ events in the LJ channel with 0, 1, and 2 b-tags. Assuming $B(t \to Wq) = 1$ for any kinematically allowed quark q, the result was $\Gamma_t = 2.00^{+0.47}_{-0.43}$ GeV, corresponding to a top-quark lifetime of $\tau_t = (3.29^{+0.90}_{-0.63}) \times 10^{-25}$ s. Under the assumption of a heavy fourth-generation b' quark and unitarity of the four-generation mixing matrix, an upper limit of $|V_{tb'}| < 0.59$ at 95% C.L. was obtained [342].

The first direct measurement of the top-quark width was performed by ATLAS at $\sqrt{s} = 8$ TeV,

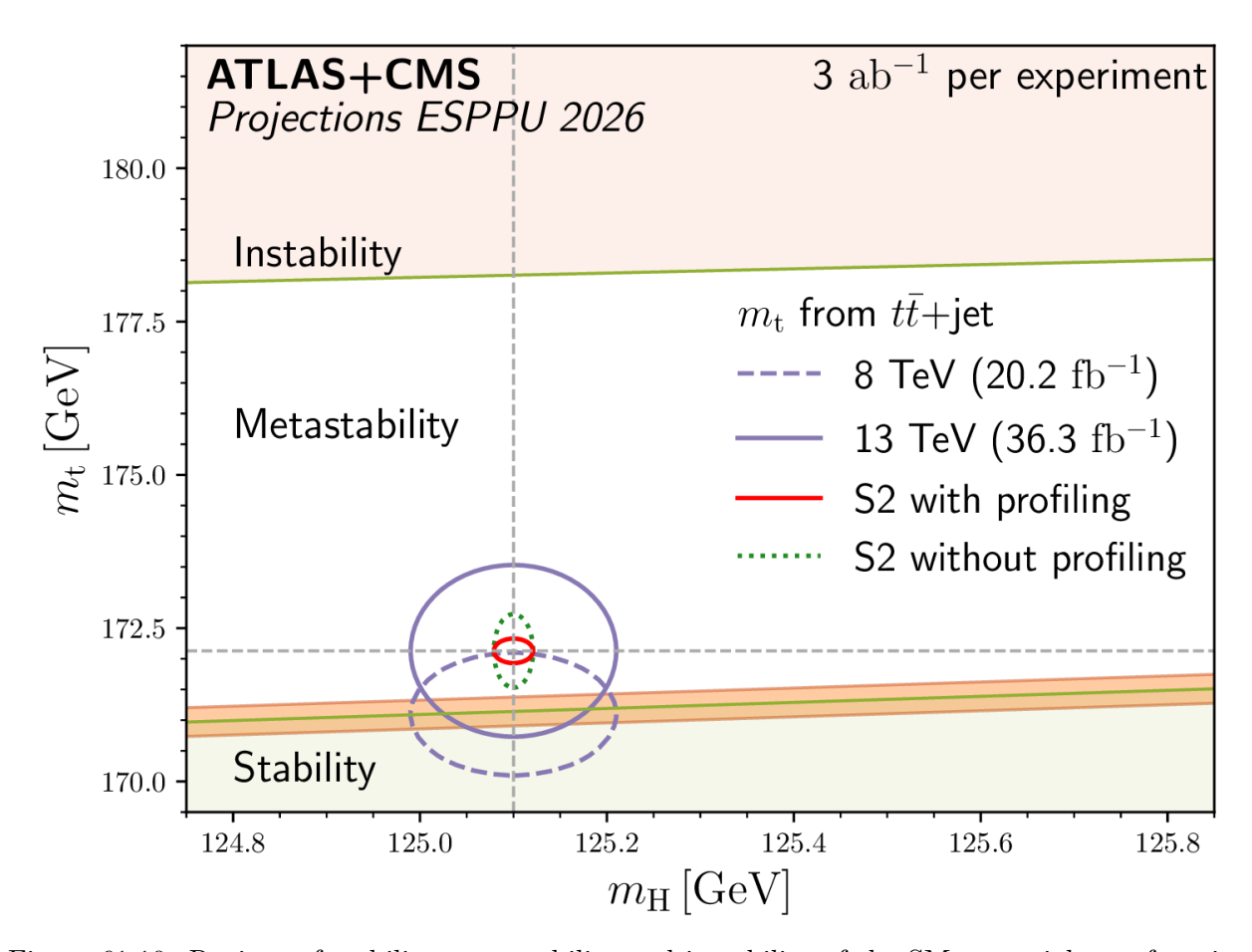


Figure 61.10: Regions of stability, metastability and instability of the SM potential as a function of the top-quark and the Higgs-boson masses [333]. The input measurements from ATLAS and CMS were used to extrapolate the size of the dataset to 3 ab⁻¹, using different assumptions on the systematic uncertainties and analysis methods.

fitting reconstructed LJ events, and yielded $\Gamma_t = 1.76 \pm 0.33$ (stat.) $^{+0.79}_{-0.68}$ (syst.) GeV [343]. A more recent ATLAS analysis at $\sqrt{s} = 13$ TeV, based on a template fit to the lepton–b-quark invariant mass in DL final states, obtained $\Gamma_t = (1.9 \pm 0.5)$ GeV [344].

A similar analysis performed by CMS at $\sqrt{s}=8$ TeV provided a more precise determination of the width, yielding $\Gamma_t=1.36\pm0.02$ (stat.) $^{+0.14}_{-0.11}$ (syst.) GeV [345].

61.2.5.3 Top Quark Spin Correlations, Polarization, and Entanglement

One of the unique features of the top quark is that it decays before QCD interactions can flip its spin. Thus, the top quark polarization is directly observable via the angular distribution of its decay products, and it is possible to define and measure observables sensitive to the top quark spin and its production mechanism. Although the top and antitop-quarks produced by QCD interactions in hadron collisions are essentially unpolarized, the spins of t and \bar{t} are correlated. For QCD production at threshold, the $t\bar{t}$ system is produced in a 3S_1 state with parallel spins for $q\bar{q}$ annihilation or in a 1S_0 state with antiparallel spins for gluon-gluon fusion, as shown in Fig. 61.11.

The production mechanisms at the Tevatron, where $t\bar{t}$ pairs are predominantly produced via $q\bar{q}$ annihilation, and at the LHC, where gluon–gluon fusion dominates, are therefore complementary. At the LHC, $t\bar{t}$ production at large invariant mass arises mainly from gluons with opposite helicities, resulting in $t\bar{t}$ pairs with parallel spins, similar to the configuration produced at the Tevatron

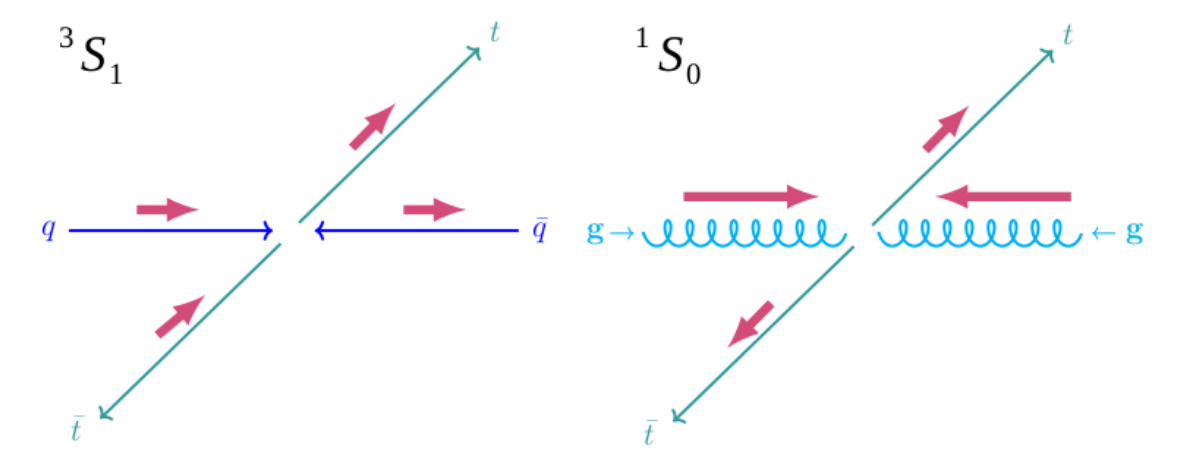


Figure 61.11: Spin state of the $t\bar{t}$ system at the production threshold for $q\bar{q}$ annihilation (left) and gluon-gluon fusion (right). The thin arrows describe the momentum direction of the particles, while the thicker arrows reflect the spin direction of the gluons (long arrows) and the quarks (short arrows).

through $q\bar{q}$ annihilation.

The top-quark spin is fully correlated with the angular distributions of the down-type fermion (charged lepton or d-type quark) in the decay. The corresponding joint angular distribution is given in Refs. [346–348]

$$\frac{1}{\sigma} \frac{d^2 \sigma}{d(\cos \theta_+^i) d(\cos \theta_-^j)} = \frac{1}{4} (1 + B_+^i \cos \theta_+^i + B_-^j \cos \theta_-^j + C_{ij} \cdot \cos \theta_+^i \cdot \cos \theta_-^j), \tag{61.5}$$

where θ_+^i and θ_-^j are the angles of the daughters in the top-quark (antitop-quark) rest frame with respect to a particular spin quantization axis i (j). The maximum value for C, 0.782 at NLO at the Tevatron [349], is found in the off-diagonal basis [346], while at the LHC the value at NLO is 0.326 in the helicity basis [349]. The coefficients B_+ and B_- are near zero in the SM because the top quarks are unpolarized in $t\bar{t}$ production. In place of C, $A\alpha_+\alpha_-$ is often used, where α_i is the spin analyzing power, and A is the spin correlation coefficient, defined as

$$A = \frac{N(\uparrow\uparrow) + N(\downarrow\downarrow) - N(\uparrow\downarrow) - N(\downarrow\uparrow)}{N(\uparrow\uparrow) + N(\downarrow\downarrow) + N(\uparrow\downarrow) + N(\downarrow\uparrow)},\tag{61.6}$$

where the first arrow represents the direction of the top quark spin along a chosen quantization axis, and the second arrow represents the same for the antitop-quark. The spin analyzing power α_i at parton level is +0.998 for positively charged leptons, -0.966 for down-type quarks from W decays, and -0.393 for bottom quarks [350]. The sign of α flips for the respective antiparticles. The spin correlation could be modified by a new $t\bar{t}$ production mechanism such as through a Z' boson, Kaluza-Klein gluons, a dark-matter mediator, or a Higgs boson.

Measurement of SM spin correlation fraction

The experiments typically use Monte Carlo simulation to provide templates for the measured distributions, or a matrix-element method, and fit a parameter $f_{\rm SM}$, representing the fraction of events with the expected SM correlation, with $(1-f_{\rm SM})$ the fraction with no correlation. The correlation coefficient is extracted via $A_{\rm meas} = f \cdot A_{\rm SM}$. A 'fraction' $f_{\rm SM} > 1$ means that the

measured correlation coefficient is larger than the SM expectation. DØ pioneered the study of spin correlations in $t\bar{t}$ production during Run 1 [351], setting the first limits of $\kappa > -0.25$ at the 68% confidence level using the DL channel. In Run 2, both CDF and DØ extended the studies to the DL and LJ channels. Although the sensitivity was limited, these analyses provided the first evidence for spin-correlation effects [352–355].

Spin correlations have been conclusively established at the LHC by both ATLAS and CMS. In the dominant gluon-gluon-fusion production mode for $t\bar{t}$ pairs, the angular separation between the two leptons in the DL channel is sensitive to the degree of spin correlation [356].

Measurements have been performed at $\sqrt{s}=7$, 8, and 13 TeV, with the corresponding values of $f_{\rm SM}$ summarized in Tab. 61.21. While the \sqrt{s} dependence of the correlations is of interest as a probe of the production mechanism ($q\bar{q}$ annihilation versus gluon-gluon fusion) and as a potential window to new physics, the 7 and 8 TeV results [357–363] were limited by relatively large uncertainties. These have since been superseded by the high-statistics measurements at 13 TeV, which are reviewed here in more detail.

Table 61.21: Measurements of the SM spin correlation fraction $f_{\rm SM}$ in $t\bar{t}$ events at the LHC, performed at $\sqrt{s}=7$, 8 TeV and 13 TeV. The results are shown together with their overall uncertainties. The precision is mainly limited by the systematic uncertainties. For the 13 TeV results, the precision is mainly limited by signal-modeling uncertainties. Only the most precise measurement per channel and publication is listed below. Further results are given in the individual publications.

Exp. [Ref.]	Lumi.	Measurement	Channel	Observable
	$[fb^{-1}]$	Value \pm Unc.		
		7 T	eV results	
ATLAS [357]	2.1	$f_{\rm SM} = 1.30 \pm ^{+0.30}_{-0.26}$	DL	$\Delta \Phi(\ell^+,\ell^-)$
ATLAS [358]	4.6	$f_{\rm SM} = 1.19 \pm 0.20$	DL	$\Delta\Phi(\ell^+,\ell^-)$
ATLAS [358]	4.6	$f_{\rm SM} = 0.87 \pm 0.18$	DL	S-ratio of matrix-elements
ATLAS [358]	4.6	$f_{\rm SM} = 1.12 \pm 0.25$	SL	$\Delta \Phi(\ell,d) + \Delta \Phi(\ell,b)$
CMS [361]	5.0	$f_{\rm SM} = 0.98 \pm 0.15$	DL	From asymmetry $A_{\varDelta\varPhi}$ measurement
		8 T	eV results	
ATLAS [359]	20.3	$f_{\rm SM} = 1.20 \pm 0.14$	DL	$\Delta\Phi(\ell^+,\ell^-)$
CMS [362]	19.7	$f_{\rm SM} = 0.72^{+0.17}_{-0.15}$	DL	matrix-element method
CMS [363]	19.5	$f_{\rm SM} = 1.12^{+0.12}_{-0.15}$	DL	$A_{\Delta\phi}$ measurement as function of $m_{t\bar{t}}$
13 TeV results				
ATLAS [364]	36.1	$f_{\rm SM} = 1.249^{+0.094}_{-0.111}$	DL	$\Delta \Phi(\ell^+,\ell^-)$
ATLAS [197]	140	$f_{\rm SM} = 1.20 \pm 0.68$	$t\bar{t}Z$ ev.	combination of 9 observables
CMS [365]	35.9	$f_{\rm SM} = 0.98 \pm 0.05$	DL	From D measurement

At $\sqrt{s}=13$ TeV, the most recent ATLAS measurement of $f_{\rm SM}$ is based on $\Delta\phi$, the azimuthal angle between the two charged leptons in $e\mu$ events, within an analysis that also measures the differential cross sections in $\Delta\phi$ and $\Delta\eta$ [364]. The comparison with NLO Monte Carlo generators yields $f=1.249\pm0.024$ (stat.) ±0.061 (syst.) $^{+0.067}_{-0.090}$ (theo.). While earlier measurements were statistically consistent with the SM expectation of f=1.0, the current result lies above this value

by about 2.2σ . The NLO predictions considered are based on QCD corrections only and correspond to the production level. When EW corrections are included, the SM prediction becomes compatible with the measurement within uncertainties, although it is affected by a relatively large uncertainty, $f = 1.03 \pm 0.13$.

The CMS measurement at $\sqrt{s}=13$ TeV was obtained from DL events by measuring parton-level normalized differential cross sections, which are sensitive to each of the independent coefficients of the spin-dependent parts of the $t\bar{t}$ production density matrix. These measured distributions and extracted coefficients were compared with SM predictions from simulations at NLO accuracy in QCD, and from NLO QCD calculations including EW corrections. The comparison with the simulation yields $f=0.98\pm0.03$ (stat.) ±0.04 (syst.) ±0.01 (theo.). The normalized differential cross sections are used in fits to constrain the anomalous chromomagnetic and chromoelectric dipole moments of the top quark [154]: $-0.24 < C_{tG}/\Lambda^2 < 0.07$ TeV⁻² and $-0.33 < C_{tG}^I/\Lambda^2 < 0.20$ TeV⁻², respectively, at 95% C.L. [365].

These results are part of a comprehensive study of the top quark spin density matrix at $\sqrt{s} = 13$ TeV, as measured through the coefficients of Eq. 61.5, which will be discussed further below.

Measurement of the full spin density matrix

Instead of extracting a single overall correlation coefficient or the fraction of SM-like spin correlation, the full spin density matrix can be measured. This requires determining the top- and antitop-quark polarizations P in the three spatial directions and the nine components of the spin-correlation matrix C^1 . An introduction to the spin-density-matrix formalism is given in Ref. [30].

To extract all coefficients, spin-quantization axes must first be defined. A full reconstruction of the $t\bar{t}$ final state is required. In the notation of the first ATLAS measurement [366], the helicity axis is denoted k, the transverse axis n, and the r axis orthogonal to both. Spin analyzers are boosted into the rest frames of the respective top or antitop quark, and the angular distribution $\cos \theta$ of their momenta relative to the chosen axis is reconstructed. The 15 parameters are then obtained from data using one observable per parameter, as listed in Fig. 61.12 from Ref. [366].

The most precise individual measurement of these 15 coefficients has recently been performed by CMS in LJ events at $\sqrt{s} = 13\,$ TeV [35], using the down-type quark and the charged lepton as spin analyzers. In this analysis, the coefficients are extracted from a combined fit to data. Events are categorized according to $m_{t\bar{t}}$, $p_{\rm T}^{\rm top}$, and the absolute value of the top-quark scattering angle $|\cos\theta|$. The templates are parametrized as functions of the angular distributions of the top- and antitop-quark decay products. The setup achieving the best precision is based on event categories in bins of $p_{\rm T}^{\rm top}$ and $|\cos\theta|$.

61.2.5.4 Measurement of spin entanglement in pair production

Entanglement, such as between the spin states of two particles, is a fundamental property of quantum mechanics [367–369]. Two particles are entangled if the state of one cannot be described independently of the state of the other. While entanglement has been observed in many physical systems, its study at high-energy colliders has been limited until recently. Notable examples include flavor entanglement in $\Upsilon(4S) \to B_0 \bar{B}_0$ decays [370] and tests of Bell non-locality in $B_0 \to J/\psi K^*(892)^0$ decays [371]. The idea of probing entanglement in top-quark pairs through their spin correlations was first proposed in 2020 [32, 372–378].

At the LHC, $t\bar{t}$ pairs are predominantly produced via gluon–gluon fusion. Near production threshold ($m_{t\bar{t}} \approx 2m_t \approx 350 \text{ GeV}$), they are expected to form dominantly a spin-singlet state (1S_0), which is maximally entangled. The different spin states are illustrated in Fig. 61.11. Since the spin state of an individual top quark cannot be determined directly in a collision experiment, the presence

¹Some publications denote the polarizations by P instead of B, and the correlations by C instead of A, as the notation has varied over time.

Expectation values	NLO predictions	Observables
B_+^k	0.0030 ± 0.0010	$\cos heta_+^k$
B^k	0.0034 ± 0.0010	$\cos heta^k$
B^n_+	0.0035 ± 0.0004	$\cos heta_+^n$
B^n	0.0035 ± 0.0004	$\cos heta^n$
B^r_+	0.0013 ± 0.0010	$\cos heta_+^r$
B^r	0.0015 ± 0.0010	$\cos heta^r$
C(k,k)	0.318 ± 0.003	$\cos heta_+^k \cos heta^k$
C(n,n)	0.332 ± 0.002	$\cos \theta_+^n \cos \theta^n$
C(r,r)	0.055 ± 0.009	$\cos heta_+^r \cos heta^r$
C(n,k) + C(k,n)	0.0023	$\cos\theta_+^n\cos\theta^k + \cos\theta_+^k\cos\theta^n$
C(n,k) - C(k,n)	0	$\cos\theta_+^n\cos\theta^k - \cos\theta_+^k\cos\theta^n$
C(n,r) + C(r,n)	0.0010	$\cos\theta_+^n\cos\theta^r + \cos\theta_+^r\cos\theta^n$
C(n,r) - C(r,n)	0	$\cos\theta_+^n\cos\theta^r - \cos\theta_+^r\cos\theta^n$
C(r,k) + C(k,r)	-0.226 ± 0.004	$\cos\theta_+^r\cos\theta^k + \cos\theta_+^k\cos\theta^r$
C(r,k) - C(k,r)	0	$\cos\theta_+^r\cos\theta^k - \cos\theta_+^k\cos\theta^r$

Figure 61.12: Expected values and corresponding observables for the measurement of spin correlations and polarizations of the top and antitop quarks [366].

of quantum entanglement must be inferred statistically from ensembles of $t\bar{t}$ events. The spin singlet is rotationally invariant, which motivates the use of the trace of the spin-correlation matrix C as an entanglement witness. A sufficient condition for entanglement is given by tr[C] + 1 < 0, measuring entanglement, a natural extension of spin-correlation studies. This can be rewritten as

$$D = tr[C]/3, (61.7)$$

which can be experimentally measured as:

$$D = -3 \cdot \langle \cos \varphi \rangle. \tag{61.8}$$

Here $\langle \cos \varphi \rangle$ is the average of the opening angle between the two spin analyzers in their respective parent-top rest frames. If D < -1/3, the top quarks are entangled [32].

The first measurement of D at $\sqrt{s} = 13$ TeV was performed by CMS using a partial dataset [365]. In that analysis, the full $m_{t\bar{t}}$ spectrum was included, which reduced the sensitivity and prevented a significant deviation from zero.

The first observation of quantum entanglement in $t\bar{t}$ events was reported by ATLAS using the full Run 2 dataset at 13 TeV [33]. The analysis employed the mean value of the $\cos\phi$ distribution to construct a calibration curve relating detector-level to particle-level observables. This calibration was then applied to the detector-level measurement of D in data, and the resulting particle-level value was compared with theoretical predictions. Since entanglement effects are expected to be most pronounced near threshold, the analysis was restricted to events with $340 < m_{t\bar{t}} < 380$ GeV. The precision of the measurement is limited by signal-modeling uncertainties, particularly those arising from differences between parton-shower algorithms.

Subsequently, CMS observed entanglement in $t\bar{t}$ events in both the DL channel [34] and the LJ channel [35]. In the DL analysis, a template fit to the full $\cos \phi$ spectrum was performed using a partial Run 2 dataset, with phase-space selections listed in Tab. 61.22. Non-relativistic bound-state effects were included in the prediction, improving agreement with the data. The LJ result forms

part of the measurement of the full spin density matrix discussed above. Although the sensitivity to entanglement near threshold in this channel is insufficient for an observation, it provides access to a second phase space where entanglement is present: events at high $m_{t\bar{t}}$, where the top quarks are produced more widely separated in a 3S_1 state. Since in this region C_{rr} and C_{kk} become negative, the entanglement witness \tilde{D} is defined as

$$\tilde{D} = \frac{1}{3}(C_{nn} - C_{rr} - C_{kk}) \tag{61.9}$$

and has to fulfill the criterion: $3\tilde{D} > 1$ [375]. This was achieved for events with $m_{t\bar{t}} > 800$ GeV and $|\cos\theta| < 0.4$. The ATLAS and CMS experiments have observed entanglement at the highest energy to date, both for $t\bar{t}$ events almost at rest and for more space-like separated top quarks. The measured values are summarized in Tab. 61.22.

Table 61.22: Measurements of different entanglement witnesses at $\sqrt{s} = 13$ TeV. The results are shown together with their overall uncertainties. The precision for the threshold measurements is mainly limited by signal-modeling uncertainties, while the measurement in the boosted phase-space is limited by statistical uncertainties. The CMS results include the modeling of threshold effects. Only the most precise measurement per channel and publication is listed below. Further results are given in the individual publications.

Exp. [Ref.]	Measurement	Significance Obs. (Exp.)	Topology	Method/Phase space
CMS [365]	$D = -0.237 \pm 0.011$		DL	Fit to $\cos \phi$ distribution
				inclusive in $m_{t\bar{t}}$
ATLAS [33]	$D = -0.547 \pm 0.021$	$> 5\sigma \ (> 5\sigma)$	DL	Calibration curve
				$340 < m_{t\bar{t}} < 380 \text{ GeV}$
				Particle level
CMS [34]	$D = -0.480^{+0.026}_{-0.029}$	$5.1\sigma \ (4.7\sigma)$	DL	Fit to $\cos \phi$ distribution
				$\beta_z^{t\bar{t}} < 0.9, m_{t\bar{t}} < 400 \text{GeV}$
				Parton level
CMS [35]	$\tilde{D} = 0.652 \pm 0.052$	$6.7\sigma~(5.6\sigma)$	SL	Fit to multi-differential distr.
				$m_{t\bar{t}} > 800 \text{ GeV}, \cos \theta < 0.4$

61.2.5.5 Pseudo-bound $t\bar{t}$ states at the production threshold

During the development of quantum entanglement measurements, it became clear that modeling of the $t\bar{t}$ threshold region required improvements. As shown in the CMS analyses [34, 35], the inclusion of threshold effects leads to better agreement between the data and the prediction. Because the top quark decays before forming hadrons, bound states cannot occur in the usual sense. However, a $t\bar{t}$ pair produced nearly at rest can exchange gluons before one quark decays weakly [16, 379].

Threshold effects from non-relativistic QCD (NRQCD) have two main contributions: the potential has an attractive component from $t\bar{t}$ pairs in a color-singlet configuration (produced in gg fusion), corresponding to the ${}^1S_0^{[1]}$ spin-angular-momentum-color state. The second component of the potential is repulsive and originates from $t\bar{t}$ pairs produced in a color-octet configuration. The latter component is small and not included in the measurements discussed here. The resummation

of Coulomb gluon exchange enhances $t\bar{t}$ production just below threshold. For $m_t = 172.5$ GeV and a binding energy of about 2 GeV, the expected mass of this state is $\simeq 343$ GeV, with a width of $2\Gamma_t$.

Standard Monte Carlo $t\bar{t}$ samples do not include these pseudo-bound-state effects, or other QCD effects occurring at the production threshold and discussed in Ref. [380]. Although these contributions amount to less than 1% of the total cross section and have negligible impact on most top-quark measurements, they become important for precision studies close to threshold, such as entanglement or top-quark Yukawa coupling measurements using the $m_{t\bar{t}}$ spectrum, and for newphysics searches in the low- $m_{t\bar{t}}$ region. To address this, CMS developed a dedicated cross-section measurement of this contribution using the full Run 2 dataset [90]. The analysis, performed in the DL channel, fitted the full $m_{t\bar{t}}$ spectrum, which was divided into nine signal regions defined by angular variables. This strategy significantly improved sensitivity compared with a single inclusive distribution. The signal was simulated with MG5_AMC@NLO using a simplified resonance model $(\eta_{t\bar{t}})$ decaying into $t\bar{t}$. The predicted cross section is 6.43 pb, and the measurement, limited by systematic uncertainties, yielded $\sigma(\eta_{t\bar{t}}) = 8.8^{+1.2}_{-1.4}$ pb with a significance greater than 5σ .

ATLAS carried out a similar analysis [91], also extracting the cross section from the $m_{t\bar{t}}$ distribution split into angular regions. The fit range was restricted to 300–500 GeV to avoid potential mis-modeling at high invariant masses. A more complete pseudo-bound state model was employed, in which LO $t\bar{t}$ matrix elements were reweighted using the NRQCD-resummed Green's function [16, 379]. The ATLAS result, also limited by systematic uncertainties, is $\sigma(t\bar{t}_{\rm NRQCD}) = 9.0 \pm 1.3$ pb with an observed significance of 7.7 σ .

Both measurements are consistent with the production of a pseudo-bound color-singlet state. However, with the current invariant-mass resolution, a clear observation of the peak structure predicted by NRQCD cannot yet be claimed, and the enhancement can also be described within more inclusive approaches [380]. Further theoretical and experimental studies will be needed to clarify the nature of this enhancement.

61.2.5.6 W-boson helicity in top-quark decay

In the SM, the top quark couples to the W boson through the vector-minus-axial-vector (V-A) charged-current interaction, $-i\frac{g}{\sqrt{2}}V_{tb}\gamma^{\mu}\frac{1}{2}(1-\gamma_5)$. Because the fraction of decays to longitudinally polarized W bosons is proportional to the top-quark Yukawa coupling, it is enhanced relative to the weak coupling. The expected fraction is [381] $\mathcal{F}_0^{\text{SM}} \approx x/(1+x)$, with $x = m_t^2/(2M_W^2)$, giving $\mathcal{F}_0^{\text{SM}} \simeq 70\%$ for $m_t = 173$ GeV. The fractions of left-handed, right-handed, and longitudinal W bosons are denoted \mathcal{F}_- , \mathcal{F}_+ , and \mathcal{F}_0 , with SM expectations $\mathcal{F}_- \simeq 30\%$ and $\mathcal{F}_+ \simeq 0\%$. Predictions at NNLO in QCD are available [382].

Measurements of the W helicity in top-quark decays have been performed by both Tevatron and LHC experiments, in $t\bar{t}$ events reconstructed in the LJ and DL channels. As for the extraction of the top-quark mass, the template technique is widely used, although the matrix-element method and its variants have also been employed to determine the helicity fractions \mathcal{F} .

In Run 1 at the Tevatron, the charged-lepton $p_{\rm T}$ spectrum [383] and the invariant mass M_{tb}^2 of the lepton-b-quark system [384] in top-quark decays were used as template observables. In Run 2, both of these observables [385] the helicity angle $\cos \theta^*$, defined as the angle between the lepton and the b quark in the W-boson rest frame, became the primary observable [386–388]. In the DL channel, reconstruction is further improved by applying the neutrino-weighting technique (see Sec. 61.2.5.1), or both. The matrix element method has also been developed for this measurement, in which a likelihood is constructed from event probabilities expressed as functions of the W-helicity fractions \mathcal{F} [389]. CDF and DØ combined their Run 2 results, based on 2.7–5.4 fb⁻¹ of data [390], assuming a top-quark mass of 172.5 GeV. From the combination of measurements that simultaneously deter-

mined the fractions of W bosons, the results are $\mathcal{F}_0 = 0.722 \pm 0.081 \ [\pm 0.062 \ (\mathrm{stat.}) \pm 0.052 \ (\mathrm{syst.})]$ and $\mathcal{F}_+ = -0.033 \pm 0.046 \ [\pm 0.034 \ (\mathrm{stat.}) \pm 0.031 \ (\mathrm{syst.})]$. In an alternative combination, where one of the helicity fractions was fixed to the SM expectation, the results are $\mathcal{F}_0 = 0.682 \pm 0.057 \ [\pm 0.035 \ (\mathrm{stat.}) \pm 0.046 \ (\mathrm{syst.})]$ and $\mathcal{F}_+ = -0.015 \pm 0.035 \ [\pm 0.018 \ (\mathrm{stat.}) \pm 0.030 \ (\mathrm{syst.})]$. Both sets of results are consistent with SM predictions.

The large LHC datasets make it possible to perform simultaneous fits of $\mathcal{F}0$, $\mathcal{F}-$, and \mathcal{F}_+ ; the corresponding ATLAS and CMS results are summarized in Fig. 61.13.

At $\sqrt{s} = 7$ TeV, ATLAS used a template method for the $\cos \theta^*$ distribution and extracted angular asymmetries from the unfolded $\cos \theta^*$ distribution in both the LJ and DL channels [391]. CMS performed a similar measurement in the LJ channel, also based on template fits to the $\cos \theta^*$ distribution [392].

Since the polarization of W bosons in top-quark decays is directly sensitive to the Lorentz structure of the Wtb vertex and to possible anomalous couplings, both collaborations derived limits on non-SM contributions to the Wtb interaction. ATLAS and CMS also combined their 7 TeV results, also assuming a top-quark mass of 172.5 GeV, to obtain joint values of the W-boson helicity fractions and corresponding limits on anomalous couplings [393].

At $\sqrt{s}=8$ TeV, ATLAS measured the W-boson helicity fractions in LJ events with at least one b tag [394]. CMS carried out complementary measurements: in LJ events with two b-tags [395] Using the same dataset, CMS also presented the first measurement of W-boson helicity in EW single-top production [396], obtaining results of similar precision and in agreement with the SM. The 8 TeV results from ATLAS and CMS in both $t\bar{t}$ and single-top events were subsequently combined [397]. The combined analysis, consistent with the SM predictions at NNLO in QCD, improved the precision by 25% (29%) for F_0 (F_L) compared to the most precise individual measurement, and set limits on anomalous right-handed vector (V_R) and left- and right-handed tensor (g_L , g_R) tWb couplings, as well as on the corresponding Wilson coefficients.

At $\sqrt{s} = 8$ TeV, ATLAS analyzed DL events with at least two b tags, measuring the normalized differential $t\bar{t}$ cross section with respect to $\cos\theta^*$ at parton level and, from template fits, extracting the W-boson helicity fractions [398]. The results are complementary to earlier measurements and consistent with SM expectations, with the precision limited by systematic uncertainties.

61.2.5.7 Yukawa coupling

The top-Higgs Yukawa coupling is expected to be the largest among all Yukawa couplings. It can be accessed directly by measurements of the $t\bar{t}$ cross section in association with a Higgs boson, $t\bar{t}H$, or indirectly via loop processes in $gg \to H$ production as well as $H \to \gamma\gamma$ or $H \to WW$ decays or in the rare process of $t\bar{t}t\bar{t}$ production. A discussion of the former can be found in Chapter 11 of this review. Searches for and recent observations of $t\bar{t}t\bar{t}$ production are discussed in Sec. 61.2.2. Measurements of y_t in kinematic distributions of $t\bar{t}$ production are providing additional information [399, 400].

61.2.5.8 Top-quark asymmetries

In $t\bar{t}$ production at hadron colliders, the SM predicts different predicts characteristic angular distributions that differ between the top and antitop quarks. Unlike most observables in the top-quark sector, measurements of asymmetries are still largely limited by statistical precision. This is particularly true for analyses probing the extreme regions of phase space, such as those targeting boosted top quarks, and for rare production modes like $t\bar{t}W$ and $t\bar{t}\gamma$. With the increasing luminosity delivered during Run 3 of the LHC and in future runs, significant improvements in these measurements are anticipated. Theoretical predictions for these asymmetries, however, have already reached a high level of precision.

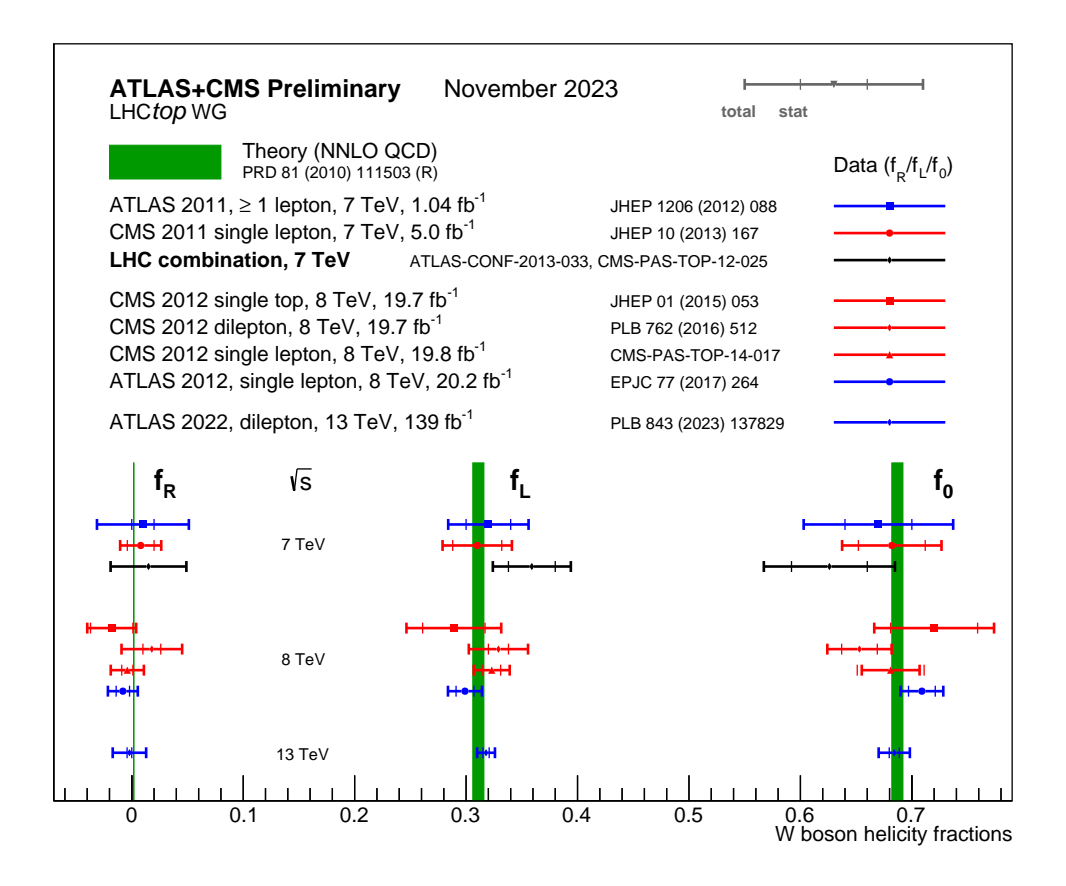


Figure 61.13: W-boson helicity fractions measured at the ATLAS and CMS experiments at different center-of-mass energies, compared to the theoretical NNLO predictions. The LHCtopWG working group kindly provides the plot, status as of November 2023, see https://twiki.cern.ch/twiki/bin/view/LHCPhysics/LHCTopWGSummaryPlots.

Measurement of the forward-backward asymmetry A_{FB}

In $p\bar{p}$ collisions at the Tevatron collider, a forward-backward asymmetry arises in $t\bar{t}$ production starting at order α_S^3 in QCD. The asymmetry originates from the interference between the Born amplitude $q\bar{q} \to t\bar{t}$ with 1-loop box production diagrams and between diagrams with initial- and final-state gluon radiation. The asymmetry, A_{FB} , is defined by

$$A_{FB} = \frac{N(x>0) - N(x<0)}{N(x>0) + N(x<0)}. (61.10)$$

Three types of asymmetries are discussed in the following:

- $A_{FB}^{t\bar{t}}$, where x is the rapidity difference between the top- and the antitop quark: $\Delta y = y_t y_{\bar{t}}$. This asymmetry requires the full reconstruction of the $t\bar{t}$ final state.
- A_{FB}^{ℓ} , where x is the product of the charge and the rapidity of the lepton: $q_{\ell} \cdot \eta_{\ell}$. This asymmetry is only defined in the SL channel.
- $A_{FB}^{\ell\ell}$, where x is the rapidity difference between the two charged leptons: $\Delta \eta = \eta_{\ell^+} \eta_{\ell^-}$. This asymmetry is only defined in the DL channel.

Calculations at α_S^3 predict a measurable A_{FB} at the Tevatron. Both CDF and DØ measured asymmetry values exceeding the SM prediction, which prompted considerable interest and speculation about possible contributions from new physics (see, for example, [401] and references therein). An overview of the early Tevatron measurements and the combined CDF and DØ results is given in Tab. 61.23. More recent calculations, extended to order α_S^4 and including EM and EW corrections, predict $A_{FB} \approx 0.095 \pm 0.007$ [402]. This value is about 10% larger than the previous NLO prediction [403, 404], leading to improved agreement with experimental results.

Table 61.23: Forward-backward asymmetry measurements in $t\bar{t}$ events at the Tevatron, performed at $\sqrt{s} = 1.96$ TeV. If only one uncertainty is given, it reflects the total uncertainty on the measurement or prediction.

Experiment [Ref.]	$\begin{array}{c} \textbf{Luminosity} \\ \textbf{(fb}^{-1} \textbf{)} \end{array}$	$\begin{array}{l} \text{Measurement} \\ \text{Value} \pm \text{(stat.)} \pm \text{(syst.)} \end{array}$	Note
DØ [405] CDF [406]	0.9 1.9	$A_{FB}^{t\bar{t}} = 0.12 \pm 0.08$ $A_{FB}^{t\bar{t}} = 0.24 \pm 0.14$	first DØ result first CDF result, parton level
Theory [402]		$A_{FB}^{t\bar{t}} = 0.095 \pm 0.007$	NNLO QCD + NLO EW
Comb. [407]	9-10	$A_{FB}^{t\bar{t}} = 0.128 \pm 0.021 \pm 0.014$	$D\emptyset+CDF$ combination
Theory [404]		$A_{FB}^{\ell} = 0.038 \pm 0.003$	NLO QCD + NLO EW
Comb. [407]	9-10	$A_{FB}^{\ell} = 0.073 \pm 0.016 \pm 0.012$	$D\emptyset+CDF$ combination
Theory [404]		$A_{FB}^{\ell\ell} = 0.048 \pm 0.004$	NLO QCD + NLO EW
Comb. [407]	9-10	$A_{FB}^{\ell\ell} = 0.108 \pm 0.043 \pm 0.016$	$D\emptyset+CDF$ combination

The first measured values at DØ and CDF were higher, though statistically consistent, with the SM expectation. With the addition of more data, the uncertainties were reduced, and the central values, if somewhat smaller, have remained consistent with the first measurements. At the same time, the improved calculations based on theory have increased the predicted asymmetry values, thereby improving the agreement between theory and experiment. Both experiments have also measured differential asymmetries, in bins of $m_{t\bar{t}}$, Δy , $q_{\ell} \cdot \eta_{\ell}$, and $\Delta \eta_{\ell\ell}$, with consistent results, though the growth of $A_{FB}^{t\bar{t}}$ with increasing $m_{t\bar{t}}$ and Δy appears somewhat more rapid than the SM prediction [407].

Charge asymmetry A_C

At the LHC, where $t\bar{t}$ production is dominated by charge-symmetric gluon–gluon fusion, the measurement is intrinsically different from that at the Tevatron. In the subdominant $q\bar{q}$ production mode, the symmetry of the pp initial state does not provide a natural definition of forward and backward directions. Instead, charge and energy asymmetries are defined based on Eq. 61.10 as follows:

- $A_C^{t\bar{t}}$, where x is the difference between the absolute rapidities of the top- and the antitop quark: $\Delta |y| = |y_t| |y_{\bar{t}}|$. The asymmetry requires the full $t\bar{t}$ event reconstruction.
- $A_C^{\ell\ell}$, where x is the difference between absolute pseudorapidities of the two charged leptons: $\Delta |\eta| = |\eta_{\ell^+}| |\eta_{\ell^-}|$. This asymmetry is only defined in the DL channel and is referred to as "leptonic charge asymmetry."
- A_E , which is defined as the difference between the top- and antitop-quark energies, and can be measured as a function of the associated high- p_T jet angle, θ_i . The energies and jet angle are

measured in the $t\bar{t}j$ rest frame. This asymmetry is referred to as "energy asymmetry" [408].

Both CMS and ATLAS have measured the charge asymmetry in different channels and at various center-of-mass energies. Results from the individual experiments at 7 and 8 TeV, as well as their combination, are summarized in Tab. 61.24. Statistical uncertainties primarily limit the precision; however, in some measurements, the statistical and systematic components are of comparable size. In addition to inclusive values, differential measurements as functions of $m_{t\bar{t}}$, and of the $p_{\rm T}$ and rapidity y of the $t\bar{t}$ system, have also been performed.

To reduce model dependence, CMS performed a measurement in a reduced fiducial phase space [409], obtaining $A_C = (-0.35 \pm 0.72 \text{ (stat.)} \pm 0.31 \text{ (syst.)})\%$, consistent with the SM prediction. To probe the $m_{t\bar{t}}$ dependence, ATLAS carried out a measurement in boosted $t\bar{t}$ events with $m_{t\bar{t}} > 0.75$ TeV, and also reported results in three bins of $m_{t\bar{t}}$ [410].

Overall, the measurements from both experiments are in agreement with SM expectations.

At 13 TeV, the measurements are more diverse, targeting not only $t\bar{t}$ events but also $t\bar{t}$ +jet and $t\bar{t}$ +boson final states [217, 411–413]. The size and sign of the asymmetries differ for the various final states. While the $t\bar{t}$ asymmetry is diluted in inclusive measurements at the LHC owing to the large fraction of gluon–gluon-initiated $t\bar{t}$ events which increases as a function of the center-of-mass energy, it is enhanced in other topologies such as $t\bar{t}\gamma$ due to an increased fraction of the quark initiated production mode. Another interesting quantity is the leptonic charge asymmetry in $t\bar{t}W$ events using final states with exactly three charged light leptons (electrons or muons). Here, the events are also enhanced in quark-initiated production processes. Additionally, the W boson in the initial state causes polarization of the $t\bar{t}$ pair, which further leads to a sizeable asymmetry. The results for the $t\bar{t}$ +boson and $t\bar{t}$ +jet final states are still strongly limited by statistical uncertainties and will benefit from the increased dataset at 13.6 TeV and beyond.

The most precise measurement to date was performed by ATLAS at $\sqrt{s}=13$ TeV, combining LJ and DL channels with reconstruction techniques for both resolved and boosted topologies [424]. Differential results are reported as functions of the invariant mass, $p_{\rm T}$, and longitudinal boost of the $t\bar{t}$ system. Both inclusive and differential measurements are compatible with SM predictions at NLO QCD with NLO EW corrections. The results are also interpreted in SMEFT, setting bounds on several Wilson coefficients.

CMS measured the charge asymmetry in $t\bar{t}$ events with highly Lorentz-boosted top quarks for $m_{t\bar{t}} > 0.75$ TeV, a phase space particularly relevant for BSM searches [425]. The measurement, corrected for detector and acceptance effects using a binned maximum-likelihood fit, was performed in three $m_{t\bar{t}}$ ranges. The results are in good agreement with the SM.

A model-independent comparison of the Tevatron and LHC results is made difficult by the differing $t\bar{t}$ production mechanisms at work at the two accelerators and by the symmetric nature of the pp collisions at the LHC. An early analysis from the CMS collaboration [427] using LJ events at $\sqrt{s}=13$ TeV, uses a likelihood analysis to separate the $q\bar{q}$ process from production via gluon-gluon and gluon-quark interactions. The values found for the asymmetry parameters are $A_{FB}=0.048^{+0.095}_{-0.087} ({\rm stat.})^{+0.020}_{-0.029} ({\rm syst.})$, for the anomalous chromomagnetic dipole moment $\mu^t=-0.024^{+0.013}_{-0.009} ({\rm stat.})^{+0.016}_{-0.011} ({\rm syst.})$, and a limit is placed on the magnitude of a possible anomalous chromoelectric dipole moment $|d^t|<0.03$ at 95% C.L. [427].

61.2.5.9 Electric charge

The top quark is the only quark whose electric charge has not been measured through threshold production in e^+e^- collisions, and its electromagnetic coupling has only recently been studied in detail. Early CDF and DØ analyses of top-quark production did not uniquely associate the b, \bar{b} , and W^{\pm} to the top or antitop quark, so that exotic decays such as $t \to W^+\bar{b}$ and $\bar{t} \to W^-b$ could not be excluded. A quark with charge 4/3 is, in fact, compatible with EW precision data. In

Table 61.24: Charge asymmetry measurements in $t\bar{t}$ events at the LHC, performed at $\sqrt{s} = 7$ and 8 TeV. The results are shown together with their overall uncertainties and are compared to the theoretical prediction. The precision is primarily limited by the dataset's size.

${\text{Exp./Pred.}}$ [Ref.]	$egin{aligned} \mathbf{Lumi.} \ [\mathbf{fb}^{-1}] \end{aligned}$	Measurement	Note		
7 TeV results					
Theory [404]		$A_C^{t\bar{t}} = (1.23 \pm 0.05)\%$	NLO QCD + NLO EW		
ATLAS [414]	4.7	$A_C^{t\bar{t}} = (0.6 \pm 1.0)\%$	LJ		
CMS [415]	5.0	$A_C^{t\bar{t}} = (0.4 \pm 1.5)\%$	LJ		
ATLAS [416]	4.6	$A_C^{t\bar{t}} = (2.1 \pm 3.0)\%.$	DL, neutrino weighting		
CMS [417]	5.0	$A_C^{t\bar{t}} = (1.0 \pm 1.6)\%,$	DL, matrix weighting technique		
Combin. [418]		$A_C^{t\bar{t}} = (0.5 \pm 0.9)\%$	LJ, ATLAS+CMS combination		
Theory [404]		$A_C^{\ell\ell} = (0.70 \pm 0.03) \%$	NLO QCD + NLO EW		
ATLAS [416]	4.6	$A_C^{\ell\ell} = (2.4 \pm 1.8)\%$	DL		
CMS [417]	5.0	$A_C^{\ell\ell} = (0.9 \pm 1.2)\%$	DL		
8 TeV results					
Theory [404]		$A_C^{t\bar{t}} = (1.11 \pm 0.04)\%$	NLO QCD + NLO EW		
Theory [419]		$A_C^{t\bar{t}} = (0.95^{+0.05}_{-0.07})\%$	NNLO QCD + NLO EW		
ATLAS [420]	20.3	$A_C^{t\bar{t}} = (0.9 \pm 0.5)$	LJ		
CMS [421]	19.7	$A_C^{t\bar{t}} = (0.33 \pm 0.43)\%$	LJ (*) stat=syst		
ATLAS [422]	20.3	$A_C^{t\bar{t}} = (2.1 \pm 1.6)\%$	DL		
CMS [423]	19.5	$A_C^{t\bar{t}} = (1.1 \pm 1.3)\%$	DL		
Combin. [418]		$A_C^{t\bar{t}} = (0.55 \pm 0.34)\%$	LJ, ATLAS+CMS combination (*)		
Theory [404]		$A_C^{\ell\ell} = (0.64 \pm 0.03)\%$	NLO QCD + NLO EW		
ATLAS [422]	20.3	$A_C^{\ell\ell} = (0.8 \pm 0.6)\%$	DL		
CMS [423]	19.5	$A_C^{\ell\ell} = (0.3 \pm 0.7)\%$	DL		

particular, the $Z \to \ell^+ \ell^-$ and $Z \to b\bar{b}$ measurements, including the discrepancy between A_{LR} at SLC and $A_{FB}^{0,b}$ and $A_{FB}^{0,\ell}$ at LEP, can be fitted with a 270 GeV quark of charge 4/3, provided the right-handed b mixes with the isospin +1/2 component of an exotic doublet $(Q_1, Q_4)_R$ with charges -1/3 and -4/3 [428, 429]. The third component of the top-quark weak isospin has likewise not been measured directly.

DØ studied the top-quark charge in double-tagged LJ events, while CDF analyzed single-tagged LJ and DL events. Assuming the top and antitop quarks carry equal and opposite charges, the b-quark charge was reconstructed using jet-charge discrimination to test the $|Q_{top}| = 2/3$ SM scenario against the exotic $|Q_{top}| = 4/3$ hypothesis. Within the framework of the exotic model of Chang et al. [429], CDF excluded $Q_{top} = 4/3$ at 99% C.L. [430], while DØ excluded it at more than 5σ and limited the fraction of such quarks in the data to below 0.46 [431]. These results firmly established that the observed particle is consistent with the SM quark of charge +2/3. At the LHC, ATLAS performed a similar measurement at $\sqrt{s} = 7$ TeV using jet-charge techniques and

Table 61.25: Asymmetry measurements in $t\bar{t}$ and $t\bar{t}+X$ events at the LHC, performed at 13 TeV. The results are shown together with their overall uncertainties and are compared to the theoretical prediction. The dataset's size primarily limits the precision.

Exp./Pred. [Ref.]	$egin{aligned} \mathbf{Lumi.} \ [\mathbf{fb}^{-1}] \end{aligned}$	Measurement	Note			
$tar{t}$						
Theory [419]		$A_C^{t\bar{t}} = (0.64^{+0.05}_{-0.06}) \%$	NNLO (QCD) + NLO (EW)			
ATLAS [424]	139	$A_C^{t\bar{t}} = (0.68 \pm 0.15) \%$	DL+LJ, resolved+boosted			
			Bayesian unfolding, 4.7σ			
Theory [404]		$A_C^{\ell\ell} = (0.40^{+0.02}_{-0.01}) \%$	NLO (QCD + EW)			
ATLAS [424]	139	$A_C^{\ell\ell} = (0.54 \pm 0.26) \%$,			
Theory [419]		$A_C^{t\bar{t}} = (0.94^{+0.05}_{-0.07}) \%$	NNLO (QCD) + NLO (EW)			
CMS [425]	138	$A_C^{t\bar{t}} = (0.42^{+0.64}_{-0.69}) \%$	LJ, boosted topology, $m_{t\bar{t}} > 750 \text{ GeV}$			
$tar{t}+{ m jet}$						
Theory		$A_E = (-3.7 \pm 0.3) \%$	MG5_aMC@NLO			
ATLAS [426]	139	$A_E = (-4.3 \pm 2.0) \%$	Bayesian unfolding, EFT interpretation			
$tar{t}\gamma$						
Theory		$A_C^{t\bar{t}} = (-1.4 \pm 0.1) \%$	MG5_aMC@NLO			
ATLAS [411]	139	$A_C^{t\bar{t}} = (-0.3 \pm 2.9) \%$	stat limited, PL unfolding			
Theory		$A_C^{t\bar{t}} = (-0.5 \pm 0.2) \%$	MG5_aMC@NLO			
CMS [217]	138	$A_C^{t\bar{t}} = (-1.2 \pm 4.2) \%$				
$tar{t}W$						
Theory		$A_C^{\ell\ell} = (-8.4^{+0.8}_{-0.7}) \%$	Sherpa 2.2.10 (NLO QCD +EW)			
ATLAS [412]	139	$A_C^{\ell\ell} = (-12 \pm 15) \%$	PL fit, reco level, 3ℓ events			
Theory		$A_C^{\ell\ell} = (-9^{+12}_{-14}) \%$	NLO simulation			
CMS [413]	138	$A_C^{\ell\ell} = (-19^{+16}_{-18}) \%$	3ℓ events			
Theory		$A_C^{\ell\ell} = (-6.3^{+0.8}_{-0.6}) \%,$	Sherpa 2.2.10 (NLO QCD +EW)			
ATLAS [412]	139	$A_C^{\ell\ell} = (-11 \pm 18) \%$	PL fit, particle level			

soft-lepton tagging in b decays combined with a kinematic likelihood fit. The measured top-quark charge was 0.64 ± 0.02 (stat.) ±0.08 (syst.), excluding the exotic Q=-4/3 hypothesis at more than 8σ [432]. CMS also tested the exotic-charge scenario at $\sqrt{s}=7$ TeV in the muon+jets channel, exploiting the correlation between high- $p_{\rm T}$ muons from W decays and soft muons from B-hadron decays inside b-jets. Using an asymmetry variable A, with A=-1 corresponding to Q=-4/3 and A=+1 to Q=+2/3, CMS preliminary measured $A=0.97\pm0.12$ (stat.) ±0.31 (syst.), in agreement with the SM and excluding the exotic scenario at 99.9% C.L. [433].

61.2.6 Physics beyond the SM

The top quark plays a special role in the SM. Being the only quark with a coupling to the Higgs boson of order one, it provides the most important contributions to the quadratic radiative corrections to the Higgs mass exposing the issue of the naturalness of the SM. It is therefore very common for models where the naturalness problem is addressed to have new physics associated with the top quark. In SUSY, for instance, naturalness predicts the scalar top-quark partners to be the lightest among the squarks and to be accessible at the LHC energies (see the review "Supersymmetry: Theory"). In models where the Higgs is a pseudo-Goldstone boson, such as Little Higgs models, naturalness predicts the existence of partners of the top quarks with the same spin and color, but with different EW couplings, the so-called vectorial t'. Stops and t''s are expected to have sizeable branching ratios to top quarks. Another intriguing prediction of SUSY models with universal couplings at the unification scale is that for a top-quark mass close to the measured value, the running of the Yukawa coupling down to 1 TeV naturally leads to the radiative breaking of the EW symmetry [434]. In fact, the top quark plays a role in the dynamics of EW symmetry breaking in many models [435]. One example is topcolor [436], where a large top-quark mass can be generated through the formation of a dynamic $t\bar{t}$ condensate, X, which is formed by a new strong gauge force coupling preferentially to the third generation. Another example is topcolor-assisted technicolor [437], predicting the existence of a heavy Z' boson that couples preferentially to the third generation of quarks. If light enough, such a state might be directly accessible at the present hadron collider energies, or if too heavy, lead to four-top interactions possibly visible in the tttt final state.

61.2.6.1 Direct searches for physics beyond the SM

In this section, the most recent direct searches for effects beyond the SM in top-quark production and decay are reviewed. These searches can be broadly divided into two categories: (i) searches for $t\bar{t}$ resonances, and (ii) searches for rare non-SM interactions involving top quarks, including flavor-changing neutral currents (FCNC). Resonance searches in the top sector include (a) $t\bar{t}$ resonances, in which a hypothetical heavy particle X decays into a $t\bar{t}$ pair, and (b) searches where a non-SM decay product of the top quark is identified through its resonant signature. The most recent results belong to the latter class. For comprehensive discussions of $X \to t\bar{t}$ searches, see Refs. [438–440]. Searches for rare non-SM interactions and FCNC processes are interpreted within the EFT framework described in Section 61.1.3. Here we focus on the limits on branching ratios obtained from these searches, while the corresponding EFT interpretations are discussed in Section 61.2.6.2.

FCNC searches. The most recent FCNC searches target the decay $t \to qH$ in $t\bar{t}$ production, or an FCNC vertex in single-top-quark production associated with a Higgs boson.

ATLAS probes both processes using $H \to VV$ decays. Neural-network outputs are used to define four signal regions, two each for production and decay, further divided into categories with two samesign leptons or three leptons [441]. Despite the small branching ratio, this channel provides the best sensitivity. The results are combined with complementary searches using Higgs-boson decays to $b\bar{b}$ [442], $\tau\tau$ [443], and $\gamma\gamma$ [444], accounting for correlations among parameters. The combined upper limits on the branching ratios are $\mathcal{B}(t \to Hu) < 2.6 \times 10^{-4}$ and $\mathcal{B}(t \to Hc) < 3.4 \times 10^{-4}$.

CMS uses Higgs decays to vector bosons and $\tau\tau$ [445], and combines these results with analyses targeting $H \to b\bar{b}$ [446] and $H \to \gamma\gamma$ [447]. As in the ATLAS case, the $H \to VV$ decay mode yields the highest sensitivity. The combined limits are $\mathcal{B}(t \to Hu) < 1.9 \times 10^{-4}$ and $\mathcal{B}(t \to Hc) < 3.7 \times 10^{-4}$. A comparison of the ATLAS and CMS results with predictions from representative BSM models is shown in Fig. 61.14.

Searches targeting tZq couplings use leptonic decays of the Z-boson and a trilepton final state.

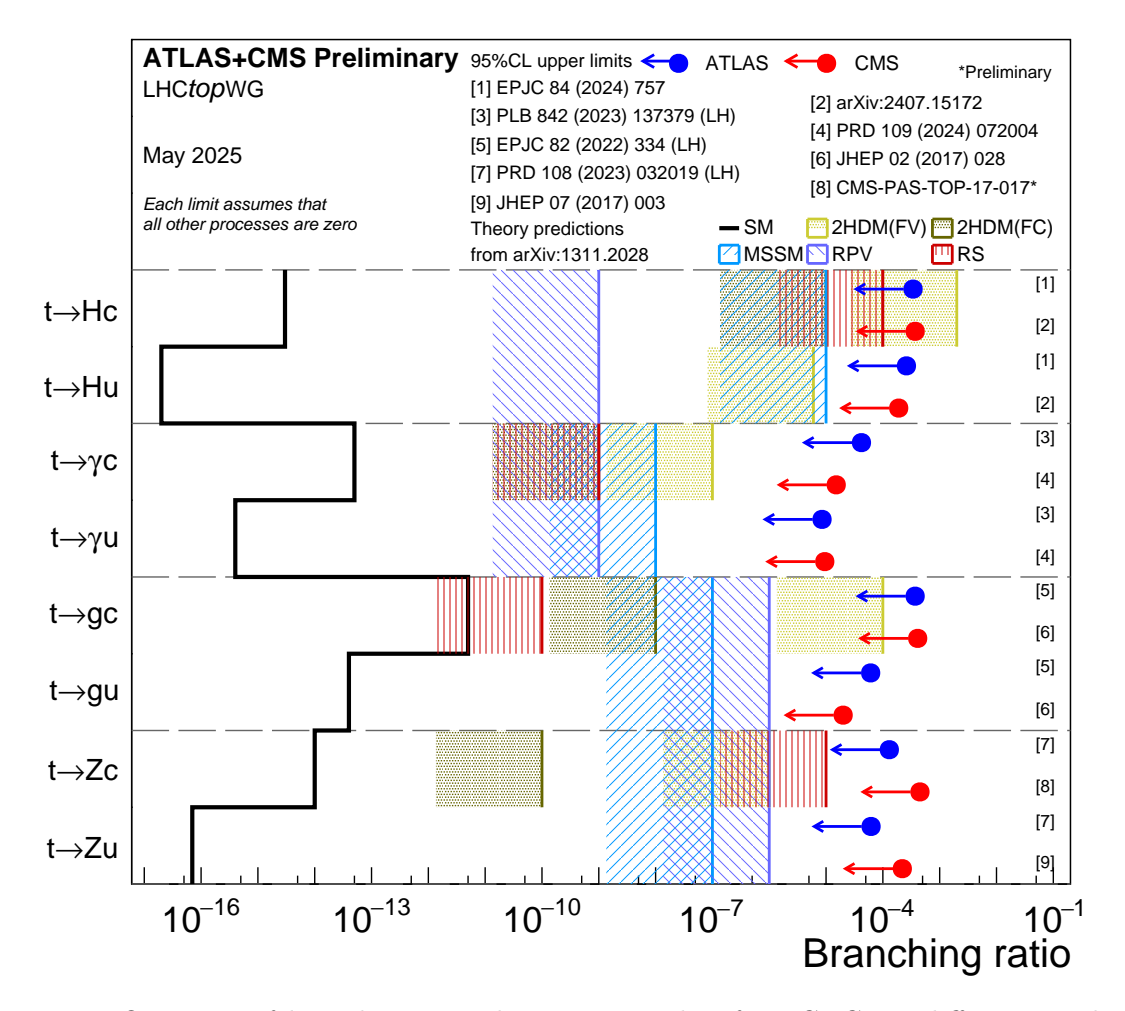


Figure 61.14: Overview of branching-ratio limits in searches for FCNCs in different production and decay channels, compared to different theory predictions. The LHCtopWG working group kindly provides the plot, status as of May 2025, see https://twiki.cern.ch/twiki/bin/view/LHCPhysics/LHCTopWGSummaryPlots.

In $t\bar{t}$ events, the signal occurs through the FCNC decay $t \to Zq$, in single-top quark the signal occurs through the associated production of a top quark and a Z-boson. The branching-ratio limits shown in Fig. 61.14 are for tZu and tZc left-handed couplings and assume, for tZu, that the tZc coupling is zero and vice versa. Reference [448] presents limits for right-handed couplings, which are close to the values quoted in Fig. 61.14 for left-handed couplings.

Searches targeting $t\gamma q$ couplings focus on a high- $p_{\rm T}$ photon in the final state. As with tZq couplings, signal events occur through top-quark decay in $t\bar{t}$ and through associated production of a top quark and a photon in single-top events. ATLAS has set limits on the corresponding EFT couplings, shown in Fig. 61.18 [449]. The limits are derived assuming left-handed couplings; those for right-handed couplings are also provided and are only slightly weaker.

FCNC couplings tgq between a top quark, a gluon, and an up or charm quark have been probed by ATLAS in single-top-quark production [450]. Such couplings enhance the single-top-quark production cross section and, in the case of the tgc interaction, modify the rapidity distribution of the top quark due to the different PDFs of valence and sea quarks.

Searches for charged-lepton flavor violation. CMS has searched for for charged-lepton-flavor-violating (CLFV) interactions in both production, $q \to e\mu t$, and decay, $t \to e\mu q$, with q = u or c [451] in final states with two leptons. Additional searches have been performed in final states with three leptons [452] and, more recently, in single-lepton final states targeting $\mu\tau qt$ interactions [453]. Limits on scalar, vector, and tensor couplings are summarized in Tab. 61.26. These limits are also shown in Fig. 61.17 and compared with the corresponding ATLAS search for CLFV $\mu\tau qt$ interactions [454], which uses final states containing a same-sign dimuon pair.

Searches for baryon number violation. CMS recently reported a search for baryon-number violation (BNV) in top-quark production and decay [455], using events with two same-sign leptons and at least one b-tagged jet. Both single-top and top-quark-pair production modes are considered. Boosted decision trees are employed to discriminate signal from background processes. No significant excess is observed, and upper limits are set on the corresponding couplings. The obtained limits improve upon previous constraints by several orders of magnitude.

Table 61.26: 95% C.L. limits on branching ratios (BR) of the top quark in searches for charged-lepton flavor violation. All searches were carried out at $\sqrt{s} = 13$ TeV.

Exp.	Process	$N(\ell)$	BR limit	Reference
CMS	$t \to e\mu u \text{ (scalar)}$	2ℓ	0.07×10^{-6}	[451]
CMS	$t \to e\mu u \text{ (vector)}$	2ℓ	0.13×10^{-6}	[451]
CMS	$t \to e\mu u \text{ (tensor)}$	2ℓ	0.25×10^{-6}	[451]
CMS	$t \to e\mu c \text{ (scalar)}$	2ℓ	0.89×10^{-6}	[451]
CMS	$t \to e\mu c \text{ (vector)}$	2ℓ	1.31×10^{-6}	[451]
CMS	$t \to e\mu c \text{ (tensor)}$	2ℓ	2.59×10^{-6}	[451]
CMS	$t \to e\mu u \text{ (scalar)}$	3ℓ	0.012×10^{-6}	[452]
CMS	$t \to e\mu u \text{ (vector)}$	3ℓ	0.022×10^{-6}	[452]
CMS	$t \to e\mu u \text{ (tensor)}$	3ℓ	0.032×10^{-6}	[452]
CMS	$t \to e\mu c \text{ (scalar)}$	3ℓ	0.216×10^{-6}	[452]
CMS	$t \to e\mu c \text{ (vector)}$	3ℓ	0.369×10^{-6}	[452]
CMS	$t \to e\mu c \text{ (tensor)}$	3ℓ	0.498×10^{-6}	[452]
ATLAS	$t \to \mu \tau u \text{ (scalar)}$	$2\ell SS$	0.20×10^{-6}	[454]
CMS	$t \to \mu \tau u \text{ (scalar)}$	1ℓ	0.04×10^{-6}	[453]
ATLAS	$t \to \mu \tau u \text{ (vector)}$	$2\ell SS$	0.33×10^{-6}	[454]
CMS	$t \to \mu \tau u \text{ (vector)}$	1ℓ	0.08×10^{-6}	[453]
ATLAS	$t \to \mu \tau u \text{ (tensor)}$	$2\ell SS$	0.52×10^{-6}	[454]
CMS	$t \to \mu \tau u \text{ (tensor)}$	1ℓ	0.12×10^{-6}	[453]
ATLAS	$t \to \mu \tau c \text{ (scalar)}$	$2\ell SS$	3.40×10^{-6}	[454]
CMS	$t \to \mu \tau c \text{ (scalar)}$	1ℓ	0.81×10^{-6}	[453]
ATLAS	$t \to \mu \tau c \text{ (vector)}$	$2\ell SS$	5.30×10^{-6}	[454]
CMS	$t \to \mu \tau c \text{ (vector)}$	1ℓ	1.71×10^{-6}	[453]
ATLAS	$t \to \mu \tau c \text{ (tensor)}$	$2\ell SS$	6.70×10^{-6}	[454]
CMS	$t \to \mu \tau c \text{ (tensor)}$	1ℓ	2.05×10^{-6}	[453]

Resonance searches. While technically an FCNC search, a decay of the type $t \to qX$ where q = u or c, could be missed when X is not the expected quark or boson. ATLAS has searched for

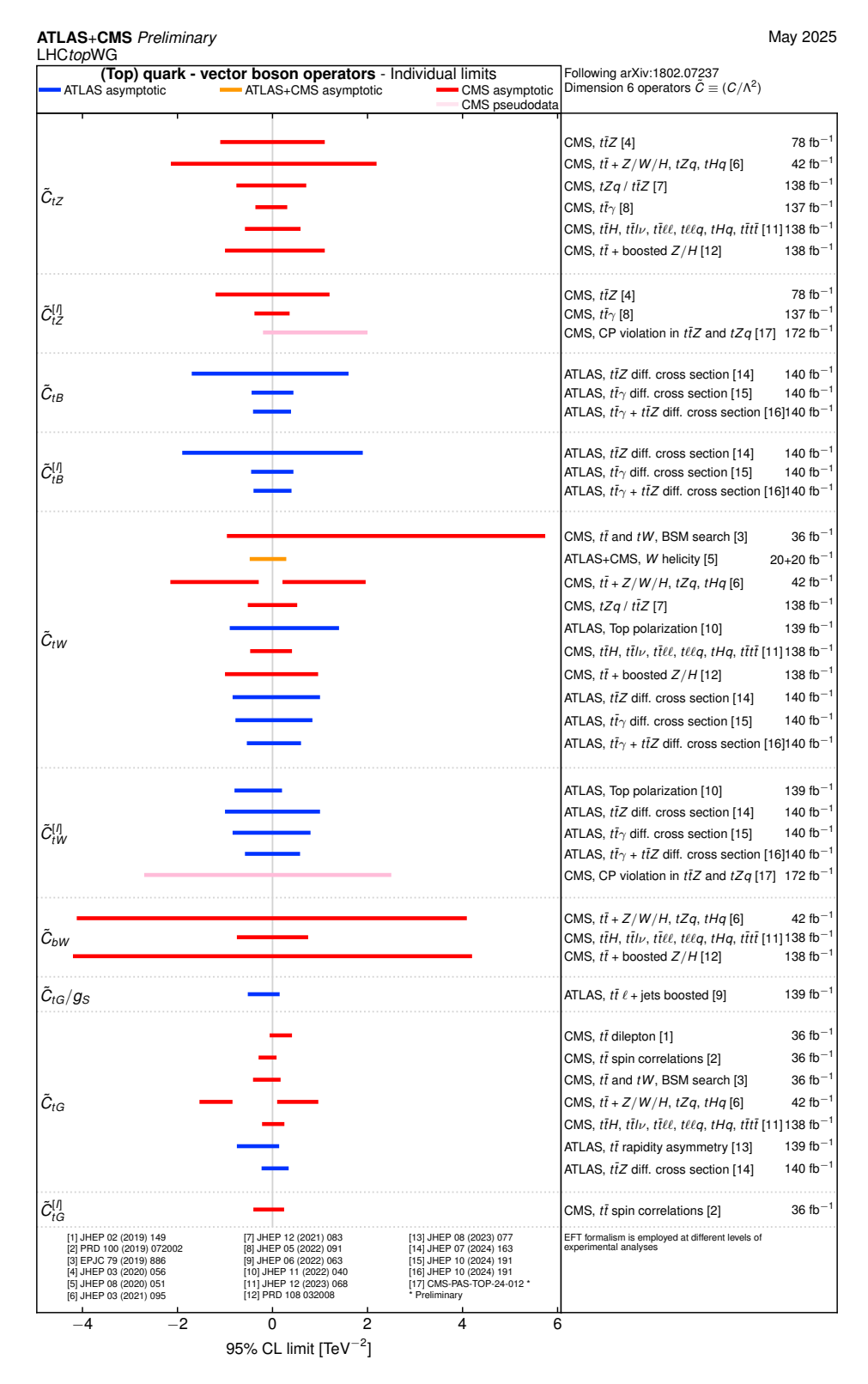


Figure 61.15: Wilson coefficients (WCs) corresponding to vector boson operators and related BSM search references. The LHCtopWG working group kindly provides the plot, status as of May 2025, see https://twiki.cern.ch/twiki/bin/view/LHCPhysics/LHCTopWGSummaryPlots.

 $t \to qX$ where X is a light scalar with a mass below the top quark that decays to $b\bar{b}$ [442]. Such phenomena exist in composite Higgs models [456]. The ATLAS search used $t\bar{t}$ events and separated signal from background by categorizing events according to the number of jets and the number of jets tagged as originating from b-quarks. The observed limits correspond to the product of the BR $t \to qX$ and $X \to b\bar{b}$. The limit in the $t \to uX(t \to cX)$ channel is 0.019% (0.018%) for $M_X = 20$ GeV and 0.062% (0.078%) for $M_X = 160$ GeV.

There is a wide range of searches for new resonances decaying into $t\bar{t}$ events which are partially covered in the section "Hypothetical particles and concepts" of this review.

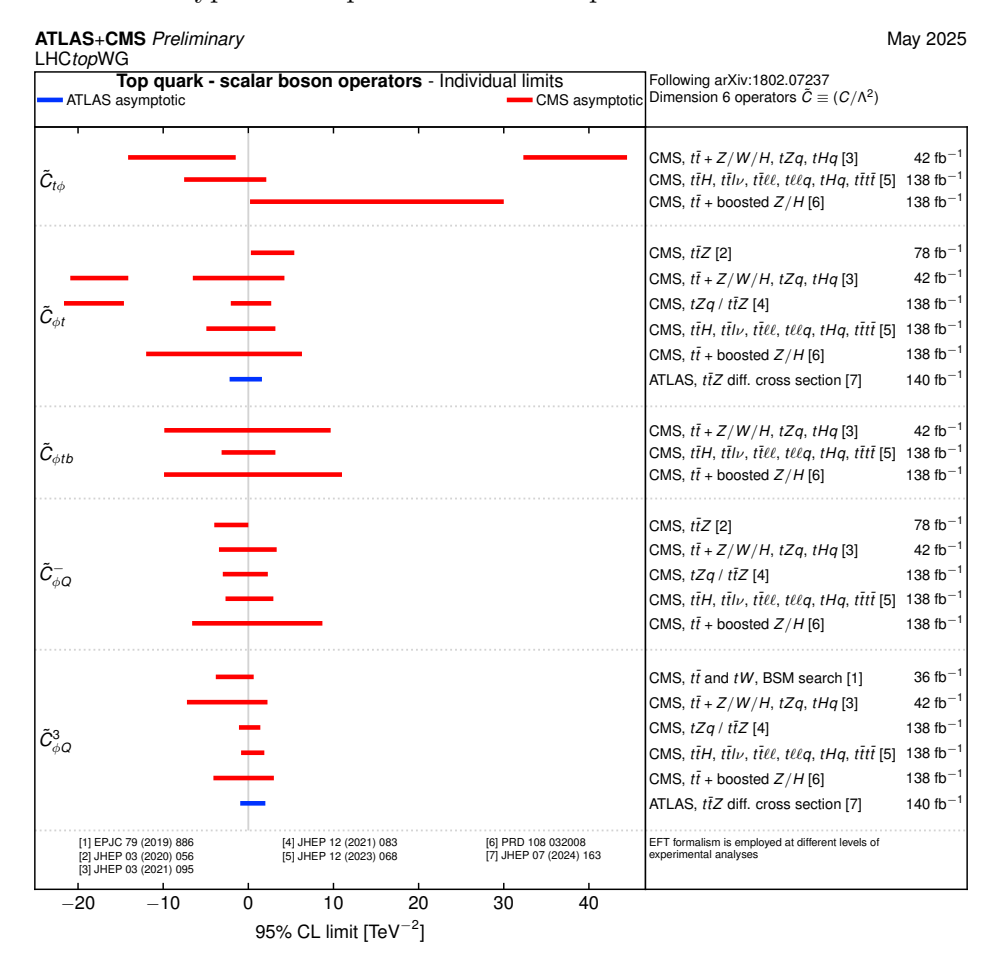


Figure 61.16: Wilson coefficients (WCs) corresponding to scalar boson operators and related BSM search references. The LHCtopWG working group kindly provides the plot, status as of May 2025, see https://twiki.cern.ch/twiki/bin/view/LHCPhysics/LHCTopWGSummaryPlots.

61.2.6.2 Effective field theory

As described in Sec. 61.1.3, EFTs have become an important tool to search for new physics processes. The EFT interpretations benefit from the increasing datasets, as this allows for very precise inclusive and differential measurements of top processes. These precision measurements of diverse sets of observables allows to improve the EFT interpretations by combining these measurements in a global analysis, as can be done using tools such as SMEFit [457]. In Ref. [458], Zhang and Willenbrock elucidate the advantages of the EFT approach compared to the vertex-function approach for searching for BSM effects in top-quark interactions, including the fact that the EFT approach incorporates the SM gauge symmetry and contact interactions that are neglected in the

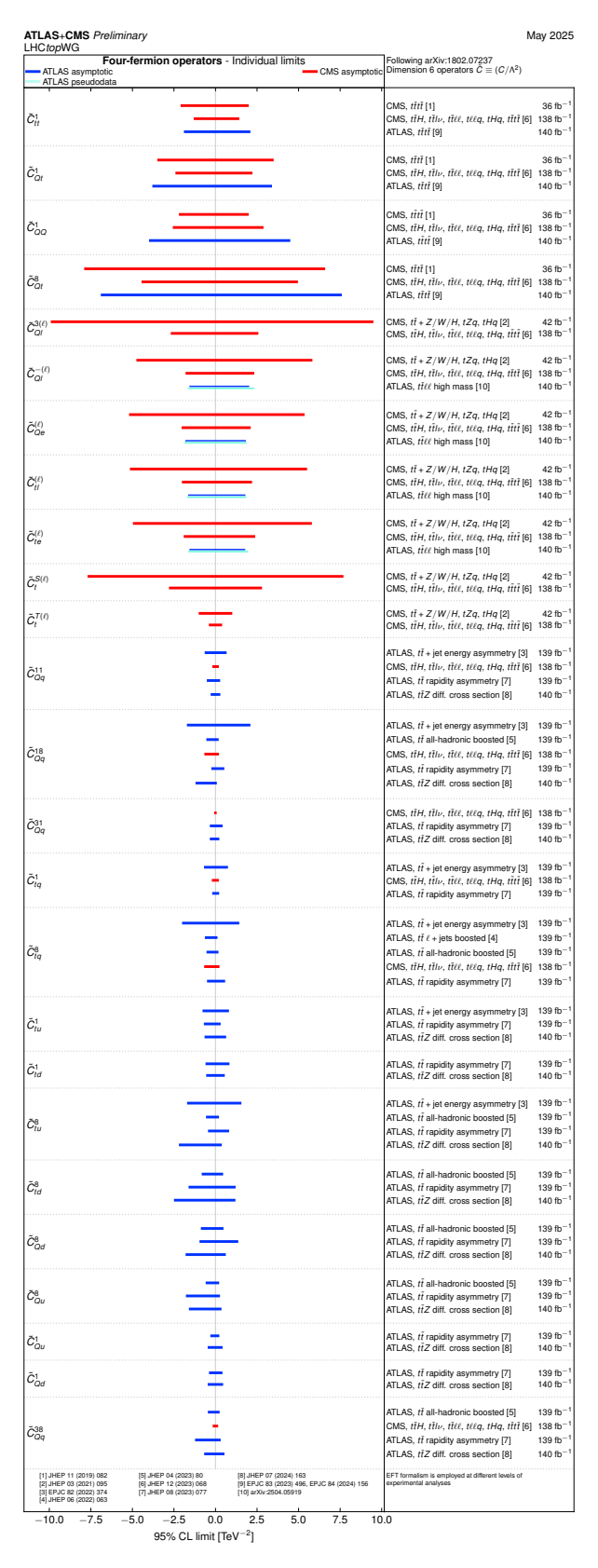


Figure 61.17: Wilson coefficients (WCs) corresponding to four-fermion operators and related BSM search references. The LHCtopWG working group kindly provides the plot, status as of May 2025, see https://twiki.cern.ch/twiki/bin/view/LHCPhysics/LHCTopWGSummaryPlots.

vertex-function approach. As a result of these advantages, EFTs have become the dominant technique for evaluating search limits, and the most recent results are reviewed in this section.

The top-EFT operators are categorized as follows: operators involving the contact-interaction of four fermions together (four-fermion operators), operators involving the interaction between top quarks and a vector boson (vector-boson operators) and between top quarks and scalar bosons (scalar-boson operators). Operators can change the overall rate of top-quark production, modify the kinematics of production and/or decay, or produce new interactions, such as FCNCs. To date, all results are consistent with the SM expectation of zero for each Wilson coefficient C. The bounds are set on C/Λ^2 and have a dimension of TeV⁻2. Once the value for the unknown coupling strength C of the interaction is set, the size of the interval is inversely proportional to the square of the new physics scale.

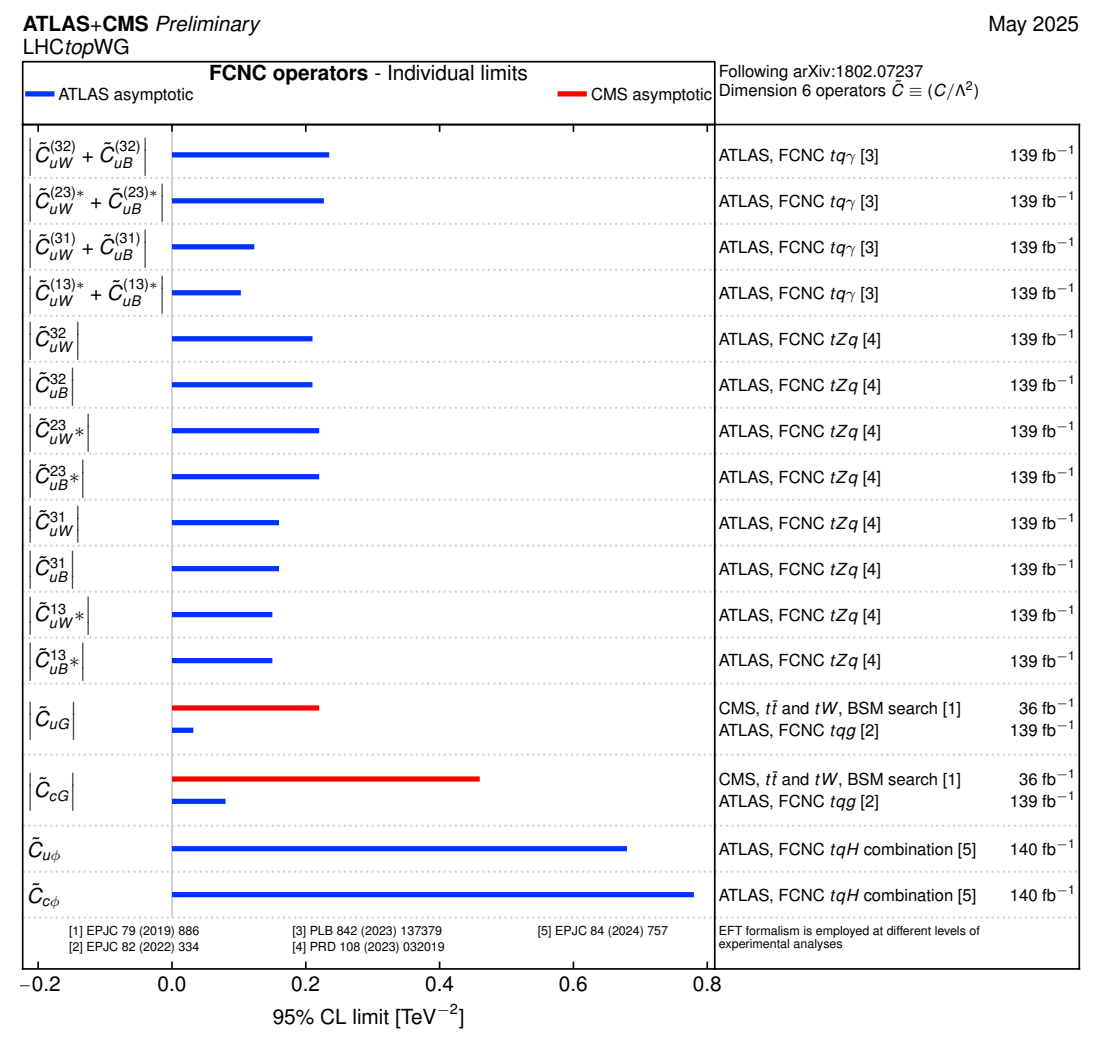


Figure 61.18: Wilson coefficients (WCs) corresponding to flavor-changing-neutral-current (FCNC) operators and related BSM search references. The LHCtopWG working group kindly provides the plot, status as of May 2025, see https://twiki.cern.ch/twiki/bin/view/LHCPhysics/LHCTopWGSummaryPlots.

The individual limits from the ATLAS and CMS results provided by the LHCtopWG can be found in Figs. 61.15–61.18. Marginalised limits and different representations can be found on the

LHCtopWG page linked from the individual figure captions. Additional limits and references can be found in the listings and for example in the references [199, 216, 451, 459, 460, 460–468].

61.3 Summary and outlook

In the three decades since its discovery, top-quark physics has evolved from the observation of a single particle into a precision field that probes the SM at the highest energy scales. With the large datasets collected at the LHC, a wide range of top-quark properties have been measured with unprecedented accuracy. Production cross sections and other \sqrt{s} -dependent quantities have been determined at multiple energies, enabling stringent tests of QCD and EW production mechanisms. All results to date are consistent with SM predictions, providing strong validation of the theory. The precision will continue to improve as larger datasets and refined theoretical and experimental techniques become available, enhancing sensitivity to potential deviations from the SM.

The large top-quark samples recorded in Run 2 have enabled detailed studies of both $t\bar{t}$ production and single-top processes, all now firmly established at the LHC. Many associated production modes have also become accessible: while Run 1 provided the first evidence and observations of processes such as $t\bar{t}\gamma$, $t\bar{t}Z$, $t\bar{t}W$, $t\bar{t}H$, and $t\bar{t}t\bar{t}$, Run 2 has opened the path to precision studies of these reactions. Rare single-top associated modes, including tZ, $t\gamma$, and tWZ, are now being measured as well, extending sensitivity to the structure of top-quark couplings and to possible new physics. Many of these results are interpreted within the framework of EFT, providing global constraints on higher-dimensional operators that parameterize deviations from the SM.

The complexity of top-quark final states and the precision they demand have driven major advances in analysis techniques, notably multivariate methods and machine learning, which are now standard in collider physics. The large top-quark mass, its unique role in electroweak symmetry breaking, and its potential link to new dynamics continue to make it a central focus of particle physics.

For many measurements, uncertainties in event simulation remain the dominant limitation on precision. Differential measurements are essential to further reduce these uncertainties, particularly in complex final states such as $t\bar{t}$ +heavy-flavor jets.

While most of the Run 2 dataset at $\sqrt{s}=13$ TeV has been analyzed, Run 3 at $\sqrt{s}=13.6$ TeV, with an expected integrated luminosity exceeding 300 fb⁻¹, will more than double the available statistics. The forthcoming High-Luminosity LHC (HL-LHC) phase, expected to deliver up to 3 ab⁻¹ of data, will mark the next major step in this progression—from discovery to precision characterization. It will enable sub-percent precision in key measurements, stringent global EFT constraints, and unprecedented sensitivity to rare processes and possible new interactions. With many results already published and more to come, top-quark physics continues to provide one of the most powerful tools for testing the SM and exploring physics at the TeV scale.

CDF and DØ notes can be retrieved from

```
https://inspirehep.net
with the search command "find CDF-NOTE-XXXXX" or "find D0 Note XXXX",
and ATLAS note references from
```

https://twiki.cern.ch/twiki/bin/view/AtlasPublic/TopPublicResults, and CMS note references from

https://twiki.cern.ch/twiki/bin/view/CMSPublic/PhysicsResultsTOP, and plots provided by the LHC Top Working Group from

https://twiki.cern.ch/twiki/bin/view/LHCPhysics/LHCTopWGSummaryPlots.

References

- [1] A. Hayrapetyan et al. (ATLAS, CMS), Phys. Rev. Lett. 132, 26 (2024), [arXiv:2402.08713].
- [2] G. Degrassi et al., JHEP 08, 098 (2012), [arXiv:1205.6497].

- [3] D. Buttazzo et al., JHEP 12, 089 (2013), [arXiv:1307.3536].
- [4] A. Andreassen, W. Frost and M. D. Schwartz, Phys. Rev. D **97**, 5, 056006 (2018), [arXiv:1707.08124].
- [5] A. H. Hoang et al., JHEP **04**, 003 (2018), [arXiv:1704.01580].
- [6] P. Marquard et al., Phys. Rev. Lett. 114, 14, 142002 (2015), [arXiv:1502.01030].
- [7] P. Nason, The Top Mass in Hadronic Collisions, 123–151 (2019), [arXiv:1712.02796].
- [8] A. H. Hoang, Ann. Rev. Nucl. Part. Sci. 70, 225 (2020), [arXiv:2004.12915].
- [9] M. Jezabek and J. H. Kuhn, Nucl. Phys. **B314**, 1 (1989).
- [10] A. Czarnecki and K. Melnikov, Nucl. Phys. B544, 520 (1999), [hep-ph/9806244]; K. G. Chetyrkin et al., Phys. Rev. D60, 114015 (1999), [hep-ph/9906273].
- [11] L.-B. Chen et al., Phys. Rev. D 108, 5, 054003 (2023), [arXiv:2212.06341].
- [12] I. I. Y. Bigi et al., Phys. Lett. **B181**, 157 (1986).
- [13] A. H. Hoang et al., Phys. Rev. **D65**, 014014 (2002), [hep-ph/0107144].
- [14] K. Hagiwara, Y. Sumino and H. Yokoya, Phys. Lett. **B666**, 71 (2008), [arXiv:0804.1014].
- [15] Y. Kiyo et al., Eur. Phys. J. C 60, 375 (2009), [arXiv:0812.0919].
- [16] B. Fuks et al., Phys. Rev. D 104, 3, 034023 (2021), [arXiv:2102.11281].
- [17] G. Eilam, J. L. Hewett and A. Soni, Phys. Rev. D 44, 1473 (1991), [Erratum: Phys.Rev.D 59, 039901 (1999)].
- [18] J. A. Aguilar-Saavedra, Acta Phys. Polon. B **35**, 2695 (2004), [hep-ph/0409342].
- [19] S. Weinberg, Phys. Rev. Lett. 43, 1566 (1979).
- [20] W. Buchmuller and D. Wyler, Nucl. Phys. B **268**, 621 (1986).
- [21] B. Grzadkowski et al., JHEP 10, 085 (2010), [arXiv:1008.4884].
- [22] D. Barducci et al. (2018), [arXiv:1802.07237].
- [23] J. A. Aguilar-Saavedra, Nucl. Phys. B 812, 181 (2009), [arXiv:0811.3842].
- [24] C. Zhang and S. Willenbrock, Phys. Rev. **D83**, 034006 (2011), [arXiv:1008.3869].
- [25] I. Brivio, JHEP **04**, 073 (2021), [arXiv:2012.11343].
- [26] C. Degrande et al., Phys. Rev. D 103, 9, 096024 (2021), [arXiv:2008.11743].
- [27] R. S. Chivukula and H. Georgi, Phys. Lett. B 188, 99 (1987).
- [28] L. J. Hall and L. Randall, Phys. Rev. Lett. 65, 2939 (1990).
- [29] G. D'Ambrosio et al., Nucl. Phys. B **645**, 155 (2002), [hep-ph/0207036].
- [30] W. Bernreuther, D. Heisler and Z.-G. Si, JHEP 12, 026 (2015), [arXiv:1508.05271].
- [31] A. Behring et al., Phys. Rev. Lett. 123, 8, 082001 (2019), [arXiv:1901.05407].
- [32] Y. Afik and J. R. M. de Nova, Eur. Phys. J. Plus 136, 9, 907 (2021), [arXiv:2003.02280].
- [33] G. Aad et al. (ATLAS), Nature 633, 8030, 542 (2024), [arXiv:2311.07288].
- [34] A. Hayrapetyan et al. (CMS), Rept. Prog. Phys. 87, 11, 117801 (2024), [arXiv:2406.03976].
- [35] A. Hayrapetyan et al. (CMS), Physical Review D 110, 11 (2024), [arXiv:2409.11067].
- [36] S. Frixione, P. Nason and B. R. Webber, JHEP 08, 007 (2003), [hep-ph/0305252]; W. Kim and H. Shin, JHEP 07, 070 (2007), [arXiv:0706.3563]; J. M. Campbell et al., JHEP 04, 114 (2015), [arXiv:1412.1828].
- [37] T. Ježo *et al.*, Eur. Phys. J. **C76**, 12, 691 (2016), [arXiv:1607.04538].

- [38] S. Frixione et al., JHEP 03, 092 (2006), [hep-ph/0512250]; V. Marotta and A. Naddeo, JHEP 08, 029 (2008), [arXiv:0810.4759]; S. Alioli et al., JHEP 09, 111 (2009), [Erratum: JHEP02,011(2010)], [arXiv:0907.4076]; E. Re, Eur. Phys. J. C71, 1547 (2011), [arXiv:1009.2450]; R. Frederix, E. Re and P. Torrielli, JHEP 09, 130 (2012), [arXiv:1207.5391]; R. Frederix et al., JHEP 06, 027 (2016), [arXiv:1603.01178].
- [39] S. Frixione, P. Nason and G. Ridolfi, JHEP 09, 126 (2007), [arXiv:0707.3088].
- [40] S. Frixione and B. R. Webber, JHEP **06**, 029 (2002), [hep-ph/0204244].
- [41] P. Nason, JHEP 11, 040 (2004), [hep-ph/0409146].
- [42] J. Mazzitelli et al., Phys. Rev. Lett. 127, 6, 062001 (2021), [arXiv:2012.14267].
- [43] J. Mazzitelli et al., JHEP 04, 079 (2022), [arXiv:2112.12135], URL https://doi.org/10. 1007/JHEP04(2022)079.
- [44] M. Czakon, P. Fiedler and A. Mitov, Phys. Rev. Lett. 110, 252004 (2013), [arXiv:1303.6254].
- [45] S. Catani et al., JHEP 07, 100 (2019), [arXiv:1906.06535].
- [46] M. Czakon et al., JHEP 10, 186 (2017), [arXiv:1705.04105].
- [47] M. Czakon and A. Mitov, Comput. Phys. Commun. 185, 2930 (2014), [arXiv:1112.5675].
- [48] M. Botje et al. (2011), [arXiv:1101.0538].
- [49] A. D. Martin et al., Eur. Phys. J. C 64, 653 (2009), [arXiv:0905.3531].
- [50] J. Gao et al., Phys. Rev. D 89, 3, 033009 (2014), [arXiv:1302.6246].
- [51] R. D. Ball et al., Nucl. Phys. B 867, 244 (2013), [arXiv:1207.1303].
- [52] L. Lönnblad and S. Prestel, JHEP **03**, 166 (2013), [arXiv:1211.7278].
- [53] R. Frederix and S. Frixione, JHEP 12, 061 (2012), [arXiv:1209.6215].
- [54] A. Bredenstein et al., JHEP 03, 021 (2010), [arXiv:1001.4006].
- [55] R. Frederix and T. Moskalets, Eur. Phys. J. C 84, 7, 763 (2024), [arXiv:2403.14419].
- [56] L. Apolinário et al., Phys. Rev. Lett. 120, 23, 232301 (2018), [arXiv:1711.03105].
- [57] A. Broggio et al., JHEP 08, 039 (2019), [arXiv:1907.04343].
- [58] S. Catani *et al.*, Phys. Rev. Lett. **130**, 11, 111902 (2023), [arXiv:2210.07846].
- [59] L. Buonocore et al., Phys. Rev. Lett. 131, 23, 231901 (2023), [arXiv:2306.16311].
- [60] N. Kidonakis and C. Foster, Physics Letters B 860, 139146 (2025), revised to match the published version, [arXiv:2410.01214], URL https://arxiv.org/abs/2410.01214.
- [61] D. Stremmer and M. Worek, JHEP **07**, 091 (2024), [arXiv:2403.03796].
- [62] S. Devoto et al., JHEP **03**, 189 (2025), [arXiv:2411.15340].
- [63] E. Boos and L. Dudko, Int. J. Mod. Phys. A 37, 05, 2250023 (2022), [arXiv:2107.07629].
- [64] R. Frederix, D. Pagani and M. Zaro, JHEP **02**, 031 (2018), [arXiv:1711.02116].
- [65] M. van Beekveld, A. Kulesza and L. M. Valero (2022), [arXiv:2212.03259].
- [66] D. Pagani et al., JHEP **09**, 155 (2021), [arXiv:2106.02059].
- [67] R. Balsach et al. (2025), [arXiv:2503.15043].
- [68] S. S. D. Willenbrock and D. A. Dicus, Phys. Rev. **D34**, 155 (1986).
- [69] S. Cortese and R. Petronzio, Phys. Lett. **B253**, 494 (1991).
- [70] N. Kidonakis, Phys. Rev. **D82**, 054018 (2010), [arXiv:1005.4451].
- [71] T. M. P. Tait and C. P. Yuan, Phys. Rev. **D63**, 014018 (2000), [hep-ph/0007298].

- [72] J. Campbell, T. Neumann and Z. Sullivan, JHEP **02**, 040 (2021), [arXiv:2012.01574].
- [73] M. Brucherseifer, F. Caola and K. Melnikov, Phys. Lett. **B736**, 58 (2014), [arXiv:1404.7116].
- [74] E. L. Berger, J. Gao and H. X. Zhu, JHEP 11, 158 (2017), [arXiv:1708.09405].
- [75] N. Kidonakis, Phys. Rev. **D81**, 054028 (2010), [arXiv:1001.5034].
- [76] S. Frixione et al., JHEP 07, 029 (2008), [arXiv:0805.3067].
- [77] C. D. White et al., JHEP 11, 074 (2009), [arXiv:0908.0631].
- [78] Z. L. Liu and J. Gao, Phys. Rev. D 98, 7, 071501 (2018), [arXiv:1807.03835].
- [79] C. Degrande et al., JHEP 10, 005 (2018), [arXiv:1804.07773].
- [80] D. Pagani, I. Tsinikos and E. Vryonidou, JHEP 08, 082 (2020), [arXiv:2006.10086].
- [81] H. E. Faham et al., JHEP **01**, 100 (2022), [arXiv:2111.03080].
- [82] F. Abe et al. (CDF), Phys. Rev. Lett. 74, 2626 (1995).
- [83] Abachi et al. (D0), Phys. Rev. Lett. 74, 2632 (1995).
- [84] R. Aaij et al. (LHCb), Phys. Rev. Lett. 115, 11, 112001 (2015), [arXiv:1506.00903].
- [85] A. M. Sirunyan et al. (CMS), Phys. Rev. Lett. 125, 22, 222001 (2020), [arXiv:2006.11110].
- [86] G. Aad et al. (ATLAS), Phys. Rev. Lett. 134, 142301 (2025), [arXiv:2411.10186].
- [87] (2025), cMS Collaboration, CMS-PAS-HIN-24-021, URL https://inspirehep.net/literature/2970211.
- [88] A. M. Sirunyan et al. (CMS), Phys. Rev. Lett. 119, 24, 242001 (2017), [arXiv:1709.07411].
- [89] G. Aad et al. (ATLAS), JHEP 11, 101 (2024), [arXiv:2405.05078].
- [90] A. Hayrapetyan et al. (CMS), ROPP 88, 8, 087801 (2025), [arXiv:2503.22382].
- [91] ATLAS Collaboration, ATLAS-CONF-2025-008.
- [92] M. Czakon, D. Heymes and A. Mitov, Phys. Rev. Lett. 116, 8, 082003 (2016), [arXiv:1511.00549].
- [93] G. D'Agostini, Nucl. Instrum. Meth. A **362**, 487 (1995).
- [94] T. Adye, in "PHYSTAT 2011," 313–318, CERN, Geneva (2011), [arXiv:1105.1160].
- [95] G. Aad et al. (ATLAS), Eur. Phys. J. C 80, 10, 957 (2020), [Erratum: Eur.Phys.J.C 81, 29 (2021), Erratum: Eur.Phys.J.C 81, 398 (2021)], [arXiv:2004.03447].
- [96] A. M. Sirunyan et al. (CMS), JHEP **01**, 183 (2019), [arXiv:1807.03825].
- [97] A. Hocker and V. Kartvelishvili, Nucl. Instrum. Meth. A 372, 469 (1996), [hep-ph/9509307].
- [98] V. Blobel, in "Conference on Advanced Statistical Techniques in Particle Physics," 258–267 (2002), [hep-ex/0208022].
- [99] T. Affolder et al. (CDF), Phys. Rev. D 64, 032002 (2001), [hep-ex/0101036].
- [100] V. M. Abazov et al. (D0), Phys. Rev. **D67**, 012004 (2003), [hep-ex/0205019].
- [101] V. M. Abazov et al. (D0), Phys. Rev. **D94**, 092004 (2016), [arXiv:1605.06168].
- [102] T. Aaltonen et al. (CDF), Phys. Rev. **D88**, 091103 (2013), [arXiv:1304.7961].
- [103] T. A. Aaltonen et al. (CDF, D0), Phys. Rev. **D89**, 7, 072001 (2014), [arXiv:1309.7570].
- [104] T. A. Aaltonen et al. (CDF), Phys. Rev. **D89**, 9, 091101 (2014), [arXiv:1402.6728].
- [105] T. Aaltonen et al. (CDF), Phys. Rev. Lett. 105, 012001 (2010), [arXiv:1004.3224].
- [106] G. Aad et al. (ATLAS), JHEP **06**, 138 (2023), [arXiv:2207.01354].
- [107] A. Hayrapetyan et al. (CMS), JHEP **04**, 099 (2025), [arXiv:2410.21631].

- [108] G. Aad *et al.* (ATLAS), Eur. Phys. J. **C74**, 10, 3109 (2014), [Addendum: Eur. Phys. J.C76,no.11,642(2016)], [arXiv:1406.5375].
- [109] V. Khachatryan et al. (CMS), JHEP 08, 029 (2016), [arXiv:1603.02303].
- [110] M. Aaboud et al. (ATLAS), Phys. Rev. D 108, 3, 032014 (2023), [arXiv:2212.00571].
- [111] S. Chatrchyan et al. (CMS), Phys. Lett. **B720**, 83 (2013), [arXiv:1212.6682].
- [112] S. Chatrchyan et al. (CMS), JHEP 11, 067 (2012), [arXiv:1208.2671].
- [113] G. Aad et al. (ATLAS), JHEP **05**, 059 (2012), [arXiv:1202.4892].
- [114] S. Chatrchyan et al. (CMS), JHEP **05**, 065 (2013), [arXiv:1302.0508].
- [115] S. Chatrchyan et al. (CMS), Phys. Rev. **D85**, 112007 (2012), [arXiv:1203.6810].
- [116] G. Aad et al. (ATLAS), Phys. Lett. **B717**, 89 (2012), [arXiv:1205.2067].
- [117] S. Chatrchyan et al. (CMS), Eur. Phys. J. C73, 4, 2386 (2013), [arXiv:1301.5755].
- [118] G. Aad et al. (ATLAS), Eur. Phys. J. C73, 3, 2328 (2013), [arXiv:1211.7205].
- [119] J. Campbell et al., MCFM: parton-level Monte Carlo programhttps://mcfm.fnal.gov/.
- [120] S. Chatrchyan et al. (CMS), Eur. Phys. J. C73, 3, 2339 (2013), [arXiv:1211.2220].
- [121] V. Khachatryan et al. (CMS), Phys. Rev. **D94**, 5, 052006 (2016), [arXiv:1607.00837].
- [122] S. Chatrchyan *et al.* (CMS), Eur. Phys. J. **C74**, 3014 (2015), [Erratum: Eur. Phys. J.C75,no.5,216(2015)], [arXiv:1404.3171].
- [123] G. Aad et al. (ATLAS), Eur. Phys. J. C73, 1, 2261 (2013), [arXiv:1207.5644].
- [124] G. Aad et al. (ATLAS), Phys. Rev. **D90**, 7, 072004 (2014), [arXiv:1407.0371].
- [125] G. Aad et al. (ATLAS), JHEP **06**, 100 (2015), [arXiv:1502.05923].
- [126] G. Aad *et al.* (ATLAS), Eur. Phys. J. **C74**, 10, 3109 (2014), [Addendum: Eur. Phys. J.C76,no.11,642(2016)], [arXiv:1406.5375].
- [127] S. Chatrchyan *et al.* (CMS), JHEP **02**, 024 (2014), [Erratum: JHEP02,102(2014)], [arXiv:1312.7582].
- [128] M. Aaboud et al. (ATLAS), Eur. Phys. J. C78, 487 (2018), [arXiv:1712.06857].
- [129] V. Khachatryan et al. (CMS), Eur. Phys. J. C77, 1, 15 (2017), [arXiv:1602.09024].
- [130] M. Aaboud et al. (ATLAS), Phys. Rev. **D95**, 7, 072003 (2017), [arXiv:1702.08839].
- [131] V. Khachatryan et al. (CMS), Phys. Lett. **B739**, 23 (2014), [arXiv:1407.6643].
- [132] V. Khachatryan et al. (CMS), Eur. Phys. J. C76, 3, 128 (2016), [arXiv:1509.06076].
- [133] G. Aad et al. (ATLAS, CMS), JHEP 07, 213 (2023), [arXiv:2205.13830].
- [134] M. Aaboud et al. (ATLAS), Phys. Rev. **D94**, 9, 092003 (2016), [arXiv:1607.07281].
- [135] G. Aad et al. (ATLAS), Eur. Phys. J. C76, 10, 538 (2016), [arXiv:1511.04716].
- [136] V. Khachatryan et al. (CMS), Eur. Phys. J. C75, 11, 542 (2015), [arXiv:1505.04480].
- [137] A. M. Sirunyan et al. (CMS), Eur. Phys. J. C77, 7, 459 (2017), [arXiv:1703.01630].
- [138] G. Aad et al. (ATLAS), Phys. Rev. **D93**, 3, 032009 (2016), [arXiv:1510.03818].
- [139] V. Khachatryan et al. (CMS), Phys. Rev. **D94**, 7, 072002 (2016), [arXiv:1605.00116].
- [140] G. Aad et al. (ATLAS), JHEP 07, 141 (2023), [arXiv:2303.15340].
- [141] A. M. Sirunyan et al. (CMS), Eur. Phys. J. C79, 5, 368 (2019), [arXiv:1812.10505].
- [142] G. Aad et al. (ATLAS), Phys. Lett. B 810, 135797 (2020), [arXiv:2006.13076].
- [143] A. Tumasyan et al. (CMS) (2021), [arXiv:2108.02803].

- [144] G. Aad et al. (ATLAS), Eur. Phys. J. C 80, 6, 528 (2020), [arXiv:1910.08819].
- [145] A. M. Sirunyan et al. (CMS), JHEP **09**, 051 (2017), [arXiv:1701.06228].
- [146] A. M. Sirunyan et al. (CMS), JHEP **02**, 191 (2020), [arXiv:1911.13204].
- [147] A. Tumasyan et al. (CMS, TOTEM) (2023), [arXiv:2310.11231].
- [148] R. Aaij et al. (LHCb), JHEP 08, 174 (2018), [arXiv:1803.05188].
- [149] A. M. Sirunyan et al. (CMS), JHEP **04**, 060 (2018), [arXiv:1708.07638].
- [150] V. Khachatryan et al. (CMS), Phys. Rev. **D95**, 9, 092001 (2017), [arXiv:1610.04191].
- [151] A. M. Sirunyan et al. (CMS), JHEP **06**, 002 (2018), [arXiv:1803.03991].
- [152] A. M. Sirunyan et al. (CMS), Phys. Rev. **D97**, 11, 112003 (2018), [arXiv:1803.08856].
- [153] G. Aad *et al.* (ATLAS), Eur. Phys. J. C **79**, 12, 1028 (2019), [Erratum: Eur.Phys.J.C 80, 1092 (2020)], [arXiv:1908.07305].
- [154] W. Bernreuther and Z.-G. Si, Physics Letters B **725**, 1–3, 115–122 (2013).
- [155] A. M. Sirunyan et al. (CMS), JHEP **02**, 149 (2019), [arXiv:1811.06625].
- [156] A. M. Sirunyan et al. (CMS), Eur. Phys. J. C 80, 7, 658 (2020), [arXiv:1904.05237].
- [157] A. Hayrapetyan et al. (CMS), JHEP **2025**, 2 (2025), [arXiv:2402.08486].
- [158] G. Aad et al. (ATLAS) (2025), [arXiv:2509.15066].
- [159] G. Aad et al. (ATLAS), JHEP 01, 033 (2021), [arXiv:2006.09274].
- [160] A. M. Sirunyan et al. (CMS), Phys. Rev. D 103, 5, 052008 (2021), [arXiv:2008.07860].
- [161] G. Aad et al. (ATLAS), JHEP **06**, 063 (2022), [arXiv:2202.12134].
- [162] M. Aaboud et al. (ATLAS), Phys. Rev. **D98**, 1, 012003 (2018), [arXiv:1801.02052].
- [163] G. Aad et al. (ATLAS), Phys. Rev. D 109, 112016 (2024), [arXiv:312.03797].
- [164] G. Aad et al. (ATLAS), Eur. Phys. J. C 83, 6, 518 (2023), [arXiv:2209.07874].
- [165] G. Aad et al. (ATLAS), Phys. Rev. D **106**, 3, 032008 (2022), [arXiv:2202.13901].
- [166] A. Tumasyan et al. (CMS), JHEP 08, 204 (2023), [arXiv:2303.10680].
- [167] G. Aad et al. (ATLAS), Phys. Lett. B 848, 138376 (2024), [arXiv:2308.09529].
- [168] A. M. Sirunyan et al. (CMS), JHEP **03**, 115 (2018), [arXiv:1711.03143].
- [169] A. Tumasyan et al. (CMS), JHEP **04**, 144 (2022), [arXiv:2112.09114].
- [170] F. Buccioni et al., JHEP 12, 15 (2019), [arXiv:1907.13624].
- [171] Aad, Georges and others, Eur. Phys. J. C 72, 2043 (2012), [arXiv:1203.5015].
- [172] G. Aad et al. (ATLAS), JHEP **01**, 020 (2015), [arXiv:1407.0891].
- [173] V. Khachatryan et al. (CMS), Eur. Phys. J. C 76, 7, 379 (2016), [arXiv:1510.03072].
- [174] G. Aad et al. (ATLAS), Eur. Phys. J. C 76, 642 (2016), [arXiv:1606.09490].
- [175] G. Aad et al. (ATLAS), Eur. Phys. J. C 77, 220 (2017), [arXiv:1610.09978].
- [176] G. Aad et al. (ATLAS), JHEP 10, 159 (2018), [arXiv:1802.06572].
- [177] A. M. Sirunyan et al. (CMS), Phys. Rev. D 97, 112003 (2018), [arXiv:1803.08856].
- [178] A. M. Sirunyan et al. (CMS), JHEP 07, 125 (2020), [arXiv:2003.06467].
- [179] G. Aad et al. (ATLAS), Phys. Rev. D 89, 072012 (2014), [arXiv:1304.6386].
- [180] V. Khachatryan et al. (CMS), Phys. Lett. **B746**, 132 (2015), [arXiv:1411.5621].
- [181] G. Aad et al. (ATLAS), Eur. Phys. J. C76, 1, 11 (2016), [arXiv:1508.06868].

- [182] M. Aaboud et al. (ATLAS), JHEP **04**, 046 (2019), [arXiv:1811.12113].
- [183] A. M. Sirunyan et al. (CMS), Phys. Lett. **B776**, 355 (2018), [arXiv:1705.10141].
- [184] A. M. Sirunyan et al. (CMS), JHEP 07, 125 (2020), [arXiv:2003.06467].
- [185] A. M. Sirunyan et al. (CMS), Phys. Lett. B 803, 135285 (2020), [arXiv:1909.05306].
- [186] A. Hayrapetyan et al. (CMS), JHEP **05**, 042 (2024), [arXiv:2309.14442].
- [187] Aad, Georges and others (ATLAS), JHEP **01**, 068 (2025), [arXiv:2407.13473].
- [188] A. M. Sirunyan et al. (CMS), Phys. Lett. B 820, 136565 (2021), [arXiv:2012.09225].
- [189] G. Aad et al. (ATLAS), Physics Letters B 860, 139177 (2025), [arXiv:2409.11305].
- [190] S. Chatrchyan et al. (CMS), Phys. Rev. Lett. 110, 172002 (2013), [arXiv:1303.3239].
- [191] G. Aad et al. (ATLAS), JHEP 11, 172 (2015), [arXiv:1509.05276].
- [192] V. Khachatryan et al. (CMS), JHEP **01**, 096 (2016), [arXiv:1510.01131].
- [193] M. Aaboud et al. (ATLAS), Phys. Rev. **D99**, 7, 072009 (2019), [arXiv:1901.03584].
- [194] A. M. Sirunyan et al. (CMS), JHEP 08, 011 (2018), [arXiv:1711.02547].
- [195] A. M. Sirunyan et al. (CMS), JHEP **03**, 056 (2020), [arXiv:1907.11270].
- [196] G. Aad et al. (ATLAS), Eur. Phys. J. C 81, 737 (2021), [arXiv:2103.12603].
- [197] G. Aad et al. (ATLAS), JHEP 07, 163 (2024), [arXiv:2312.04450].
- [198] A. Hayrapetyan et al. (CMS), JHEP **02**, 177 (2025), [arXiv:2410.23475].
- [199] A. Tumasyan et al. (CMS), Phys. Rev. D 108, 032008 (2023), [arXiv:2208.12837].
- [200] A. Tumasyan et al. (CMS), JHEP 07, 219 (2023), [arXiv:2208.06485].
- [201] A. Tumasyan et al., JHEP 07, 219 (2023), [arXiv:2208.06485].
- [202] G. Aad et al. (ATLAS), JHEP 07, 096 (2024), [arXiv:2401.05299].
- [203] O. Bessidskaia Bylund et al., JHEP 05, 052 (2016), [arXiv:1601.08193].
- [204] M. Schulze and Y. Soreq, Eur. Phys. J. C 76, 466 (2016), [arXiv:1603.08911].
- [205] A. O. Bouzas and F. Larios, Phys. Rev. D 87, 074015 (2013), [arXiv:1212.6575].
- [206] P.-F. Duan et al., Phys. Lett. B 766, 102 (2017), [arXiv:1612.00248].
- [207] T. Aaltonen et al. (CDF), Phys. Rev. **D84**, 031104 (2011), [arXiv:1106.3970].
- [208] G. Aad et al. (ATLAS), Phys. Rev. **D91**, 7, 072007 (2015), [arXiv:1502.00586].
- [209] M. Aaboud et al. (ATLAS), JHEP 11, 086 (2017), [arXiv:1706.03046].
- [210] K. Melnikov, M. Schulze and A. Scharf, Phys. Rev. **D83**, 074013 (2011), [arXiv:1102.1967].
- [211] A. M. Sirunyan et al. (CMS), JHEP 10, 006 (2017), [arXiv:1706.08128].
- [212] M. Aaboud et al. (ATLAS), Eur. Phys. J. C79, 5, 382 (2019), [arXiv:1812.01697].
- [213] G. Aad et al. (ATLAS), JHEP **09**, 049 (2020), [arXiv:2007.06946].
- [214] G. Aad et al. (ATLAS), JHEP **2024**, 10 (2024), [arXiv:2403.09452].
- [215] A. Tumasyan et al. (CMS), JHEP 12, 180 (2021), [arXiv:2107.01508].
- [216] A. Tumasyan et al. (CMS), JHEP **05**, 091 (2022), [arXiv:2201.07301].
- [217] CMS Collaboration, CMS-PAS-TOP-23-002.
- [218] G. Aad et al. (ATLAS) (2025), [arXiv:2506.05018].
- [219] A. M. Sirunyan et al. (CMS), JHEP 11, 082 (2019), [arXiv:1906.02805].
- [220] A. M. Sirunyan et al. (CMS), Eur. Phys. J. C 80, 2, 75 (2020), [arXiv:1908.06463].

- [221] G. Aad et al. (ATLAS), Eur. Phys. J. C 80, 11, 1085 (2020), [arXiv:2007.14858].
- [222] G. Aad et al. (ATLAS), JHEP 11, 118 (2021), [arXiv:2106.11683].
- [223] A. Tumasyan et al. (CMS), Phys. Lett. B 844, 138076 (2023), [arXiv:2303.03864].
- [224] G. Aad et al. (ATLAS), Eur. Phys. J. C 83, 6, 496 (2023), [arXiv:2303.15061].
- [225] A. Hayrapetyan et al. (CMS), Phys. Lett. B 847, 138290 (2023), [arXiv:2305.13439].
- [226] V. M. Abazov et al. (D0), Phys. Rev. Lett. 103, 092001 (2009), [arXiv:0903.0850].
- [227] V. M. Abazov et al. (D0), Phys. Rev. **D78**, 012005 (2008), [arXiv:0803.0739].
- [228] V. M. Abazov et al. (D0), Phys. Rev. Lett. 98, 181802 (2007), [hep-ex/0612052].
- [229] T. Aaltonen et al. (CDF), Phys. Rev. Lett. 103, 092002 (2009), [arXiv:0903.0885].
- [230] T. Aaltonen et al. (CDF), Phys. Rev. **D81**, 072003 (2010), [arXiv:1001.4577].
- [231] T. Aaltonen et al. (CDF), Phys. Rev. **D82**, 112005 (2010), [arXiv:1004.1181].
- [232] A. Heinson and T. R. Junk, Ann. Rev. Nucl. Part. Sci. 61, 171 (2011), [arXiv:1101.1275].
- [233] A. Giammanco and R. Schwienhorst, Rev. Mod. Phys. **90**, 3, 035001 (2018), [arXiv:1710.10699].
- [234] Tevatron Electroweak Working Group, (2009), [arXiv:0908.2171].
- [235] T. A. Aaltonen et al. (CDF, D0), Phys. Rev. Lett. 115, 15, 152003 (2015), [arXiv:1503.05027].
- [236] N. Kidonakis, Phys. Rev. **D83**, 091503 (2011), [arXiv:1103.2792].
- [237] T. A. Aaltonen et al. (CDF, D0), Phys. Rev. Lett. 112, 231803 (2014), [arXiv:1402.5126].
- [238] G. Aad et al. (ATLAS), Phys. Lett. B 854, 138726 (2024), [arXiv:2310.01518].
- [239] C. Collaboration (CMS), Technical Report CMS-PAS-TOP-24-011 (2024).
- [240] G. Aad et al. (ATLAS), Phys. Rev. **D90**, 11, 112006 (2014), [arXiv:1406.7844].
- [241] G. Aad et al. (ATLAS), Phys. Lett. **B717**, 330 (2012), [arXiv:1205.3130].
- [242] S. Chatrchyan et al. (CMS), JHEP 12, 035 (2012), [arXiv:1209.4533].
- [243] M. Aaboud et al. (ATLAS, CMS), JHEP 05, 088 (2019), [arXiv:1902.07158].
- [244] M. Aaboud et al. (ATLAS), Eur. Phys. J. C77, 8, 531 (2017), [arXiv:1702.02859].
- [245] M. Aaboud et al. (ATLAS), JHEP 04, 124 (2017), [arXiv:1702.08309].
- [246] V. Khachatryan et al. (CMS), JHEP **06**, 090 (2014), [arXiv:1403.7366].
- [247] V. Khachatryan et al. (CMS), JHEP **04**, 073 (2016), [arXiv:1511.02138].
- [248] M. Aaboud et al. (ATLAS), JHEP **04**, 086 (2017), [arXiv:1609.03920].
- [249] A. M. Sirunyan et al. (CMS), Phys. Lett. **B772**, 752 (2017), [arXiv:1610.00678].
- [250] A. M. Sirunyan et al. (CMS), Phys. Lett. B 800, 135042 (2020), [arXiv:1812.10514].
- [251] A. M. Sirunyan et al. (CMS), Eur. Phys. J. C 80, 5, 370 (2020), [arXiv:1907.08330].
- [252] A. M. Sirunyan et al. (CMS), Phys. Lett. B 808, 135609 (2020), [arXiv:2004.12181].
- [253] Aad, Georges and others, JHEP **05**, 305 (2024), [arXiv:2403.02126].
- [254] G. Aad et al. (ATLAS), JHEP 11, 040 (2022), [arXiv:2202.11382].
- [255] V. Khachatryan et al. (CMS), JHEP **09**, 027 (2016), [arXiv:1603.02555].
- [256] G. Aad et al. (ATLAS), Phys. Lett. **B756**, 228 (2016), [arXiv:1511.05980].
- [257] G. Aad et al. (ATLAS), JHEP **06**, 191 (2023), [arXiv:2209.08990].
- [258] ATLAS Collaboration, ATLAS-CONF-2011-118.

- [259] G. Aad et al. (ATLAS), Phys. Lett. **B716**, 142 (2012), [arXiv:1205.5764].
- [260] S. Chatrchyan et al. (CMS), Phys. Rev. Lett. 110, 022003 (2013), [arXiv:1209.3489].
- [261] G. Aad et al. (ATLAS), JHEP **01**, 064 (2016), [arXiv:1510.03752].
- [262] G. Aad et al. (ATLAS), Eur. Phys. J. C 81, 8, 720 (2021), [arXiv:2007.01554].
- [263] S. Chatrchyan et al. (CMS), Phys. Rev. Lett. 112, 23, 231802 (2014), [arXiv:1401.2942].
- [264] M. Aaboud et al. (ATLAS), JHEP **01**, 063 (2018), [arXiv:1612.07231].
- [265] M. Aaboud et al. (ATLAS), Eur. Phys. J. C 78, 3, 186 (2018), [arXiv:1712.01602].
- [266] G. Aad et al. (ATLAS), Physical Review D 110, 7 (2024), [arXiv:2407.15594].
- [267] A. M. Sirunyan et al. (CMS), JHEP 10, 117 (2018), [arXiv:1805.07399].
- [268] CMS Collaboration, CMS-PAS-TOP-19-003.
- [269] CMS Collaboration, JHEP 11, 111 (2021), [arXiv:2109.01706].
- [270] A. Tumasyan et al. (CMS), JHEP 07, 046 (2023), [arXiv:2208.00924].
- [271] A. Hayrapetyan et al. (CMS), JHEP **2025**, 1 (2025), [arXiv:2409.06444].
- [272] M. Fael and T. Gehrmann, Phys. Rev. D 88, 033003 (2013), [arXiv:1307.1349].
- [273] S. M. Etesami, S. Khatibi and M. Mohammadi Najafabadi, Eur. Phys. J. C **76**, 533 (2016), [arXiv:1606.02178].
- [274] A. M. Sirunyan et al. (CMS), Phys. Rev. Lett. 121, 22, 221802 (2018), [arXiv:1808.02913].
- [275] G. Aad et al. (ATLAS), Phys. Rev. Lett. 131, 161802 (2023), [arXiv:2302.01283].
- [276] A. M. Sirunyan et al. (CMS), JHEP 07, 003 (2017), [arXiv:1702.01404].
- [277] A. M. Sirunyan et al. (CMS), Phys. Rev. Lett. 122, 13, 132003 (2019), [arXiv:1812.05900].
- [278] A. Tumasyan et al. (CMS), JHEP **02**, 107 (2022), [arXiv:2111.02860].
- [279] G. Aad et al. (ATLAS), JHEP 07, 124 (2020), [arXiv:2002.07546].
- [280] CMS Collaboration, Phys. Lett. B 855, 138815 (2024), [arXiv:2312.11668].
- [281] CMS Collaboration, CMS-PAS-TOP-24-009.
- [282] M. Aaboud et al. (ATLAS), Eur. Phys. J. C79, 4, 290 (2019), [arXiv:1810.01772].
- [283] T. Affolder et al. (CDF), Phys. Rev. D 63, 032003 (2001), [hep-ex/0006028].
- [284] B. Abbott et al. (D0), Phys. Rev. D 58, 052001 (1998), [hep-ex/9801025].
- [285] A. M. Sirunyan et al. (CMS), Eur. Phys. J. C79, 4, 313 (2019), [arXiv:1812.10534].
- [286] A. Tumasyan et al. (CMS), Eur. Phys. J. C 83, 10 (2023), [arXiv:2302.01967].
- [287] L. Sonnenschein, Phys. Rev. D 73, 054015 (2006), [hep-ph/0603011].
- [288] A. Hayrapetyan et al. (CMS), Physics Reports 116–218 (2025), [arXiv:2403.01313].
- [289] B. Abbott et al. (D0), Phys. Rev. Lett. 80, 2063 (1998), [hep-ex/9706014].
- [290] B. Abbott et al. (D0), Phys. Rev. **D60**, 052001 (1999), [hep-ex/9808029].
- [291] F. Abe *et al.* (CDF), Phys. Rev. Lett. **82**, 271 (1999), [Erratum: Phys. Rev. Lett.82,2808(1999)], [hep-ex/9810029].
- [292] M. Aaboud et al. (ATLAS), Phys. Lett. **B761**, 350 (2016), [arXiv:1606.02179].
- [293] A. Abulencia et al. (CDF), Phys. Rev. D 75, 111103 (2007), [arXiv:0705.1594].
- [294] T. Aaltonen et al. (CDF), Phys. Rev. **D80**, 051104 (2009), [arXiv:0906.5371].
- [295] G. Aad et al. (ATLAS), JHEP **2023**, 6 (2023), [arXiv:2209.00583].
- [296] V. Khachatryan et al. (CMS), JHEP 12, 123 (2016), [arXiv:1608.03560].

- [297] V. Khachatryan et al. (CMS), Phys. Rev. **D93**, 9, 092006 (2016), [arXiv:1603.06536].
- [298] A. Abulencia et al. (CDF), Phys. Rev. Lett. 96, 022004 (2006), [hep-ex/0512070].
- [299] T. Aaltonen et al. (CDF), Phys. Rev. Lett. 99, 182002 (2007), [arXiv:0707.3934].
- [300] G. Aad et al. (ATLAS), Eur. Phys. J. C 75, 4 (2015), [arXiv:1409.0832].
- [301] G. Aad et al. (ATLAS), Eur. Phys. J. C 72, 6 (2012), [arXiv:1203.5755].
- [302] F. Abe et al. (CDF), Phys. Rev. Lett. 80, 2767 (1998), [hep-ex/9801014].
- [303] B. Abbott et al. (D0), Phys. Rev. Lett. **79**, 1197 (1997), [hep-ex/9703008].
- [304] V. M. Abazov et al. (D0), Nature 429, 638 (2004), [hep-ex/0406031].
- [305] A. Abulencia et al. (CDF), Phys. Rev. D 73, 092002 (2006), [hep-ex/0702018].
- [306] A. M. Sirunyan et al. (CMS), Eur. Phys. J. C78, 11, 891 (2018), [arXiv:1805.01428].
- [307] T. Aaltonen et al. (CDF), Phys. Lett. **B698**, 371 (2011), [arXiv:1101.4926].
- [308] The Tevatron Electroweak Working Group, arXiv:1608.01881, FERMILAB-CONF-16-298-E.
- [309] F. Abe et al. (CDF), Phys. Rev. Lett. **79**, 1992 (1997).
- [310] T. Aaltonen et al. (CDF), Phys. Rev. Lett. 105, 252001 (2010), [arXiv:1010.4582].
- [311] T. Aaltonen et al. (CDF), Phys. Rev. D 81, 032002 (2010), [arXiv:0910.0969].
- [312] T. Aaltonen et al. (CDF), Phys. Rev. D 88, 011101 (2013), [arXiv:1305.3339].
- [313] T. Aaltonen et al. (CDF), Phys. Rev. D 92, 032003 (2015), [arXiv:1505.00500].
- [314] T. Aaltonen et al. (CDF), Phys. Rev. D 88, 091101 (2013), [arXiv:1309.7570].
- [315] V. M. Abazov et al. (D0), Phys. Rev. Lett. 113, 032002 (2014), [arXiv:1405.1756].
- [316] V. M. Abazov et al. (D0), Phys. Rev. **D91**, 11, 112003 (2015), [arXiv:1501.07912].
- [317] G. Aad et al. (ATLAS), Physics Reports 127–183 (2025), [arXiv:2404.10674].
- [318] G. Aad et al. (ATLAS) (2025), [arXiv:2502.18216].
- [319] V. Khachatryan et al. (CMS), Phys. Rev. **D93**, 7, 072004 (2016), [arXiv:1509.04044].
- [320] [arXiv:1403.4427].
- [321] R. Nisius, SoftwareX 11, 100468 (2020).
- [322] M. Beneke et al., Phys. Lett. **B775**, 63 (2017), [arXiv:1605.03609].
- [323] A. H. Hoang, C. Lepenik and M. Preisser, JHEP 09, 099 (2017), [arXiv:1706.08526].
- [324] A. H. Hoang, S. Plätzer and D. Samitz, JHEP 10, 200 (2018), [arXiv:1807.06617].
- [325] A. H. Hoang et al., Phys. Rev. Lett. 101, 151602 (2008), [arXiv:0803.4214].
- [326] ATLAS Collaboration, ATL-PHYS-PUB-2021-034.
- [327] A. M. Sirunyan et al., Physics Letters B 803, 135263 (2020), [arXiv:1909.09193].
- [328] S. Catani et al., JHEP 08, 08, 027 (2020), [arXiv:2005.00557].
- [329] G. Aad et al. (ATLAS) (2025), [arXiv:2507.02632].
- [330] G. Aad et al. (ATLAS), Phys. Lett. **B716**, 1 (2012), [arXiv:1207.7214].
- [331] S. Chatrchyan et al. (CMS), Phys. Lett. **B716**, 30 (2012), [arXiv:1207.7235].
- [332] S. Alekhin, A. Djouadi and S. Moch, Phys. Lett. **B716**, 214 (2012), [arXiv:1207.0980].
- [333] G. Aad et al. (ATLAS, CMS) (2025), [arXiv:2504.00672].
- [334] T. Aaltonen et al. (CDF), Phys. Rev. **D87**, 5, 052013 (2013), [arXiv:1210.6131].
- [335] V. M. Abazov et al. (D0), Phys. Rev. **D84**, 052005 (2011), [arXiv:1106.2063].

- [336] G. Aad et al. (ATLAS), Phys. Lett. **B728**, 363 (2014), [arXiv:1310.6527].
- [337] S. Chatrchyan et al. (CMS), JHEP **06**, 109 (2012), [arXiv:1204.2807].
- [338] S. Chatrchyan et al. (CMS), Phys. Lett. **B770**, 50 (2017), [arXiv:1610.09551].
- [339] A. Hayrapetyan et al. (CMS), JHEP **2021**, 12 (2021), [arXiv:2108.10407].
- [340] T. A. Aaltonen et al. (CDF), Phys. Rev. Lett. 111, 20, 202001 (2013), [arXiv:1308.4050].
- [341] CMS Collaboration, CMS-PAS-TOP-16-019.
- [342] V. M. Abazov et al. (D0), Phys. Rev. **D85**, 091104 (2012), [arXiv:1201.4156].
- [343] M. Aaboud et al. (ATLAS), Eur. Phys. J. C78, 2, 129 (2018), [arXiv:1709.04207].
- [344] ATLAS Collaboration, ATLAS-CONF-2019-038.
- [345] V. Khachatryan et al. (CMS), Phys. Lett. **B736**, 33 (2014), [arXiv:1404.2292].
- [346] G. Mahlon and S. J. Parke, Phys. Rev. D53, 4886 (1996), [hep-ph/9512264]; G. Mahlon and S. J. Parke, Phys. Lett. B411, 173 (1997), [hep-ph/9706304].
- [347] G.R. Goldstein, in Spin 96: Proceedings of the 12th International Symposium on High Energy Spin Physics, ed. C.W. Jager (World Scientific, Singapore, 1997), p. 328.
- [348] T. Stelzer and S. Willenbrock, Phys. Lett. **B374**, 169 (1996), [hep-ph/9512292].
- [349] W. Bernreuther et al., Nucl. Phys. **B690**, 81 (2004), [hep-ph/0403035].
- [350] A. Brandenburg, Z. G. Si and P. Uwer, Phys. Lett. **B539**, 235 (2002), [hep-ph/0205023].
- [351] B. Abbott et al. (D0), Phys. Rev. Lett. 85, 256 (2000), [hep-ex/0002058].
- [352] T. Aaltonen et al. (CDF), Phys. Rev. D 83, 031104 (2011), [arXiv:1012.3093].
- [353] V. M. Abazov et al. (D0), Phys. Lett. **B757**, 199 (2016), [arXiv:1512.08818].
- [354] V. M. Abazov et al. (D0), Phys. Rev. **D95**, 1, 011101 (2017), [arXiv:1607.07627].
- [355] V. M. Abazov et al. (D0), Phys. Rev. **D92**, 052007 (2015), [arXiv:1507.05666].
- [356] G. Mahlon and S. J. Parke, Phys. Rev. **D81**, 074024 (2010), [arXiv:1001.3422].
- [357] G. Aad et al. (ATLAS), Phys. Rev. Lett. 108, 21 (2012), [arXiv:1203.4081].
- [358] G. Aad et al. (ATLAS), Phys. Rev. **D90**, 11, 112016 (2014), [arXiv:1407.4314].
- [359] G. Aad et al. (ATLAS), Phys. Rev. Lett. 114, 14, 142001 (2015), [arXiv:1412.4742].
- [360] G. Aad et al. (ATLAS), Phys. Rev. **D93**, 1, 012002 (2016), [arXiv:1510.07478].
- [361] S. Chatrchyan et al. (CMS), Phys. Rev. Lett. 112, 18, 182001 (2014), [arXiv:1311.3924].
- [362] V. Khachatryan et al. (CMS), Phys. Lett. **B758**, 321 (2016), [arXiv:1511.06170].
- [363] V. Khachatryan et al. (CMS), Phys. Rev. **D93**, 5, 052007 (2016), [arXiv:1601.01107].
- [364] M. Aaboud et al. (ATLAS), Eur. Phys. J. C 80, 8, 754 (2020), [arXiv:1903.07570].
- [365] A. M. Sirunyan et al. (CMS), Phys. Rev. **D100**, 7, 072002 (2019), [arXiv:1907.03729].
- [366] M. Aaboud et al. (ATLAS), JHEP **03**, 113 (2017), [arXiv:1612.07004].
- [367] A. Einstein, B. Podolsky and N. Rosen, Phys. Rev. 47, 777 (1935).
- [368] E. Schrödinger, Mathematical Proceedings of the Cambridge Philosophical Society **31**, 4, 555–563 (1935).
- [369] J. S. Bell, Physics Physique Fizika 1, 195 (1964).
- [370] A. Go et al. (Belle), Phys. Rev. Lett. 99, 131802 (2007), [arXiv:quant-ph/0702267].
- [371] M. Fabbrichesi et al. (2023), [arXiv:2305.04982].

- [372] M. Fabbrichesi, R. Floreanini and G. Panizzo, Phys. Rev. Lett. 127, 16, 161801 (2021), [arXiv:2102.11883].
- [373] C. Severi et al., Eur. Phys. J. C 82, 4, 285 (2022), [arXiv:2110.10112].
- [374] Y. Afik and J. R. M. n. de Nova, Quantum 6, 820 (2022), [arXiv:2203.05582].
- [375] J. A. Aguilar-Saavedra and J. A. Casas, Eur. Phys. J. C 82, 8, 666 (2022), [arXiv:2205.00542].
- [376] Y. Afik and J. R. M. n. de Nova, Phys. Rev. Lett. 130, 22, 221801 (2023), [arXiv:2209.03969].
- [377] R. Ashby-Pickering, A. J. Barr and A. Wierzchucka, JHEP **05**, 020 (2023), [arXiv:2209.13990].
- [378] J. A. Aguilar-Saavedra (2023), [arXiv:2307.06991].
- [379] B. Fuks et al., The European Physical Journal C 85, 2 (2025).
- [380] P. Nason, E. Re and L. Rottoli (2025), [arXiv:2505.00096].
- [381] G. L. Kane, G. A. Ladinsky and C. P. Yuan, Phys. Rev. **D45**, 124 (1992).
- [382] A. Czarnecki, J. G. Korner and J. H. Piclum, Phys. Rev. **D81**, 111503 (2010), [arXiv:1005.2625].
- [383] T. Affolder et al. (CDF), Phys. Rev. Lett. 84, 216 (2000), [hep-ex/9909042].
- [384] D. Acosta et al. (CDF), Phys. Rev. D 71, 031101 (2005), [hep-ex/0411070].
- [385] A. Abulencia et al. (CDF), Phys. Rev. D 73, 111103 (2006), [hep-ex/0511023].
- [386] V. M. Abazov et al. (D0), Phys. Rev. D 75, 031102 (2007), [hep-ex/0609045].
- [387] V. M. Abazov et al. (D0), Phys. Rev. Lett. 100, 062004 (2008), [arXiv:0711.0032].
- [388] T. Aaltonen et al. (CDF), Phys. Lett. B 674, 160 (2009), [arXiv:0811.0344].
- [389] V. M. Abazov et al. (D0), Phys. Rev. D 70, 032004 (2004), [hep-ex/0404040].
- [390] T. Aaltonen et al. (CDF, D0), Phys. Rev. **D85**, 071106 (2012), [arXiv:1202.5272].
- [391] G. Aad et al. (ATLAS), JHEP **06**, 088 (2012), [arXiv:1205.2484].
- [392] S. Chatrchyan et al. (CMS), JHEP 10, 167 (2013), [arXiv:1308.3879].
- [393] ATLAS and CMS Collaboration, ATLAS-CONF-2013-033, CMS-PAS-TOP-12-025.
- [394] M. Aaboud *et al.* (ATLAS), Eur. Phys. J. **C77**, 4, 264 (2017), [Erratum: Eur. Phys. J.C79,no.1,19(2019)], [arXiv:1612.02577].
- [395] V. Khachatryan et al. (CMS), Phys. Lett. **B762**, 512 (2016), [arXiv:1605.09047].
- [396] V. Khachatryan et al. (CMS), JHEP **01**, 053 (2015), [arXiv:1410.1154].
- [397] G. Aad et al. (CMS, ATLAS), JHEP **08**, 08, 051 (2020), [arXiv:2005.03799].
- [398] G. Aad et al. (ATLAS), Phys. Lett. B 843, 137829 (2023), [arXiv:2209.14903].
- [399] G. Aad et al. (ATLAS) (2025), [arXiv:2509.16039], URL https://arxiv.org/abs/2509.16039.
- [400] A. M. Sirunyan et al. (CMS), Physical Review D 102, 9 (2020), [arXiv:2009.07123].
- [401] S. Jung et al., Phys. Rev. **D81**, 015004 (2010), [arXiv:0907.4112].
- [402] M. Czakon, P. Fiedler and A. Mitov, Phys. Rev. Lett. **115**, 5, 052001 (2015), [arXiv:1411.3007].
- [403] W. Hollik and D. Pagani, Phys. Rev. **D84**, 093003 (2011), [arXiv:1107.2606].
- [404] W. Bernreuther and Z.-G. Si, Phys. Rev. **D86**, 034026 (2012), [arXiv:1205.6580].

- [405] V. M. Abazov et al. (D0), Phys. Rev. Lett. 100, 142002 (2008), [arXiv:0712.0851].
- [406] T. Aaltonen et al. (CDF), Phys. Rev. Lett. 101, 202001 (2008), [arXiv:0806.2472].
- [407] T. A. Aaltonen et al. (CDF, D0), Phys. Rev. Lett. 120, 4, 042001 (2018), [arXiv:1709.04894].
- [408] S. Berge and S. Westhoff, JHEP **2013**, 7 (2013), ISSN 1029-8479, [arXiv:1305.3272].
- [409] V. Khachatryan et al. (CMS), Phys. Lett. **B757**, 154 (2016), [arXiv:1507.03119].
- [410] G. Aad et al. (ATLAS), Phys. Lett. **B756**, 52 (2016), [arXiv:1512.06092].
- [411] G. Aad et al. (ATLAS), Phys. Lett. B 843, 137848 (2023), [arXiv:2212.10552].
- [412] G. Aad et al. (ATLAS), JHEP 07, 033 (2023), [arXiv:2301.04245].
- [413] A. Hayrapetyan et al. (CMS) (2025), [arXiv:2509.13512].
- [414] G. Aad et al. (ATLAS), JHEP 02, 107 (2014), [arXiv:1311.6724].
- [415] S. Chatrchyan et al. (CMS), Phys. Lett. **B717**, 129 (2012), [arXiv:1207.0065].
- [416] G. Aad et al. (ATLAS), JHEP 05, 061 (2015), [arXiv:1501.07383].
- [417] S. Chatrchyan et al. (CMS), JHEP **04**, 191 (2014), [arXiv:1402.3803].
- [418] M. Aaboud et al. (ATLAS, CMS), JHEP 04, 033 (2018), [arXiv:1709.05327].
- [419] M. Czakon et al., Phys. Rev. **D98**, 1, 014003 (2018), [arXiv:1711.03945].
- [420] G. Aad *et al.* (ATLAS), Eur. Phys. J. **C76**, 2, 87 (2016), [Erratum: Eur. Phys. J.C77,564(2017)], [arXiv:1509.02358].
- [421] V. Khachatryan et al. (CMS), Phys. Rev. **D93**, 3, 034014 (2016), [arXiv:1508.03862].
- [422] G. Aad et al. (ATLAS), Phys. Rev. **D94**, 3, 032006 (2016), [arXiv:1604.05538].
- [423] V. Khachatryan et al. (CMS), Phys. Lett. **B760**, 365 (2016), [arXiv:1603.06221].
- [424] G. Aad et al. (ATLAS), JHEP 08, 077 (2023), [arXiv:2208.12095].
- [425] A. Tumasyan et al. (CMS), Phys. Lett. B 846, 137703 (2023), [arXiv:2208.02751].
- [426] G. Aad et al. (ATLAS), Eur. Phys. J. C 82, 4, 374 (2022), [arXiv:2110.05453].
- [427] A. M. Sirunyan et al. (CMS), JHEP 06, 146 (2020), [arXiv:1912.09540].
- [428] D. Choudhury, T. M. P. Tait and C. E. M. Wagner, Phys. Rev. D65, 053002 (2002), [hep-ph/0109097].
- [429] D. Chang, W.-F. Chang and E. Ma, Phys. Rev. **D59**, 091503 (1999), [hep-ph/9810531];
 D. Chang, W.-F. Chang and E. Ma, Phys. Rev. **D61**, 037301 (2000), [hep-ph/9909537].
- [430] T. Aaltonen et al. (CDF), Phys. Rev. **D88**, 3, 032003 (2013), [arXiv:1304.4141].
- [431] V. M. Abazov *et al.* (D0), Phys. Rev. **D90**, 5, 051101 (2014), [Erratum: Phys. Rev. D90, no.7,079904(2014)], [arXiv:1407.4837].
- [432] G. Aad et al. (ATLAS), JHEP 11, 031 (2013), [arXiv:1307.4568].
- [433] CMS Collaboration, CMS-PAS-TOP-11-031.
- [434] S. P. Martin 1–98 (1997), [Adv. Ser. Direct. High Energy Phys.18,1(1998)], [hep-ph/9709356].
- [435] C. T. Hill and E. H. Simmons, Phys. Rept. **381**, 235 (2003), [Erratum: Phys Rept.390,553(2004)], [hep-ph/0203079].
- [436] C. T. Hill, Phys. Lett. **B266**, 419 (1991).
- [437] C. T. Hill, Phys. Lett. **B345**, 483 (1995), [hep-ph/9411426].
- [438] S. Chatrchyan et al. (CMS), Phys. Rev. D 87, 072002 (2013), URL https://link.aps.org/doi/10.1103/PhysRevD.87.072002.

- [439] S. Chatrchyan et al. (CMS), JHEP 12, 015 (2012), [arXiv:1209.4397].
- [440] G. Aad et al. (ATLAS), JHEP 10, 061 (2020), [arXiv:2005.05138].
- [441] G. Aad et al. (ATLAS), The European Physical Journal C 84, 7 (2024).
- [442] G. Aad et al. (ATLAS), JHEP 07, 199 (2023), [arXiv:2301.03902].
- [443] G. Aad et al. (ATLAS), JHEP 2306, 155 (2023), [arXiv:2208.11415].
- [444] G. Aad et al. (ATLAS), JHEP 2023, 12 (2023), [arXiv:2309.12817].
- [445] A. Hayrapetyan et al. (CMS), Physical Review D 112, 3 (2025), [arXiv:2407.15172].
- [446] A. Tumasyan et al. (CMS), JHEP **02**, 169 (2022), [arXiv:2112.09734].
- [447] A. Tumasyan *et al.* (CMS), Phys. Rev. Lett. **129**, 032001 (2022), URL https://link.aps.org/doi/10.1103/PhysRevLett.129.032001.
- [448] G. Aad et al. (ATLAS), Physical Review D 108, 3 (2023), [arXiv:2301.11605].
- [449] G. Aad et al. (ATLAS), Phys. Lett. B 842, 137379 (2023), [arXiv:2205.02537].
- [450] G. Aad et al. (ATLAS), Eur. Phys. J. C 82, 4, 334 (2022), [arXiv:2112.01302].
- [451] A. Tumasyan et al. (CMS), JHEP **06**, 082 (2022), [arXiv:2201.07859].
- [452] A. Hayrapetyan (CMS), Physical Review D 111, 1 (2025), [arXiv:2312.03199].
- [453] A. Hayrapetyan et al. (CMS) (2025), [arXiv:2504.08532].
- [454] G. Aad et al. (ATLAS), Physical Review D 110, 1 (2024), [arXiv:2403.06742].
- [455] A. Hayrapetyan et al. (CMS), Physical Review Letters 132, 24 (2024), [arXiv:2402.18461].
- [456] S. Banerjee, M. Chala and M. Spannowsky, Eur. Phys. J. C **78**, 8, 683 (2018), [arXiv:1806.02836].
- [457] T. Giani, G. Magni and J. Rojo, EPJC 83, 5 (2023).
- [458] C. Zhang and S. Willenbrock, Nuovo Cim. C 033, 4, 285 (2010), [arXiv:1008.3155].
- [459] A. M. Sirunyan et al. (CMS), JHEP **03**, 095 (2021), [arXiv:2012.04120].
- [460] A. Tumasyan et al. (CMS), JHEP **2021**, 12 (2021), [arXiv:2107.13896].
- [461] A. Hayrapetyan et al. (CMS) (2025), [arXiv:2505.21206].
- [462] A. Hayrapetyan et al. (CMS) (2025), [arXiv:2507.17498].
- [463] A. Hayrapetyan, Physical Review D 109, 7 (2024), [arXiv:2312.08229].
- [464] A. a. Hayrapetyan, Physical Review D 111, 1 (2025), [arXiv:2312.03199].
- [465] A. Hayrapetyan, JHEP **2023**, 12 (2023), [arXiv:2307.15761].
- [466] G. Aad et al. (ATLAS), JHEP **2025**, 2 (2025), [arXiv:2409.14982].
- [467] G. Aad et al. (ATLAS) (2025), [arXiv:2504.05919].
- [468] G. Aad et al. (ATLAS) (2025), [arXiv:2509.19038].